Geotechnical Centrifuge Experiments to Improve Understanding of Sand Production from Heavy Oil Reservoirs

A Thesis Submitted to the College of Graduate and Postdoctoral Studies

In partial Fulfillment of the Requirements for the degree of Master of Science

In Department of Civil, Geological and Environmental Engineering

University of Saskatchewan

Saskatoon

By

Shahin Layeghpour

PERMISSION TO USE AND DISCLAIMER

In presenting this thesis/dissertation in partial fulfillment of the requirements for a Postgraduate degree from the University of Saskatchewan, I agree that the Libraries of this University may make it freely available for inspection. I further agree that permission for copying of this thesis/dissertation in any manner, in whole or in part, for scholarly purposes may be granted by the professor or professors who supervised my thesis/dissertation work or, in their absence, by the Head of the Department or the Dean of the College in which my thesis work was done. It is understood that any copying or publication or use of this thesis/dissertation or parts thereof for financial gain shall not be allowed without my written permission. It is also understood that due recognition shall be given to me and to the University of Saskatchewan in any scholarly use which may be made of any material in my thesis/dissertation.

Requests for permission to copy or to make any other use of the material in this thesis in whole or in part should be addressed to:

Head of the Department of Civil, Geological and Environmental Engineering
3B48.3 Engineering Building, 57 Campus Drive
University of Saskatchewan
Saskatoon, Saskatchewan
S7N 5A9 Canada
OR
Dean
College of Graduate and Postdoctoral Studies
University of Saskatchewan
116 Thorvaldson Building, 110 Science Place
Saskatoon, Saskatchewan S7N 5C9
Canada

ABSTRACT

Since the 1990's, Cold Heavy Oil Production with Sand (CHOPS) has been a common practice in Western Canada where sand can be easily mobilized from weakly cemented sandstones. The more sand produced, the greater the oil recovery, with recovery factors of 10% being typical. In recent years, operating companies have enhanced recovery in reservoirs previously operated using CHOPS by applying thermal and/or chemical methods; however, effective implementation of these methods requires an improved understanding of sand production mechanisms. Numerous field-based, numerical, and laboratory modelling studies have been completed to better understand the shape of the voids that form within heavy oil reservoirs during CHOPS, sand transport mechanisms, and CHOPS impact on production rate. The objective of this research was to design and implement a laboratory testing system to investigate these subjects.

A purpose-built geotechnical centrifuge model was used for this research, with a sandpack of dense, uncemented sand representing the reservoir. The results demonstrate that the predominant sanding mechanism is the development of a cone-shaped cavity at the top of the sandpack, both with stiff (steel) and compliant (clay) caprock. The results also demonstrate that erosion channels may develop around the cavity, in cases where flow rates near the top of the sandpack are greater than flow rates at depth; however, with the presence of a flexible caprock and uniform radial flow, this effect can be nullified. In addition, the results for one of the experiments, in conjunction with numerical modelling, suggest that a wormhole may form during seepage in the upper part of the reservoir where in-situ stresses are relatively low, though it might collapse once seepage is ceased. Such wormholes may have been a major cause of the high flowrates observed during the tests after sand production, enhanced to some extent by dilation-induced increase in hydraulic conductivity in the near-well and near-cavity areas. Moreover, results obtained using two-phase fluid saturations (water and oil) suggest that capillary pressures increase the effective strength of the sandpack, which reduces the tendency of sand failure as was observed in deep perforated zones in experiments conducted using single-phase oil saturation. The practical implication of this work is the suggestion that it may be possible to improve the effectiveness of enhanced recovery operations if heated fluids/solvents are injected into the deeper, less disturbed part of the reservoir in order to avoid premature breakthrough (production) of injected fluids.

ACKNOWLEDGEMENTS

I would like to give a special thanks to my supervisor, Dr. Christopher David Hawkes, for his guidance and support throughout this project. He taught me how to conduct research step by step with patience; taught me how to see different aspects of a problem or critically assess results. It is now my privilege to carry these skills forward to future projects. He helped me to learn from my errors and how to minimize them and this was a great advantage for my future professional career. I would also like to thank my co-supervisor, Dr. Gonzalo Zambrano Narvaez for his technical support during our experimental work at the University of Alberta. I would like to thank Michael Pereira who developed the physical model used in this research. I would like to express appreciation to Dmytro Pantov, Yazhao Wang, and Donna Beneteau for their help in my laboratory work and thesis. I also would like to thank my committee members, Dr. Doug Milne and Dr. Grant A. Ferguson, for their time and guidance.

I truly appreciate the support of my mother since it was her efforts and support that I could reach to the point that I am standing now. Lastly, I would like to thank the Department of Civil, Geological and Environmental Engineering for providing me the opportunity to do my research work at the University of Saskatchewan. This study was funded by Petroleum Technology Research Center (PTRC) and the Mitacs Accelerate program.

DEDICATION

I dedicate this work to my mom, Maryam Sadat Faraji, who devoted her life, youth and all her money to support me all these years from the moment I was born up to date and her plans for my future. Thank you, mom, for all the thousands of times you made me delicious food, for all the times you drove me to my classes and sitting in your car waiting for me with enthusiasm, for all the life and business facts you taught me, for your persistent that I learn English since I was a little child, for all the moments we built and enjoyed together.

I also dedicate this work to the governments to exploit more oil, and instead of using it for destroying humanity, they use it for peaceful purposes and explorations in the universe.

> “ Human beings are parts of each other,
> In creation are indeed of one essence.
> If one part is afflicted with pain,
> Other parts uneasy will remain.
> If you have no sympathy for human pain,
> The name of human you cannot retain."
> Saadi Shirazi

TABLE OF CONTENTS

LIST OF TABLES

LIST OF FIGURES

1 INTRODUCTION

1.1 CHOPS

This research focuses on Cold Heavy Oil Production with Sand (CHOPS), which has been a common practice in heavy oil reservoirs in Saskatchewan and Alberta, Canada in recent decades. CHOPS is defined as non-thermal heavy oil production where substantial quantities of sand and oil are allowed into a perforated well. This thesis contains an interpretation of data collected from experiments to better understand the sand production from these heavy oil reservoirs. As the world's conventional oil production has reached a peak, heavy oil reservoirs have been recognized by the oil industry (Pan et al., 2010) as potential fields that are required to meet future supply and demand requirements. Heavy oil deposits including bitumen, heavy oil, and conventional heavy oil in Western Canada are shown in Figure 1.1. The area labelled "Cold Production Belt" that straddles the Alberta-Saskatchewan borders is most relevant to this research. These Cretaceous-age reservoirs generally comprise uncemented sand deposits with porosities estimated to be ~30%.

1.2 Sand Production

Significant quantities of sand are produced and handled through the CHOPS process. This represents an evolution of the recovery technology. Previously, operating companies prevented sand from being produced through the pay zone by using gravel packs or screens. This resulted in a 5-8% recovery factor (Dusseault, 2007). In the late 1980s, with the advent of a new pumping technology, namely progressive cavity pumps (PCP), the industry started to allow sand to be produced with the oil instead of preventing it. This primary production technique resulted in a recovery factor of 15-20% which allowed many wells to produce at economical rates (Han et al., 2007; Solanki & Metwally, 2007).

The increased recovery percentages are still inadequate because almost 80% of the oil in these reservoirs is still in place. That said, there is a need for application of post-CHOPS EOR (enhanced oil recovery) methods involving thermal and/or continuous solvent injection methods. Cyclic Solvent injection (CSI), however, is more economical compared to thermal methods because it eliminates the costs associated with source water, generators, and recycling or disposal (Miller et al., 2003). Also, in thermal methods there are excessive heat loss to the underburden or overburden layers which is accompanied with production of greenhouses gases (Hongze et al., 2017). In

addition, continuous solvent injection has a lower potential compared to CSI due to the early breakthrough caused by wormholes. CSI increases the contact area of solvent and heavy oil in the reservoir, and the wormholes provide paths for diluted oil could flow back to the well so the recovery factors associated with CSI are generally reported to be higher than other methods (Du and Zheng, 2015). However, CSI reports are mainly based on laboratory tests since field applications of CSI have not yet been tried. Field testing is the most direct method to study sand production. However, monitoring technologies that allow the producers to accurately assess where (within the reservoir) the produced sand is coming from are not yet developed. An improved understanding of the processes associated with sand production would be beneficial to enable more effective implementation of enhanced recovery operations after sand production.

Laboratory tests can be used to study sand transport mechanisms, the shape of the formed voids within the heavy oil reservoir during CHOPS, and the impact of sanding on oil production rate. In laboratory testing, the effect of modifying a single parameter at a time can be observed. Moreover, the data obtained during the tests can be used in conjunction with numerical modelling to better understand sand failure mechanisms. Therefore, a physical model has been used in this research to further study cold heavy oil production with sand in conditions that are more representative of uncemented heavy oil reservoirs.

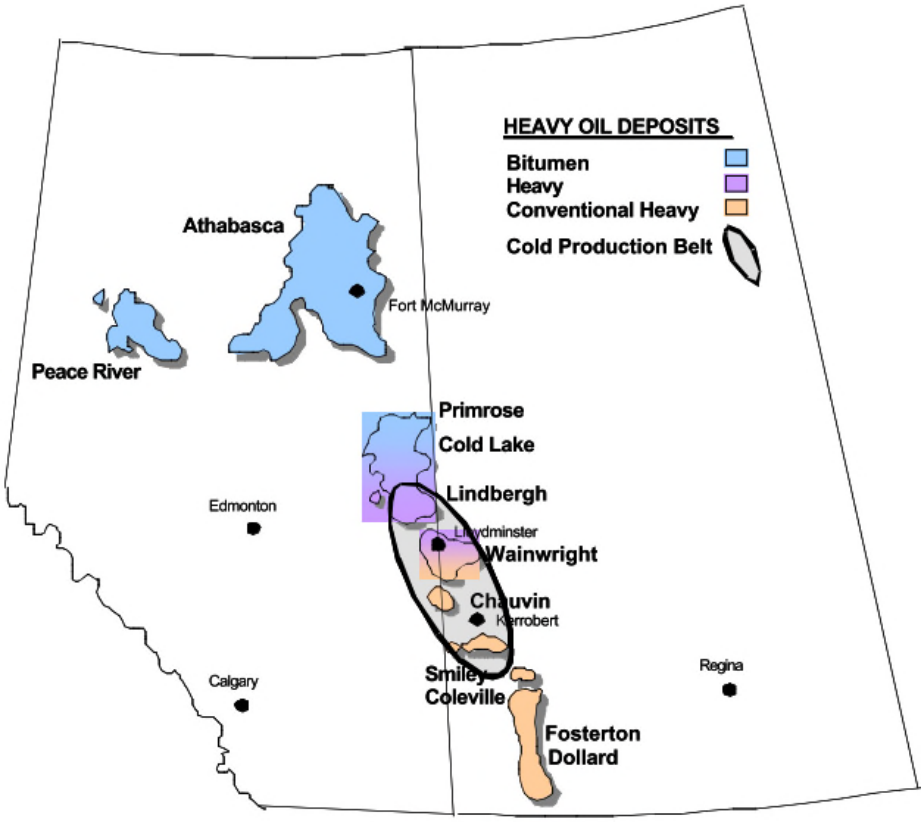

Figure 1.1. Distribution of heavy oil deposits in Western Canada (Sawatzky et al., 2002)

1.3 Research Objectives

Limited physical prototype modelling has been conducted that studies the influence of the following parameters on sand failure:

1. The effect of uniform radial flow towards the wellbore;
2. The effect of reservoir-caprock interaction in the presence of compliant caprock materials; and
3. The effect of two-phase fluid saturation during CHOPS processes.

The objective of this research was to undertake a testing sequence in an enhanced gravity environment to assess how these different parameters will affect specific aspects of sanding, including:

1. The mass of produced sand;
2. Flow rate changes resulting from sand production; and
3. The geometries of cavities, surface erosion channels and in-situ wormholes.

This should ultimately encourage more operators to consider CHOPS and post-CHOPS enhanced recovery methods where appropriate. Unlike field testing, laboratory experiments can be performed to control and vary parameters (stress distribution and anisotropy, reservoir properties, fluid viscosities, fluid saturations and other sensitivity parameters) systematically to see their influence on the results. The obtained results from laboratory experiments can be used in numerical modelling to predict sand production volumes and void geometries more precisely.

1.4 Thesis Structure

- Chapter 2 provides an overview of heavy oil reservoirs in Western Canada and explains mechanisms and advantages related to CHOPS. Also, relevant literature relating to the geology of some of the CHOPS wells, field work, numerical modelling and laboratory testing is discussed including principles of the geotechnical centrifuge and the influence of capillary forces on sand failure.
- Chapter 3 describes the geotechnical centrifuge which was used in this project, and the physical model for the testing. An outline of the procedures in different stages of the tests is presented.
- Chapter 4 shows data analysis and the results of each experiment and describes how the results can be applied to designing/redesigning future tests.
- Chapter 5 summarizes the key findings of each experiment in this project and gives recommendations for future studies relating to this project.

2 LITERATURE REVIEW

2.1 Introduction to Literature Review

This literature review focuses on advantages of CHOPS compared to other production methods, the geology of the Mannville Group in Western Canada, and effects of drilling and seepage on sand failure. There is also an overview of field observations, past numerical modelling, and previous laboratory work. The principles related to a geotechnical centrifuge are also described, because this research involved experiments conducted using such a centrifuge. Finally, the effect of water saturation on sand failure has been summarized.

2.2 Sand Production During CHOPS

A big portion of Western Canadian heavy oil reservoirs are uncemented or weakly cemented sandstone reservoirs, so the sand can be easily mobilized during production stages since there is no or weak cementation between grain particles (i.e., the sand has negligible tensile and cohesive strength which would normally arise from grain-to-grain cementation). Scientists have recognized for decades that recovery from these types of reservoirs are directly affected by sand recovery; i.e., the more sand produced, the greater the recovery factor (Han et al., 2007). The term to refer to this method has been named Cold Heavy Oil Production with Sand (CHOPS). Other methods such as thermal methods exist but these have been found to be economically unfavorable because the operational costs are too high due to heat losses from thin formations to the understrata and overburden (Han et al., 2007; Zhao et al., 2014).

CHOPS requires less energy and uses less water than steam-based processes and uses natural reservoir pressure to offset pumping costs. More attention has been paid to the extension of life of primary recovery methods in Western Canada by implementing CHOPS (Diaz et al., 2008; Pan et al., 2010). Application of advanced pumping technology, such as Progressive Cavity Pumps (PCP) to extract both sand and heavy oil has enabled Canadian heavy oil reservoirs to reach recovery factors up to 20% or more given appropriate stratigraphy, stress state and reservoir strength properties(Han et al., 2007; Tremblay et al., 1997; Vaziri et al., 2000). Producing sand with the CHOPS method increases porosity around the wellbore, which in return increases the effective permeability of the reservoir (Figure 2.1).

Another potential reason for an increase in oil production rate during CHOPS is foamy oil flow behavior, which seems to greatly enhance heavy oil production rates. The oil incorporates dissolved gas, which is exsolved as the pressure drops below the bubble point. However, the high viscosity of the fluid and the capillary effects keep the bubbles separate from each other and do not allow a continuous gas phase to be formed. This slows down the growth of the pressure drawdown transient and can maintain high pressure conditions in the reservoir, causing a pressure maintenance effect (Metwally & Solanski, 1995; Liu et al., 2008). Finally, there are other important mechanisms in the production of heavy oil in conjunction with the sand that explain why CHOPS enhances the production rates (Han et al., 2007). These mechanisms include fluid erosion due to seepage induced failure (Figure 2.2), removal of the skin (mud cake) around the wellbore, and dilation of sand in the vicinity of the wellbore due to the lateral stress reduction from sand production.

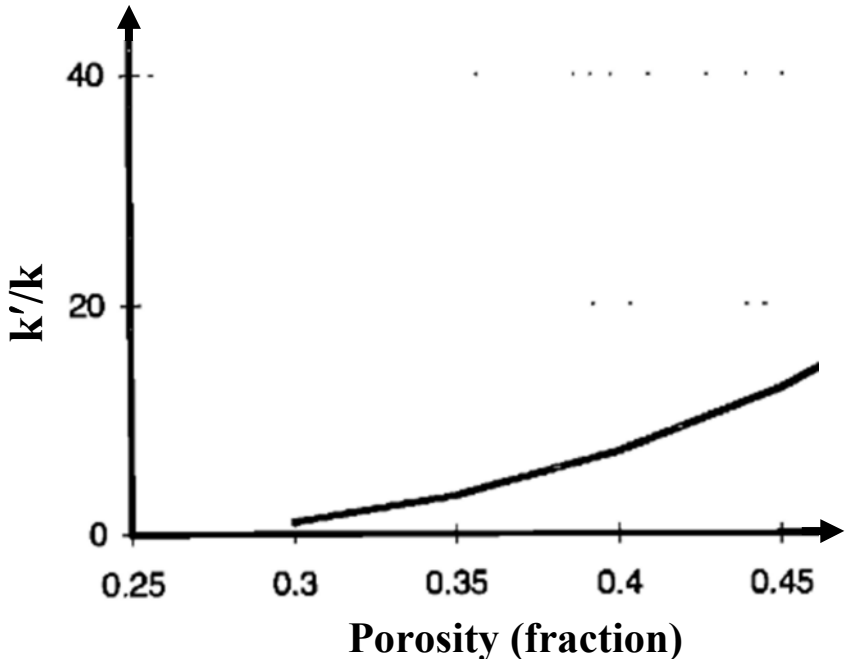

Figure 2.1. Idealized relation between permeability and porosity based on the Kozeny-Poiseuille model for a typical sand where, k is the original permeability, and k′ is the altered permeability due to the dilation and porosity changes resulting from sand production near the wellbore (after Tortike & Ali, 1991). (From this figure it can be concluded that if the porosity increases from 30% to 40%, this will result in a 8-fold increase in permeability) (Metwally & Solanski, 1995).

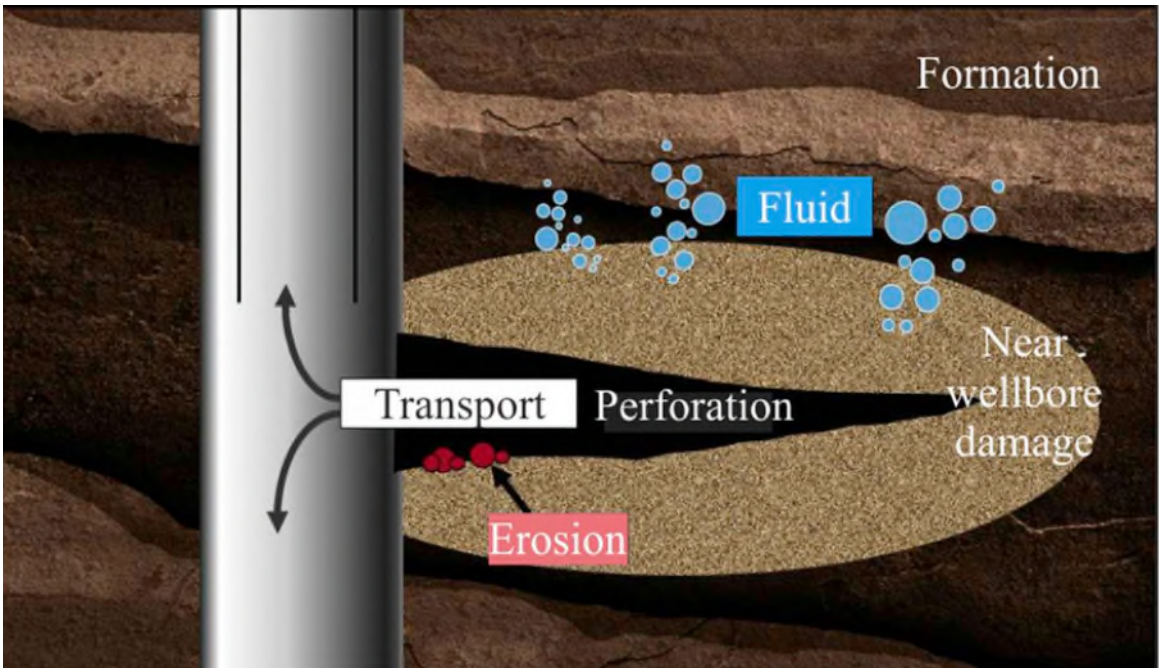

Figure 2.2. Sand failure due to the seepage induced failure because of the high velocity of viscous fluid (frictional drag) which can erode sand (Mahmud et al., 2020).

2.3 Mannville Group

The Mannville Group of south-eastern Alberta and north-western Saskatchewan consist of nine members (Figure 2.3) which have been defined in descending order as follows: Colony, McLaren, Waseca, Sparky, General Petroleum (GP), Rex, Lloydminster, Cummings and Diana (Zaitlin & Shultz, 1984). The typical heavy oil reservoirs properties in Western Canada are provided in Table 2.1.The members most commonly used for CHOPS operations are the Waseca, GP, Lloydminster and Cummings. Following are descriptions of these units in areas studied by Orr and Johnston (1977), Zaitlin & Shultz (1984), and Riediger et al. (1999). Thicknesses of the strata described here vary throughout the broader region of interest. The description given here is intended to illustrate the nature of these four units in specific areas of interest, rather than describe their regional variations in detail.

The Waseca member consists of interbedded shale and siltstone at its base with combined thicknesses of 15 to 20 meters and it is overlain by two oil producing sandstone strata named Lower Waseca and Upper Waseca. The Upper and Lower Waseca layers are separated from each other by a 1 m thick shale layer which may grade into coal as shown in Figure 2.4. The Upper Waseca is overlain by a 7 m shale that contains ironstone. The Lloydminster member is overlain by 1 to 5 m coal with interbedded carbonaceous shale at its base and is capped by shale of the Rex member. The Lloydminster member consists of two sands referred to as type 1 and type 2 (see Figure 2.5). Both sands are dominated by quartz with a clay matrix (kaolinite, minor illite, smectite) less than 8% by weight. Core studies have shown that type 1 sands have higher clay contents and higher water contents (Zaitlin & Shultz, 1984).

The GP member is located on top of lagoonal to swampy carbonaceous shale with discontinuous fine-grained laminated sand. It consists of several units mostly recognizable by beaches and burrows with finely cross laminated sand. The Cummings member mainly consist of well cemented siltstones and sandstones as stacked sheet-sands with fining-upward mudstone deposits, has interbedded limestone and shale its base and is capped by carbonaceous mudstone and coal. A correlation panel of six wells which shows the boundaries of the Cummings member (using Gamma-Ray curves) in the Frog-Lake field is shown in Figure 2.6.

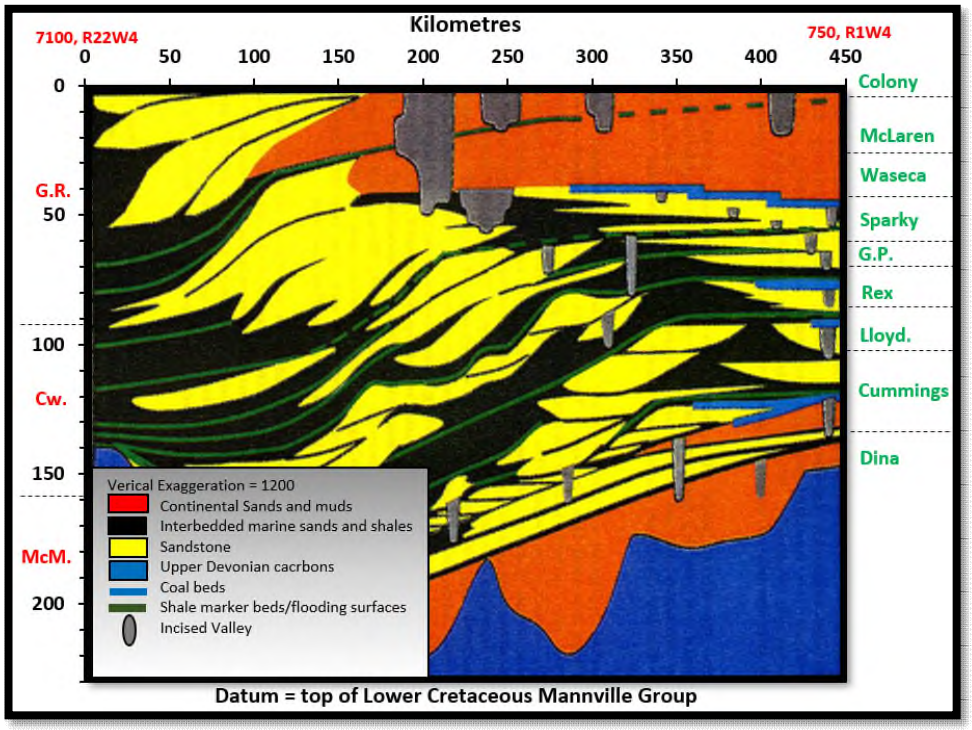

Figure 2.3. The nine members of Mannville Group (after Mcphee & Pemberton, 1994)

Table 2.1. General properties of a typical Western Canadian heavy oil reservoir (Zaitlin & Shultz, 1984; Riediger et al., 1999)

Property	Depth, m	Thickness of the pay zone, m	Porosity, %	Permeability, Darcy	Temperature, ^{o}C
Value	420-600	3-15	30-34	1-5	21

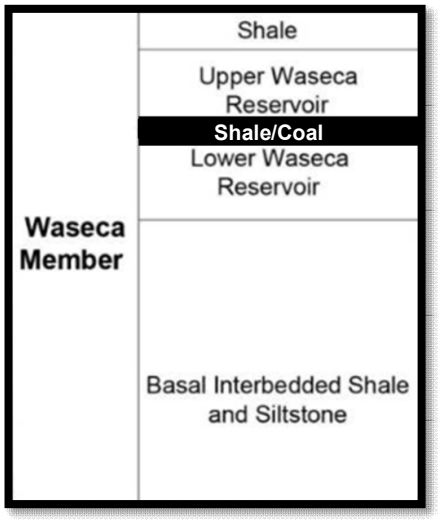

Figure 2.4. Stratigraphic chart of the Waseca member (after Hill, 2017)

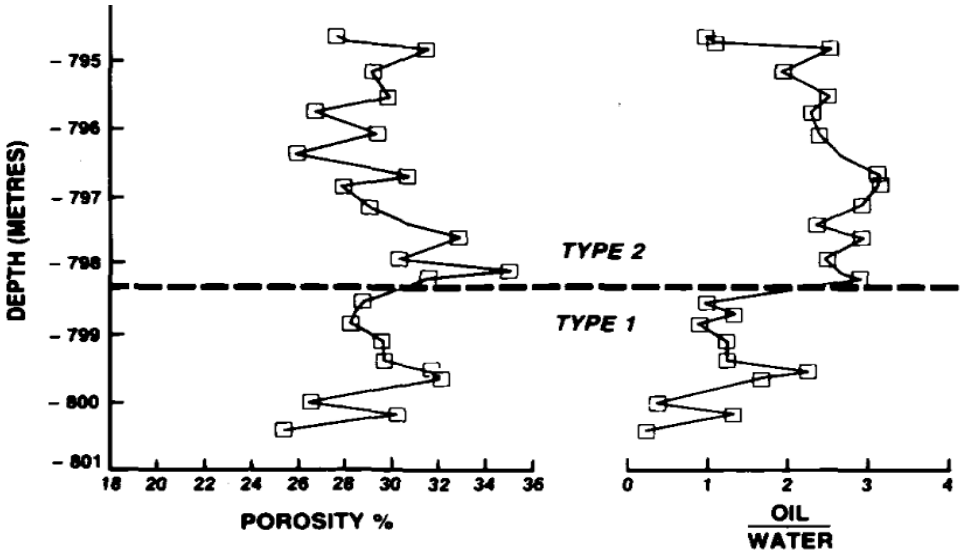

Figure 2.5. Porosity and oil-water ratio vs. depth for core samples of Type 1 and Type 2 sands (Zaitlin & Shultz, 1984)

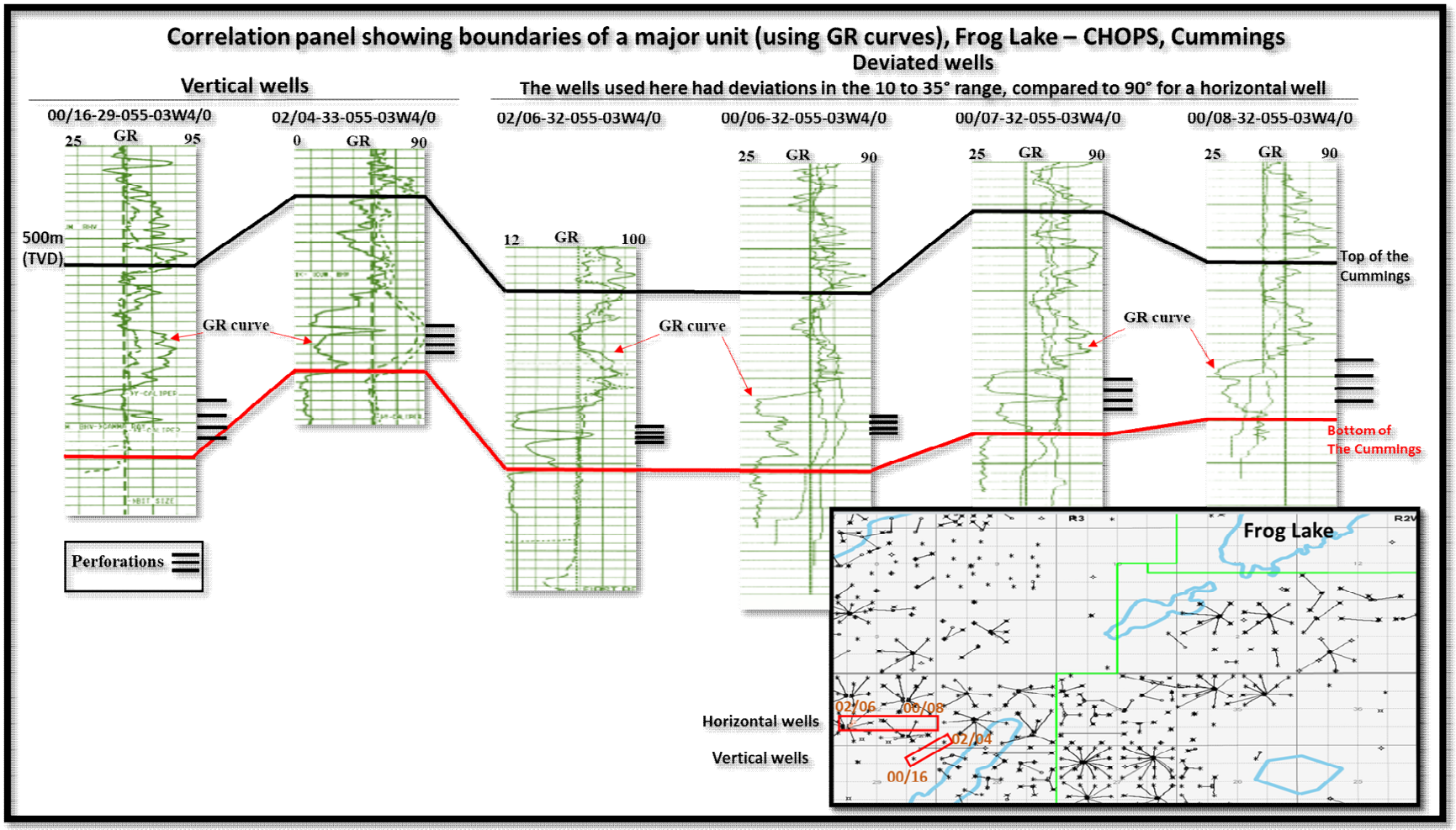

Figure 2.6. Correlation panel showing boundaries of a major unit (using GR curves), Frog Lake – CHOPS, Cummings. These data were compiled by the author from well log data obtained from Accumap. The name of the wells are mentioned above each log. The data for deviated wells are plotted against true vertical depth (TVD).

2.4 Sand Failure Mechanism

The severity and mode of sand failure during oil production depends on several parameters including fluid characteristics (foamy oil behavior, bubble point pressure, capillary tension, viscosity and multi-phase flow), level of pressure drawdown and rate of fluid flow, wellbore completion (openhole or cased hole completion), reservoir pressure, level of anisotropy, rock petrophysical and mechanical properties (permeability, strength, and stress-strain relations) and heterogeneity (Vaziri and Lemoine, 2000). One of the main recognized mechanisms of sand mobilization is seepage-induced failure. If the pore pressure gradient near a wellbore is high, as a result of fluid flow with a steep pressure gradient, the effective stress becomes negative and tensile failure can occur, and/or the drag force of the fluid may overcome the resistance forces of the formation (i.e., friction between sand grains, capillary cohesion strength, or cementation) (Vaziri & Lemoine, 2000). Another recognized mechanism is the change of stress field adjacent to wellbore due to the hydrocarbon withdrawal which causes an increase in shear stress which leads to the formation of a yielded zone. Indeed, the seepage induced failure and the stress redistribution are interrelated where stress changes can cause localized damage to the formation near the wellbore and cause sand mobilization which results in an increase in the porosity which results in increasing fluid rate and further damage to the formation (Risnes et al., 1982; Menzel and Schreiner, 1989; Vardoulakis et al.; 1996). In addition, geological properties of a reservoir can impact the outcome of sand production. For example, the presence of a competent impermeable caprock can resist deflection from the overburden stress and thus leads to a formation of a cavity around the wellbore (Figure 2.7) which causes significant changes to stresses and seepage forces (Vaziri et al., 2001; Penberthy and Shaughnessy, 1992). Also, sand arching is another factor in controlling the sand production. Sand arching is a natural mechanism that may occur outside an opening (perforation), caused by few grains interlocking together supporting a load by resolving external tangential and radial stresses (Tippie and Kohlhaas, 1973; Meza et al., 2010). Sand arching can decrease the permeability of the formation locally close to the wellbore's perforations due to the tight stable packing of sand grains which act as a filter (Bratli and Risnes, 1981). As a result of sand arching, it can negatively impact the CHOPS process by lowering the fluid rate. Then, the fluid flow does not have the capacity to transport sand grains and as a result solid particles accumulation around the wellbore, this may cause a complete shutdown of the wellbore (Economides et al., 1998). Many

studies have been done regarding sand arching and its effect on sand production. These studies suggests that sand arching is dependent on seepage rate (Bratli & Risnes, 1981), fluid viscosity (Cleary et al., 1979), confining stresses (Cleary et al., 1979; Meza and Tremblay, 2002), angularity of sand (Mccormack, 1988; Meza et al., 2010), density of sand (Meza et al., 2010), capillary cohesion strength (Cleary et al., 1979; Miller, 1994; Meza et al., 2010), and size of the perforation (Yim et al., 1994).

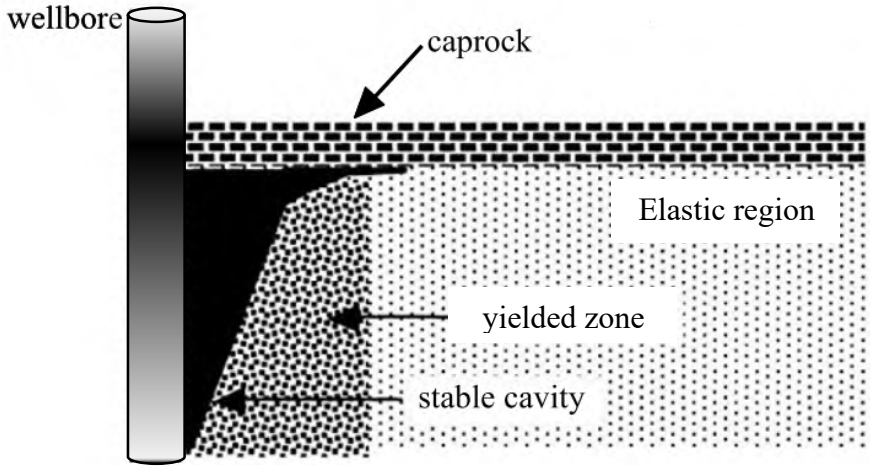

Figure 2.7. The formation of a cavity near the wellbore under the presence of a caprock with high strength which has changed the stress distribution of the formation locally (after Vaziri et al., 2001)

2.5 Field Tests to Investigate CHOPS

To optimize well spacing, operators have performed several tests including tracer injection tests (i.e., dye and radioactive tracers) in formations that have been previously operated under CHOPS to determine the effect of sand production. It has been noted in literature that the tracers' travel time from an injection well to a production well was less than what was expected, considering radial drainage between wells. This led investigators to believe that that some sort of interconnected channels (wormholes) between the injection and production well must exist (Smith, 1988; Squires, 1993; Elkins et al., 1972). The creation of high permeability channels has been observed previously in water-saturated silty clay soil and is referred to as piping failure in geotechnical engineering. However, piping was not ever observed in sand due to the lower cohesive strength of water-saturated sand compared to clay (Wolski, 1965; Townsend et al., 1987).

To assess the geometry of wormholes, Talnishnikh et al. (2015) injected millimeter-sized GPS sensors into the CHOPS wells as shown in Figure 2.8. The results of their study proved the existence of wormholes at least 7 mm in diameter. In addition, they showed that a solid sensor of mm-size can pass through such a porous medium which yielded optimism that sand grain sized GPS sensors can be used in the study of CHOPS if technology can lead to reduced diameter sensor development. Other field tests (Metwally & Solanki, 1995) claimed that as a consequence of CHOPS, a cavity had formed in the immediate vicinity of a production well.

In terms of productivity, allowing oil production in conjunction with the reservoir's sand will enhance the permeability of reservoir which can improve production rate. In Figure 2.9, the data of a heavy oil wellbore is presented which illustrates that the rate of oil production is closely related to the rate of sand production. In May 2008, large sand production rates (approaching 300 m^3/month) occur in conjunction with high oil production rates (roughly 900 m^3/month). However, by February 2011, oil production rate has declined significantly and sand production had become negligible.By July 2011 both oil and sand production ceased (Rangrizshokri, 2015).

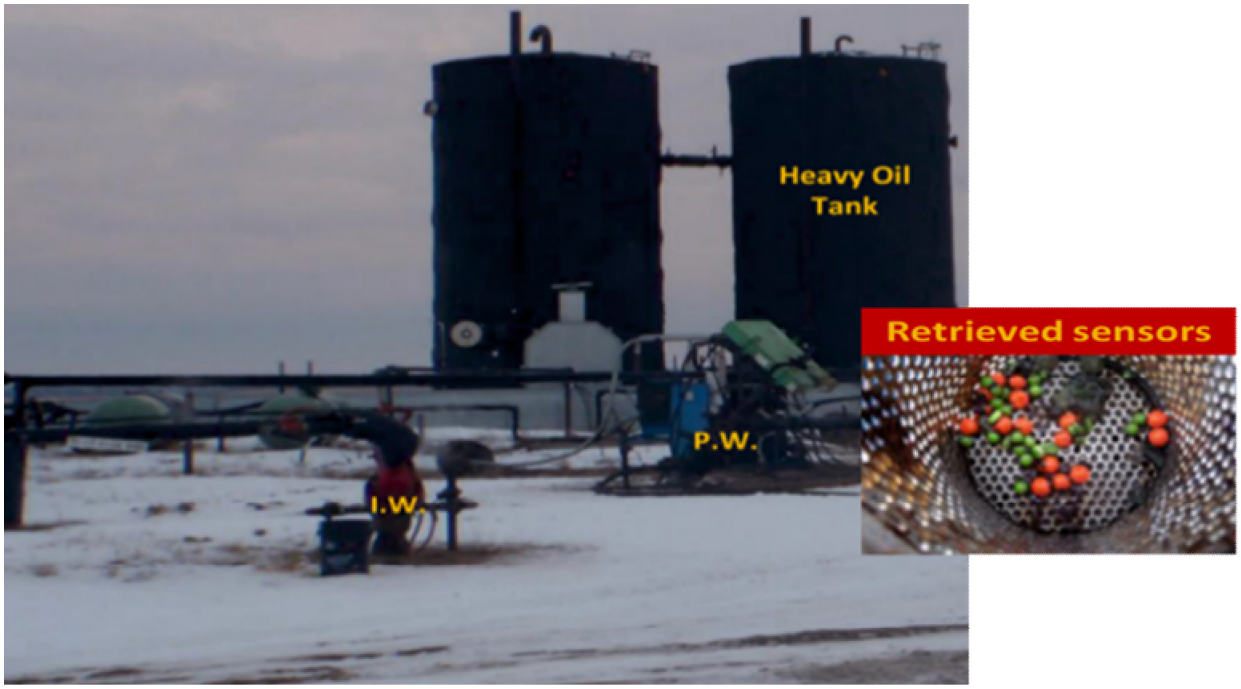

Figure 2.8. Field site with both injection well (I.W.) and production well (P.W.). A few of the retrieved GPS are shown at the right insert (Talnishnikh et al., 2015)

Though field studies would be the most direct and effective method to investigate CHOPS, detailed in-situ studies of high permeability channels or other cavity geometries that might be developed under CHOPS is currently impractical. This is due to the challenges of monitoring in-situ physical properties during CHOPS operations. Since detailed site investigations of the void geometries that might exist within the heavy oil reservoirs are not possible, the following questions remain:

1. What is the geometry of the failed zone?
2. How can this geometry be used to further improve oil production? For example, would the implementation of post-CHOPS enhanced recovery operations involving thermal and/or solvent based processes be successful in improving recovery? Would there be zones within CHOPS reservoirs that should be preferentially avoided (or selected) for injection of solvent or steam during post-CHOPS EOR?

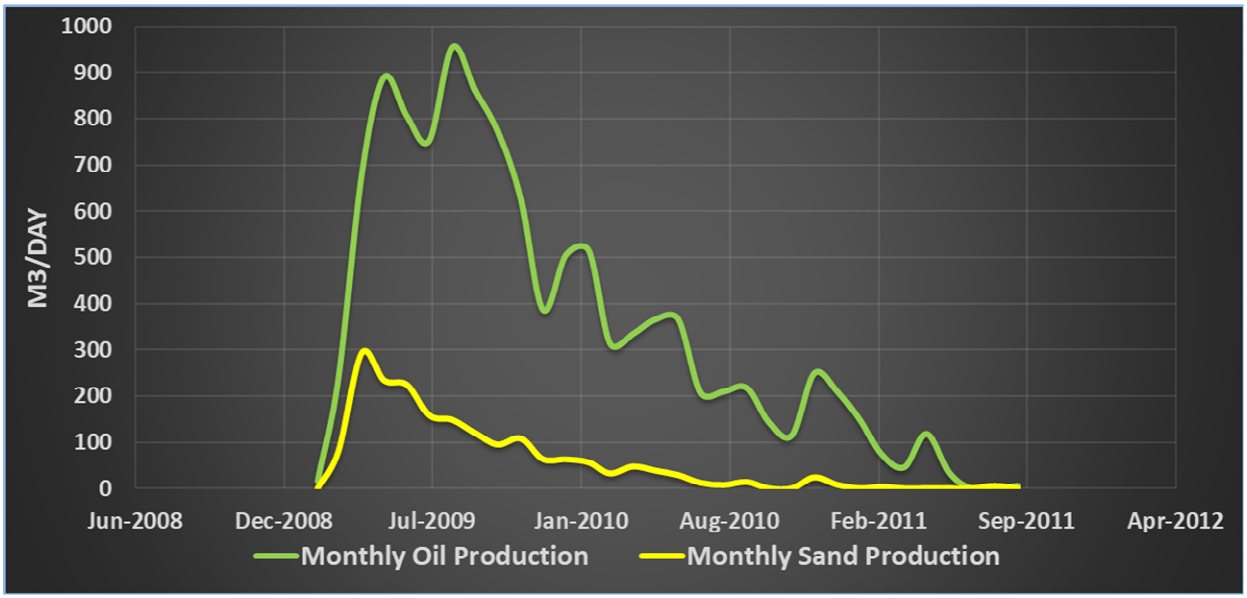

Figure 2.9. Partial production data from a Canadian oil company. The average porosity of the formation was38% with 28% residual water saturation (after Rangrizshokri, 2015).

2.6 Mathematical and Numerical Models to Study CHOPS

Numerical modelling studies have been performed to study the mechanics of wormhole development, including multilateral well simulation to mimic wormholes (Tremblay, 2009), fractal pattern simulation to mimic wormholes as a network rather than an individual pipe (Shokri & Babadagli, 2012), dynamic growth of a wormhole simulation using a dynamic wellbore model (Istchenko & Gates, 2014), and analysis of wormhole regions using flow rate versus time data and other type curves (Xiao & Zhao, 2017). All models mentioned effectively mimicked the wormhole behavior but were based on assumptions that could not be rigorously validated since no data was available to map the length, diameter and tortuosity of in-situ wormholes.

2.7 Laboratory models to study CHOPS

2.7.1 Introduction

Extensive laboratory work has been done to study sand production processes using various types of physical models. Some of this work was quite general in nature, while some was designed to represent CHOPS reservoirs – though always with some degree of simplification and/or approximation compared to field conditions. Various types of void geometries have been observed in these experiments, as discussed in the following sub-sections

2.7.2 Sand Arches

Terzaghi (1936) conducted a trap door experiment used a container full of sand with a hole at the bottom. When he opened the hole, sand was produced initially because of gravity, and after some time it stopped. He concluded that the sand flow stopped due to the sand arching which prevented further sand production. Likewise, Bratli and Risnes (1981) studied the sand arching in a container full of sand saturated with water. Before the experiment, excess water was drained to a non-drainable level. They also, simulated the overburden stress using a vertical load supplied by a piston. They used air as the producing fluid in their sandpack. They steadily increased the flowrate until an amount of sand was produced (Figure 2.10). Then, they increased the flowrate further until a new amount of sand was failed and this cycle was repeated several times. They concluded that the sand was produced when the sand arch was failed, and a cavity formed by sand arches is only stable at a certain range of seepage. They also concluded that the sand failure occurred under two failure mechanism. Shear failure because of field stress redistribution and tensile failure as a result of seepage force. Tronvoll et al. (1997) argued that the sand failure was due to the field stress redistribution rather than by seepage. To show this they manufactured weakly cemented sandstone using sand, sodium silicate and water hardened with carbon dioxide. They concluded that sand production is caused by shear failure because of filed stress redistribution and that the seepage only escalates the failure and transport.

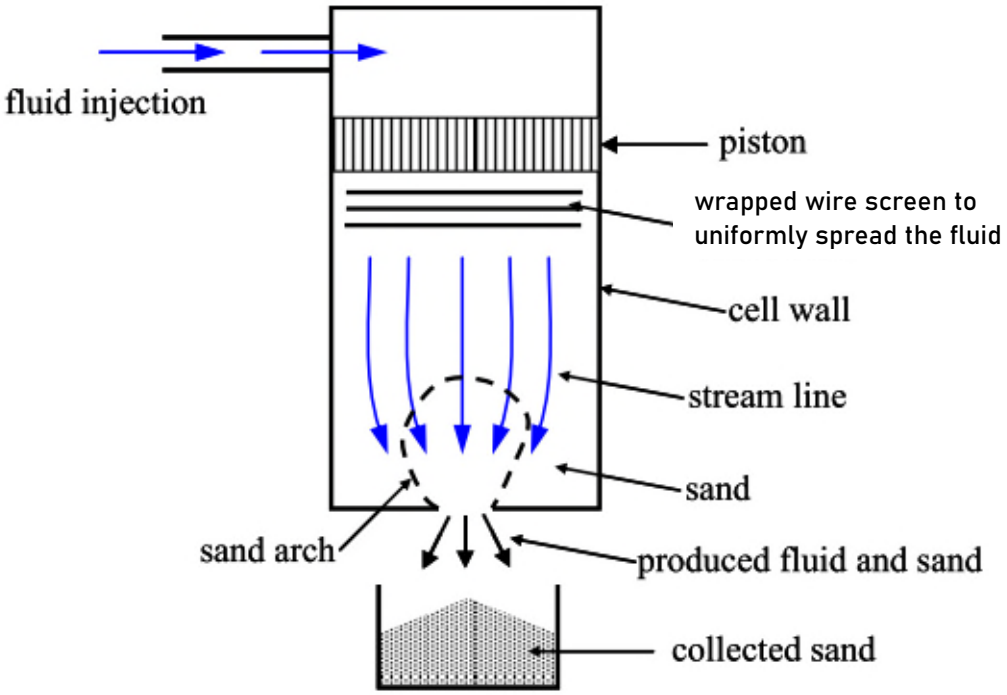

Figure 2.10. Bratli and Risnes (1981)'s experimental model

2.7.3 Wormholes and Cavities

Tremblay & Oldakowski (2003) used a horizontal cell to study sand failure. One end of the cell was perforated, and it was filled with sand, as shown in Figure 2.11. They saturated the sand with live heavy oil (i.e., crude oil containing dissolved natural gas), and they generated initial stresses by compacting the sand within the cell. The fluid pressure was then decreased at the perforation, and as a result a wormhole developed with tensile failure bands at the tip and perimeter of the wormhole. The pressure gradient within the sand pack caused the sand in the matrix to be dislodged and to be transported within the wormhole. They concluded that sand failure occurred preferentially at the tip of the wormhole rather than the perimeter because of the higher fluid velocity and pressure gradient at the tip. This experimental setup highlighted the effect of different flow regimes to wormhole creation, as shown in Figure 2.12.

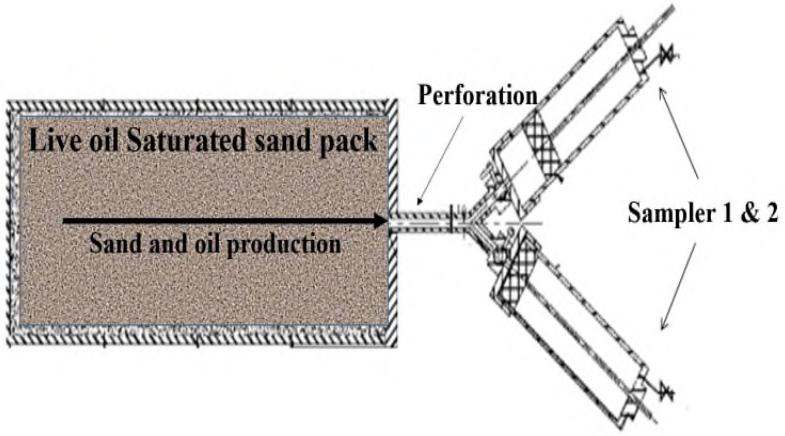

Figure 2.11. Cross section of Tremblay's physical model to study CHOPS (after Tremblay & Oldakowski, 2003)

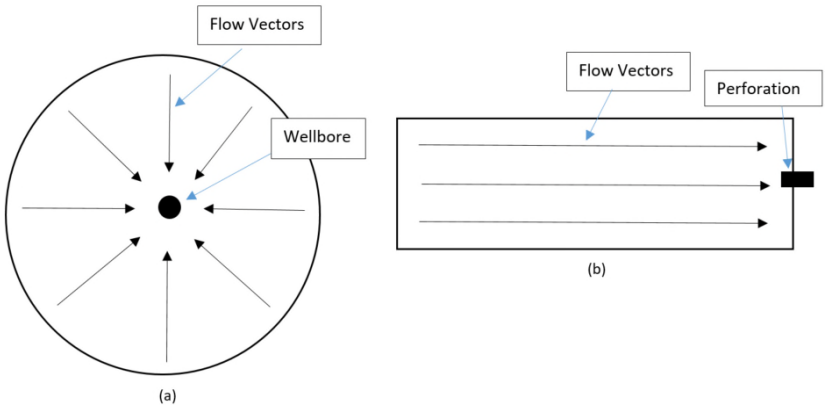

Figure 2.12. Flow regimes relevant to experimental work: (a) A cylindrical cell with radial flow into a perforation; (b) A cylindrical cell with linear flow into a wellbore (Pereira, 2021)

Experiments similar to Tremblay & Oldakowski (2003) were performed by Wong (2003) but using a triaxial cell with a perforation at the base of the cell. He reported that sand production initiates when pressure at the perforation reduces below the fluid saturation (bubble point) pressure which causes gas to exsolve. This results in a steep pressure gradient, which as described by Geilikman & Dusseault (1999), can create tensile failure. However, similar to the aforenoted experiments, their laboratory set-up only allowed for linear flow.

The effect of anisotropic horizontal stresses was studied by Oldakowski & Sawatzky (2018) using a custom built polyaxial cell. In their first five tests, they filled a polyaxial cell with a pre-saturated sand with silicone oil, and with heavy oil in their last four tests. They noticed that the wormholes' growth was in the direction of the minimum horizontal stresses. However, in spite of this observation, they concluded that the wormholes could behave independent of minimum horizontal stresses if a high fluid flux develops in the porous medium, i.e., in such a case, wormholes would tend to form in the same direction as the flux.

A beam geotechnical centrifuge was used by Vaziri et al. (1998; 2000; 2003) to study sand failure. This study stands out among other laboratory set-ups since they studied CHOPS in a scaled representation of a reservoir under hyper gravity conditions using a geotechnical centrifuge. As described in (Vaziri & Lemoine, 2000), canola oil was chosen as the pore fluid to facilitate saturating the sand prior to the test (does not require heating to lower its viscosity) . The structure of their model was a cylindrical tub with a wellbore placed in the center of the set-up to allow production. The overburden pressure during flight (centrifuge rotation) was supplied by a steel plate on top of the sand layer. A cross section of their physical model for one test is shown in

Figure 2.13. In their experiments they always observed a conical cavity; in tests that used a wellbore with three perforations at the bottom (rather than a multi perforated wellbore), they additionally observed an erosion channel that was formed at the edge of the cavity and grew radially outwards along the sand-caprock interface. These void geometries allowed for more sand production and resulted in subsidence under the caprock. The sand production noticed by Vaziri & Lemoine (2000) was not located near the perforations which was different from other works (Diaz et al., 2008, 2010, 2012; Tremblay et al., 1997, 1998; Wong, 2003). Rather, a void developed preferentially in sand zones immediately underlying the caprock. This observation is consistent with unpublished and anecdotal accounts from at least one operator suggesting that enhanced porosity/permeability zones tend to develop preferentially beneath the caprock during field operations (personal communication with Jerry Shaw of Devon Energy, January 2017). It is also consistent with field observations from the Burnt Lake Project (cold flow production of bitumen in the Cold Lake oil sands deposits in northeastern Alberta), as interpreted by Vaziri et al. (2003).

Results for one the Vaziri and Lemoine's experiment is shown in Figure 2.14. The cavity, which was formed prior to the surface erosion channel, had a narrow diameter near the perforations (at the bottom of the wellbore) and a large diameter towards the steel plate (at the top of the wellbore). Based on the series of test performed by Vaziri and Lemoine, they concluded that if a wellbore with multi perforations was used during the experiment, this would cause formation of a smaller cavity comparing to a wellbore with perforations only at its bottom, thus resulting in less sand production and subsidence. Also, in one of their tests they placed a kaolin clay stringer in the middle of the pay zone (sand) to study the effect of heterogeneity (sand-shale layering) on sand failure. They found that the clay layer stopped the cavity growth (Figure 2.15) and concluded that the mechanism governed the erosion of sand in all experiments was due to the seepage-induced failure.

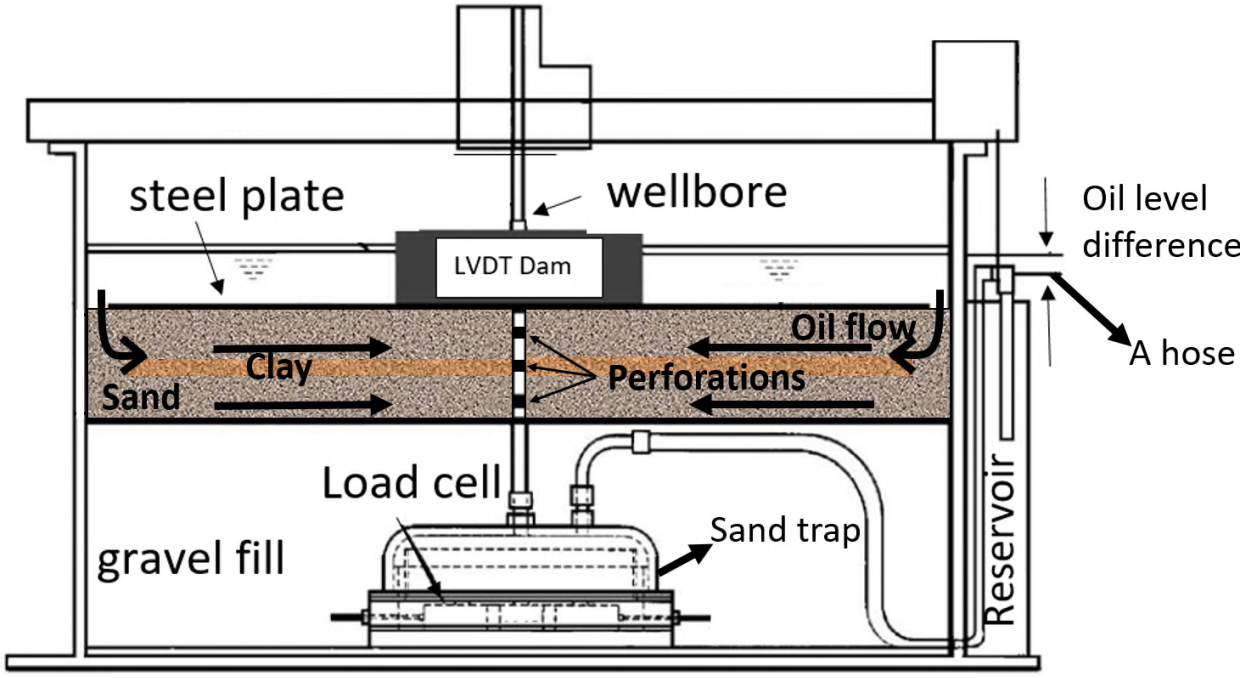

Figure 2.13. A cross section of Vaziri's physical model that was used in a geotechnical centrifuge (after Vaziri et al. 2003)

Figure 2.14. One of the test results of Vaziri et al. (2000), in which the wellbore was only perforated near the bottom of the sandpack. A cavity formed around the wellbore under the caprock, and a surface erosion channel developed at the edge of the cavity.

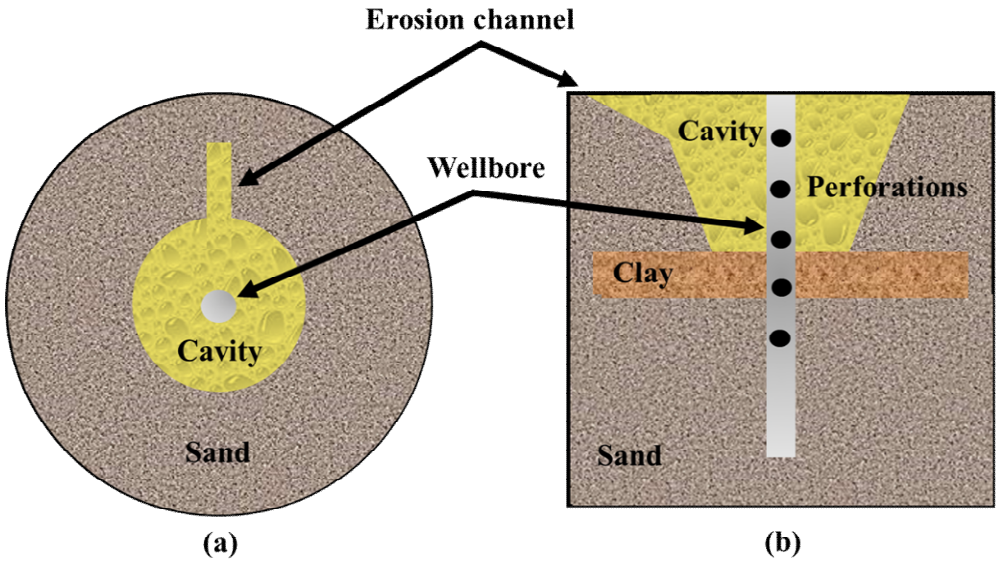

Figure 2.15. Schematic result of Vaziri & Lemoine (2000)'s experiment (TUNS 20) which shows a development of a cavity in the vicinity of a wellbore and an erosion channel in the sand matrix: (a) Plan view; and (b) Cross sectional view. Neither of these drawings are drawn to scale.

Similar to Vaziri's work, Choi (2011) observed cavities and surface erosion channels in his experiments using an uncemented sand reservoir. The differences with Choi's experiments, compared to Vaziri's experiments, were that the tests were done at 1×gwithout using a geotechnical centrifuge. This allowed him to observe surface events through a clear polycarbonate sheet representing a caprock that he placed on top of his sandpack. Also, doing experiments at 1×g gave him the flexibility to tilt his physical model. The schematic view of his physical model is shown in Figure 2.16. He noticed that by tilting his physical model at 7° and 15°, the surface erosional channels formed in the direction of the slope which, shows the significant role of gravity in the direction of sand production (Figure 2.17).

As shown, many experiments under laboratory conditions have been performed and several different geometries have been proposed. However, it is still unknown which geometry will form under which conditions in field applications. Therefore, to provide a better understanding of sand failure and the mechanisms that it relies on, integration of more representative heterogeneity, anisotropic stresses, and fluid properties in experimental tests are required.

Small physical models that were used by most of the researchers had the disadvantage of capturing data regarding the formed voids only at a perforation and near the wellbore. By comparison, laboratory testing in a centrifuge can capture useful information regarding voids at sizes similar to the scale of field operations when accounting for the centrifuge scaling factor, which is discussed in the following section.

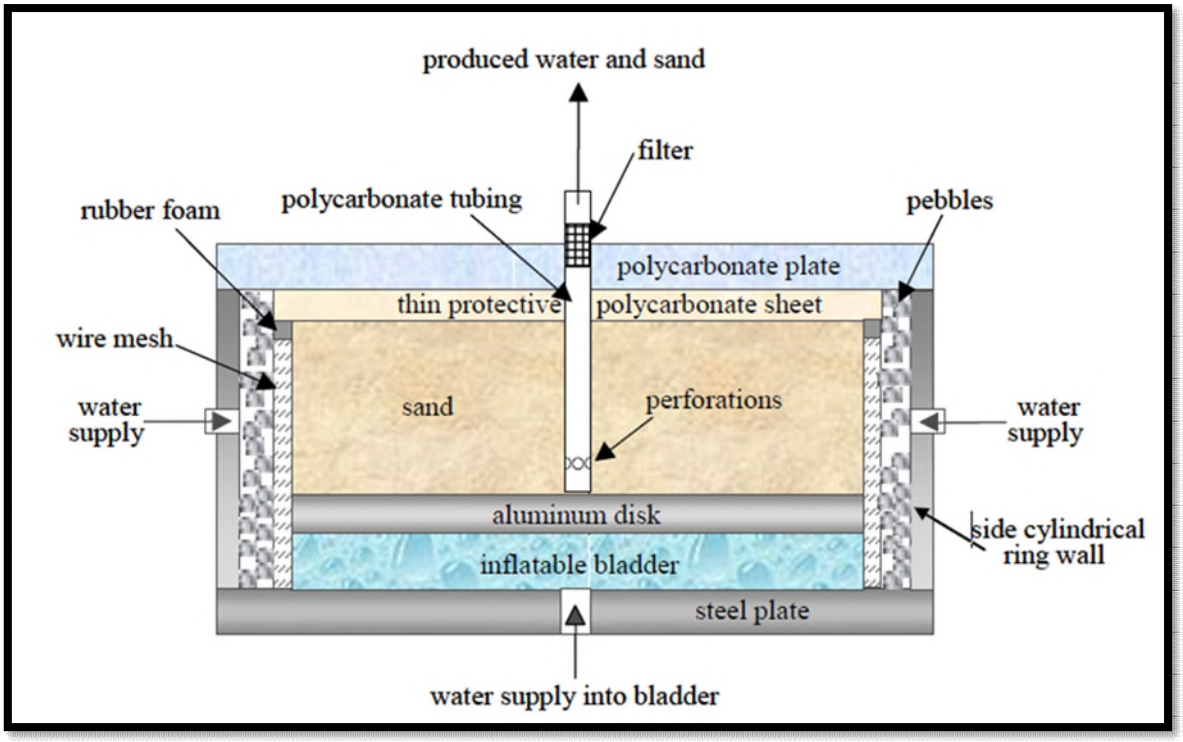

Figure 2.16. A schematic cross section of the physical model used by Choi (2011). The reservoir was under a pressure of 34.5 KPa in all tests, supplied by the inflatable bladder located below the reservoir. Instead of canola oil, Choi used water as the pore fluid. The water was introduced to the system from the edges of the reservoir.

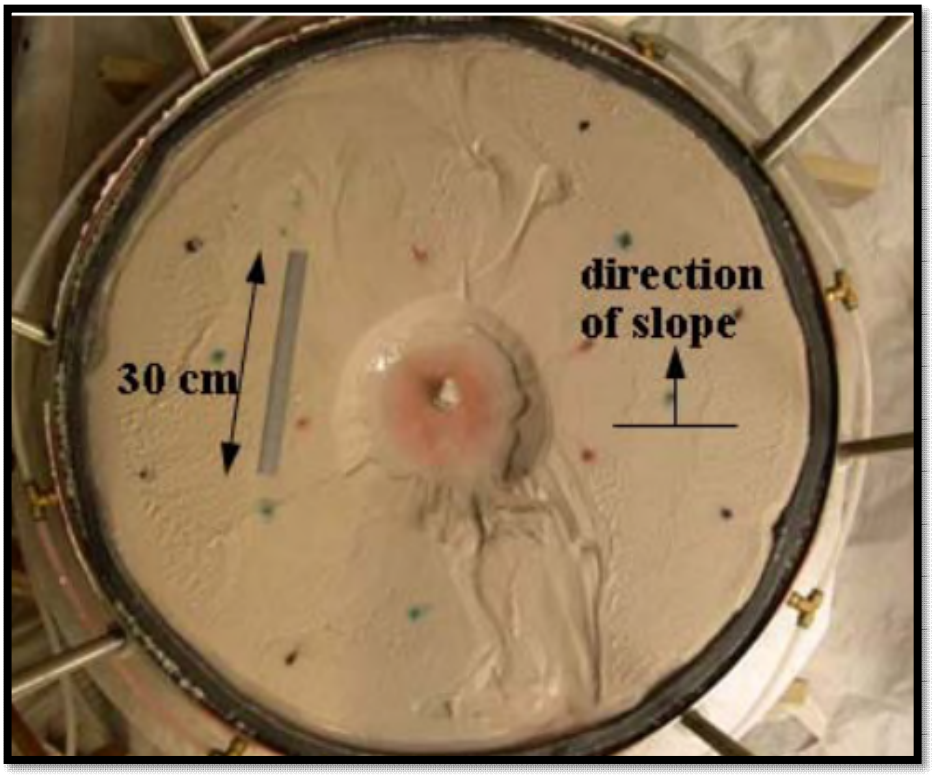

Figure 2.17. Example of post-test results obtained by Choi (2011).

2.8 Principles of Geotechnical Centrifuge

The principles of centrifuge testing relevant to CHOPS simulation are summarized in this section based on the text book by Madabhushi (2014).

2.8.1 Scaling Factor

Since it is not possible to design a test in a laboratory which is directly representative of the scale of a heavy oil reservoir, a geotechnical centrifuge is a useful tool because the test prototype is actually a scaled down version of the reservoir by a factor of N. N is the scaling factor and represents the enhanced gravity field relative to the normal earth's gravity field (1 g = 9.81 m/s^2). Some of the important parameters which can be affected by the scaling factor for a fully-saturated porous medium are shown in Table 2.2.

Table 2.2. Scaling factors (Madabhushi, 2014)

Parameter	Scaling Law (model/prototype)	Units
Length	1/N	m
Area	$1/N^2$	m^2
Volume	$1/N^3$	m^3
Mass	$1/N^3$	$N \times m^{-1}s^2$
Stress	1	$N \times m^{-2}$
Strain	1	-
Porosity	1	-
Acceleration (g)	N	$m \times s^{-2}$

2.8.2 Swing-up Effect

As the centrifuge begins to turn, the swing platform spins around a pivot until it achieves a sub-horizontal orientation as shown in Figure 2.18. The "swing-up" is a function of the radius of the centrifuge and the weight of the centrifugal model which sits on the basket at the end of the arm. It is worth mentioning that the centrifugal acceleration will act normal to the base of the test cell. Also, it should be noted that earth's gravity (1×g) still continues to act on the tub, perpendicular to the centrifugal acceleration, but it has a minor effect on the test results.

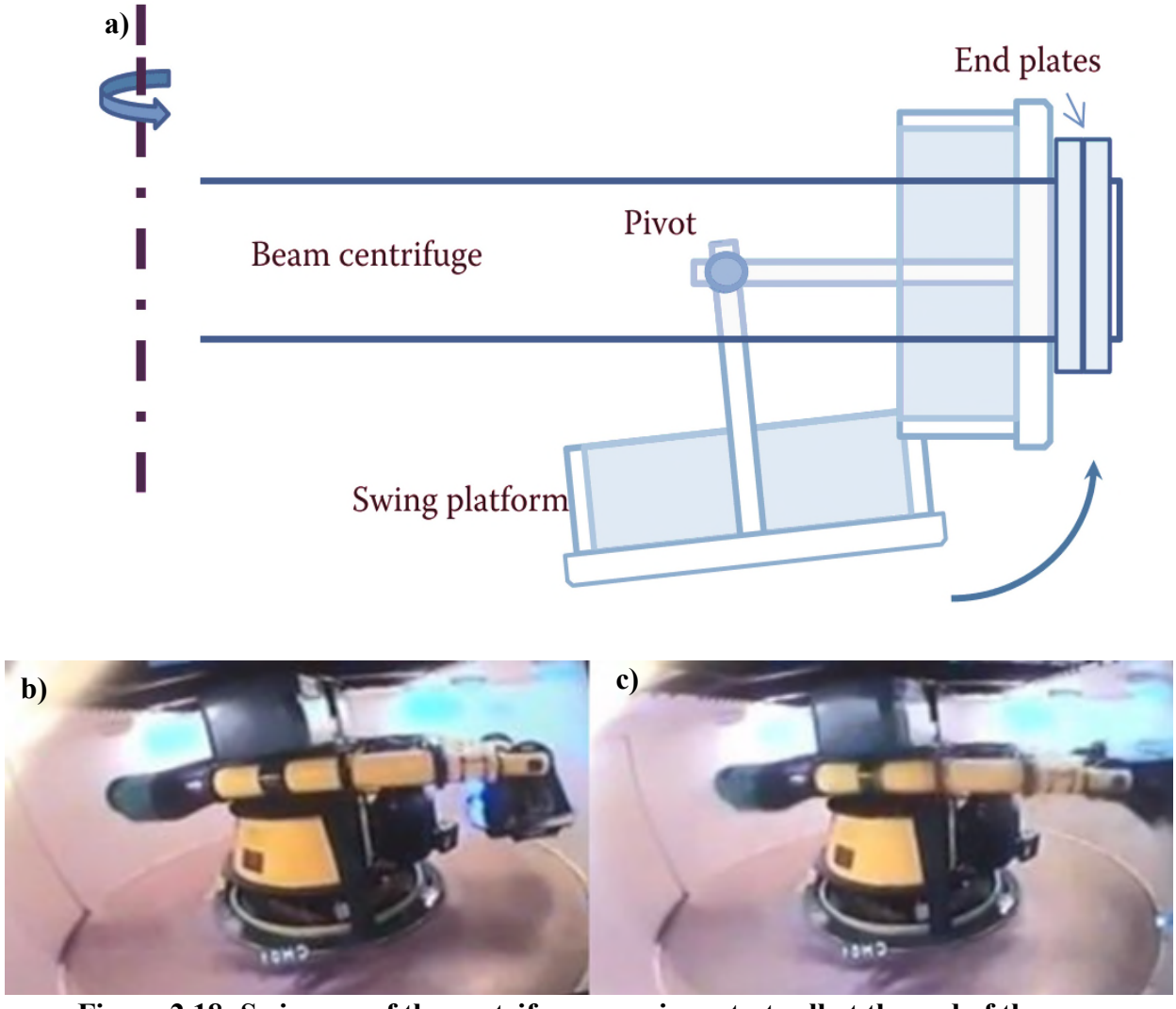

Figure 2.18. Swing-up of the centrifuge carrying a test cell at the end of the arm (Madabhushi, 2014); (a) Schematic view of swing-up; (b) Centrifuge before the flight; and (c) Centrifuge during flight and swing-up. Photo b and c have been taken during one of the centrifuges CHOPS experiments at the University of Alberta's GeoCERF facility, which is discussed in Chapter 3.

2.8.3 Stress and Strain Effects

According to Madabhushi (2014), considering a block structure of mass M with dimensions of a × b × c (see Figure 2.19.a), the vertical stress exerted to the plane below the block can be calculated as:

$$\sigma_v = \frac{M \times g}{b \times c} \tag{2.1}$$

Where:

σ_v is the vertical stress (N/m^2);

M is the mass of the prototype (kg);

g is the earth's gravity (9.81 m/s^2);

b is the length of the block (m);

c is the width of the block (m);

Likewise, the vertical strain ε imposed in the soil for a characteristic length α is:

$$\varepsilon = \frac{\delta\alpha}{\alpha} \tag{2.2}$$

Where:

ε is the vertical strain in the soil below the model;

α is a characteristic length in the soil below the model;

$\delta\alpha$ is a change in the characteristic length resulting from compression;

As per Table **2.2**, the size of the experimental block must be scaled down as compared to the original block by N in dimension and N^3 in mass (Figure 2.19.b). If this scaled block which is representative of what would be used in a centrifuge model is placed in an enhanced gravity field of N × earth's gravity (1g), the vertical stress exerted on the plane below the centrifuge model can be recalculated as:

$$\sigma_v = \frac{{}^{M}/_{N^3} \times N \times g}{{}^{b}/_{N} \times {}^{c}/_{N}} = \frac{M \times g}{b \times c} \tag{2.3}$$

Thus, the vertical stress in the centrifuge model is the same as the prototype considered in Equation 2.1. Also, the calculation of strain for the centrifuge model is as follows:

$$\varepsilon = \frac{{}^{\delta\alpha}/_{N}}{{}^{\alpha}/_{N}} = \frac{\delta\alpha}{\alpha} \tag{2.4}$$

As such, the prototype strain in Equation 2.2 is the same as the strain in the scaled block. Thus, the centrifuge model behaves mechanically in the same manner as the prototype in a N×g environment because of centrifugal acceleration.

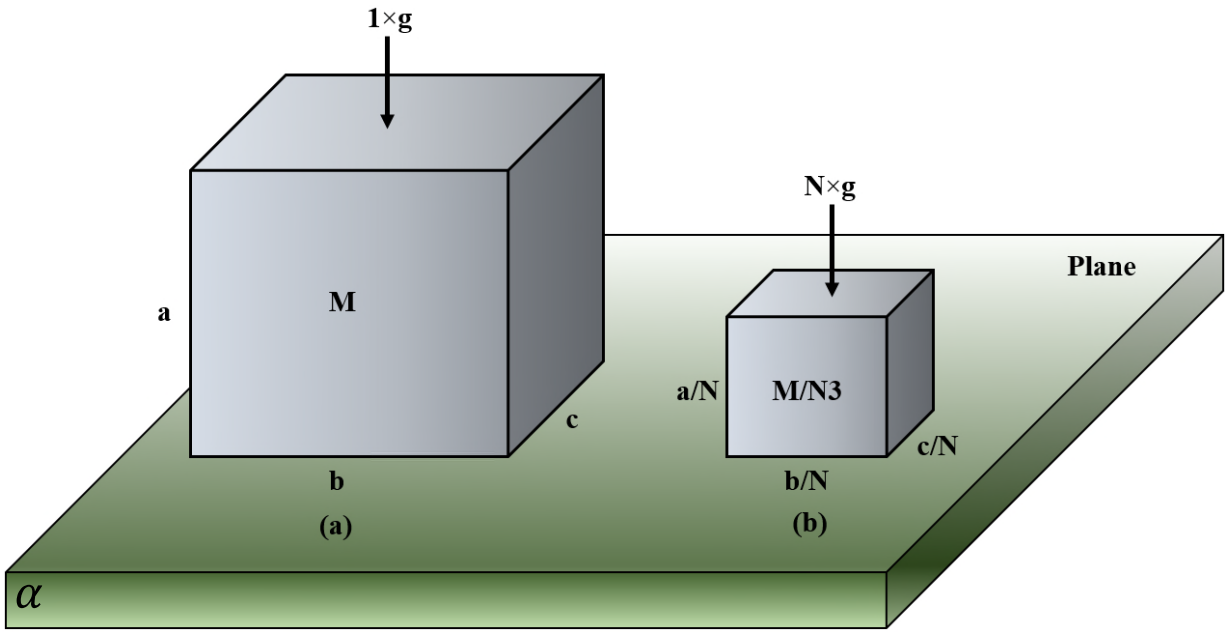

Figure 2.19. Principle of centrifuge modelling; (a) Prototype at 1×g; (b) Model ccaled down by a factor of N

2.8.4 Inertial Acceleration Field

To reach the required "g" level, angular velocity $\left(\dot{\theta^2}\right)$ needs to be set. The centrifugal acceleration at an axis of rotation of radius (r) is given by:

$$\bar{a} = r\ \dot{\theta^2} \tag{2.5}$$

Where:

$\bar{a}$ is the centrifugal acceleration ($m \times rad^2/sec^2$);

r is the length of the beam's arm (m);

$\dot{\theta}$ is the rotational speed (rad/sec);

Using the same scaling factor (N) that was used to scale down the prototype, then:

$$N \times g = r\ \times \dot{\theta^2} \tag{2.6}$$

Since the radius of a centrifuge is constant and plays a role in determining the scaling factor, and the physical model has a height which is embedded in the radius of the centrifuge, the scaling factor at different heights of the physical model is different. According to Taylor (2018), this results in a variation through the model that does not exist in the prototype, but this variation is relatively small. This depth-wise variation in scaling factor is explored using the following calculation, based on points r_1, r_2 and r_3 of a physical model which is shown in Figure 2.20. In this calculation, an angular velocity of 111 rpm or 11.6 rad/s is assumed. Using equation 2.6:

- The scaling factor at point r_1 is calculated as 22.8
- The scaling factor at point r_2 is calculated as 24.8
- The scaling factor at point r_3 is calculated as 27.4

Seeing the results of calculation for the three points, it is evident that in centrifuge modelling, the scaling factor is not constant and is dependent on the radius of the beam's arm. As such, the question arises as to which value should be used when assigning a constant scaling factor to a given experiment. So, the question is on which point should, the scaling factor be set? Rewriting equation 2.6 for any given coordinates:

$$N = \frac{r \times \dot{\theta}^2}{g} \tag{2.7}$$

Where:

r is any given point on the X-axis (m);

Considering equation 2.7, the vertical stress gradient in the physical model is non-linear compared to the prototype due to the hyper gravity environment. This issue cannot be avoided, but to reduce the stress profile error to ±3%, the scaling factor should be selected at two thirds of the centrifugal model's depth (Taylor, 2018).

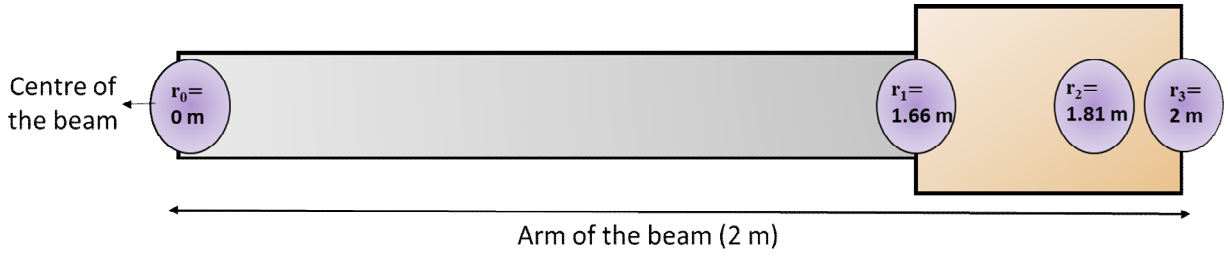

Figure 2.20. The schematic cross section of a beam and the physical model during flight as shown in Figure 2.18. The coordinates shown specify the position of points a, b, c and d in metres.

2.8.5 Particle Size Effect

Western Canadian heavy oil reservoirs generally have sand grain sizes between 100 and 250 μm (Tremblay and Sedgwick, 1999). For modelling a prototype with grain sizes in this range at 25 g hyper gravity, scaling laws would suggest particle sizes of 4 to 10 μm. This corresponds to fine silt. However, this would be erroneous because the constitutive behaviour and water retention properties of a silt are different from a sand (Madabhushi, 2014). However, Kutter (1992) proposed that by using actual particle sizes representative of heavy oil reservoir in the physical model, intergranular forces would remain the same as reservoir conditions. Madabhushi (2014), also suggested that actual reservoir particle dimensions can be used in the physical model only if the size of critical structural elements (e.g., wellbore perforations) in the physical model are large relative to the particle sizes. In essence, experiments conducted in a geotechnical centrifuge are generally designed to change the stresses and pressures, but not particle sizes.

2.9 Capillarity-Induced Strength

In weakly-cemented or uncemented porous media, the capillary forces resulting from multi-phase saturations may have a notable effect on sand failure and mobilization (Vaziri et al., 2002; Islam and george, 1989). Considering a water-wet sandpack saturated with water and oil, the wetting phase (water) is preferentially attracted to the sand grain surfaces and tends to bind those grains together. Han & Dusseault (2002) reported a model for estimating capillary forces in a sand comprised of uniformly sized spherical grains (see Figure 2.21). These capillary forces are a result of the pressure difference across the free surface formed between the water (wetting phase) and oil (non-wetting phase). The capillary bond force can be written as:

$$F_C^o = \pi(R \times \sin\alpha)^2 \, \Delta P \tag{2.7}$$

Where:

F_C^o is the capillary bond force resulting from capillary pressure (N);

R is the radius of sand grains (m);

α is the volume angle of wetting fluid (rad);

ΔP is the pressure difference between two fluids (Pa);

Lazzer et al. (1999) state that another surface tension force acting on the interface along the contact line is:

$$F_s = 2\pi \times x_p \times \gamma \times \sin(\alpha + \theta) \quad (2.8)$$

Where:

F_s is the capillary bond force resulting from surface tension (N);

x_p is the coordinate of point p;

γ is the surface tension between the two fluids;

θ is the contact angle.

Therefore, the cohesion force will be the sum of the two capillary bond forces in equations 2.7 and 2.8:

$$F_c = |F_C^o| + F_s \quad (2.9)$$

Where:

F_c is the capillary cohesion force (N).

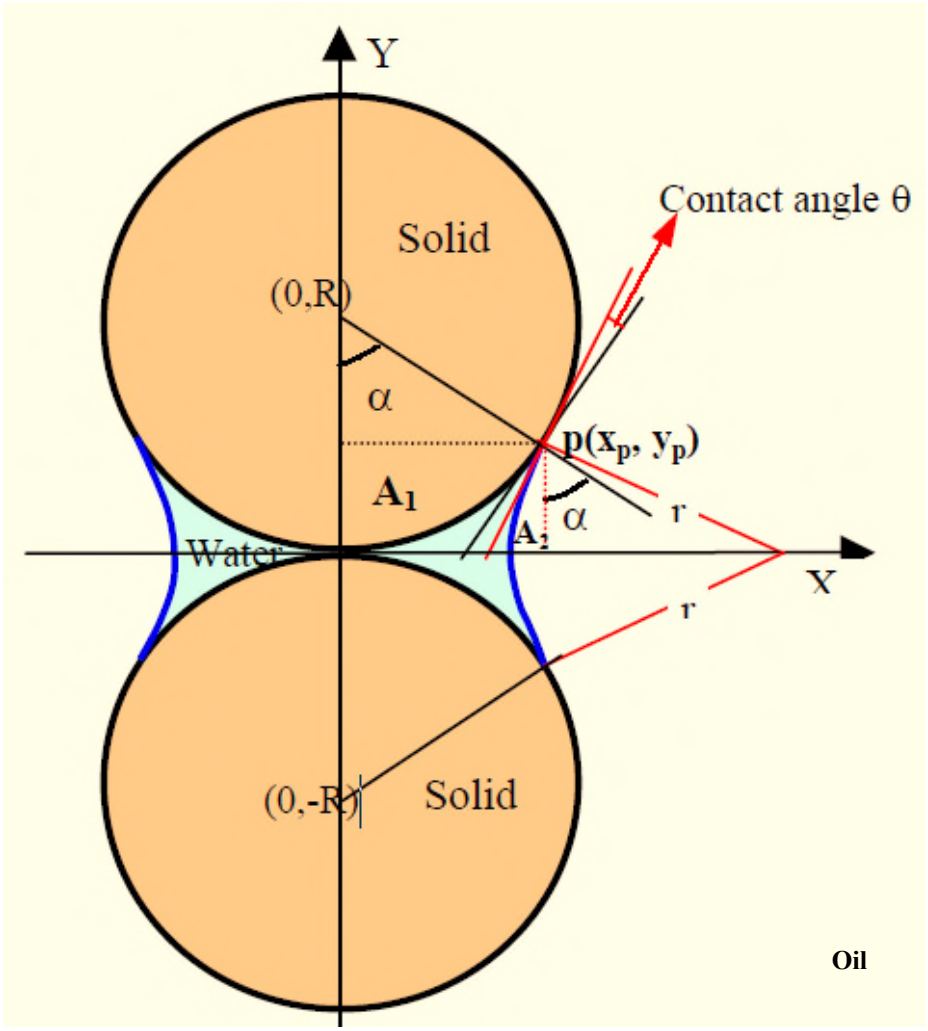

Figure 2.21. A proposed model for uniform grains in tangential contact (after Han & Dusseault, 2002)

2.9.1 Capillary Cohesive Force and Apparent Strength Relations

Schubert (1984) reported that in particulate mechanics, tensile strength (σ_T) at the macroscopic scale can be related to capillary cohesive force (Fc) based on geometrical considerations:

$$\sigma_T = \frac{1-\varphi}{\varphi}\frac{F_c}{R^2} \tag{2.10}$$

Where:

σ_T is tensile strength of the particulate medium (Pa);

φ is the porosity;

F_c is the capillary cohesive force (N);

R is the average grain radius (m).

Also, assuming a linear Mohr-Coulomb failure criterion with no tensile strength cut-off (see Figure 2.22), unconfined compressive strength (UCS) is related to tensile strength as follows:

$$\sigma_{UCS} = 2\sigma_T \frac{\sin\phi}{1-\sin\phi} \tag{2.11}$$

Where:

σ_{UCS} is Uniaxial Compressive Strength (Pa);

ϕ is the friction angle.

Therefore, combining the Equation 2.10 and 2.11:

$$\sigma_{UCS} = 2\frac{1-\varphi}{\varphi}\frac{\sin\phi}{1-\sin\phi}\frac{F_c}{R^2} \tag{2.12}$$

These equations, in combination with the capillary force equations presented in the previous section, make it possible to estimate the effect of two-phase saturations on the apparent cohesion of an uncemented sand as follows:

$$C = \frac{\sigma_{UCS\times}(1-\sin\phi)}{2\times\cos\phi} \tag{2.13}$$

Where C is the apparent cohesion resulting from capillary forces (Pa).

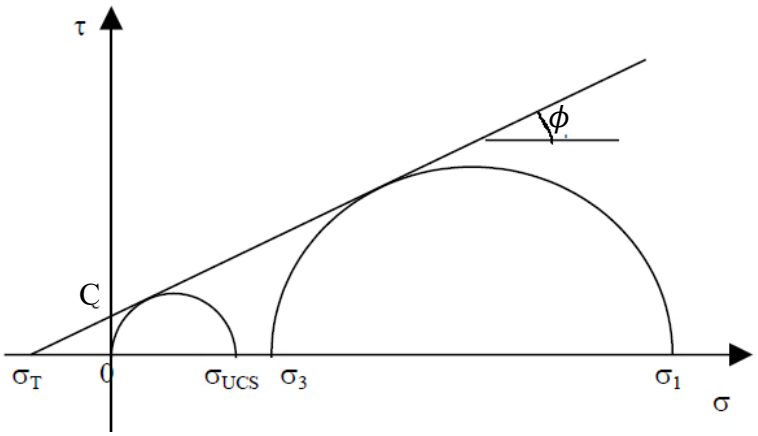

Figure 2.22. Linear Mohr-Coulomb failure criterion. For cemented rocks, it is more common to assume a tensile strength cut-off. However, this work assumes an uncemented sand with all cohesive and tensile strength derived from capillary forces, hence the criterion is extrapolated linearly into the tensile stress regime.

2.9.2 Radius of the Yielded Zone Around a Perforation

Bratli & Risnes (1981) proposed an ideal representation of the sand geometry around a perforation (Figure 2.23) which consists of two hemispherical shells in which the inner radius of the shell represents the perforation size, and the outer radius of the spherical shell represents the size of the reservoir. This model can be used to assess the size of the hemispherical yielded zone that may develop around the perforation, depending on the strength of the sand relative to the stresses around the perforation. For estimation of the yielded zone radius for a given flow rate Q, they introduced Equation 2.14, as follows:

$$\left(\frac{Rc}{R1}\right)^{T} = \frac{3\,\frac{T+1}{T+3}\,(P_0 - P_1)}{\frac{T+1}{T}\,4\,C\,\tan\alpha - Qc} \tag{2.14}$$

$$T = 2\,(tan^2\theta - 1) \tag{2.15}$$

$$\theta = \left(\frac{\pi}{4}\right) + \left(\frac{\phi}{2}\right) \tag{2.16}$$

Where:

R_c is the radius of the yielded zone;

R_1 is the radius of the perforation;

P_0 is the average in-situ stress magnitude;

P_1 is the pore pressure at the perforation surface;

ϕ is the friction angle;

C is the cohesion (e.g., derived from Equation 2.13, in the case of an uncemented medium with apparent cohesion due to capillary forces);

T and θ are parameters that depend on friction angle

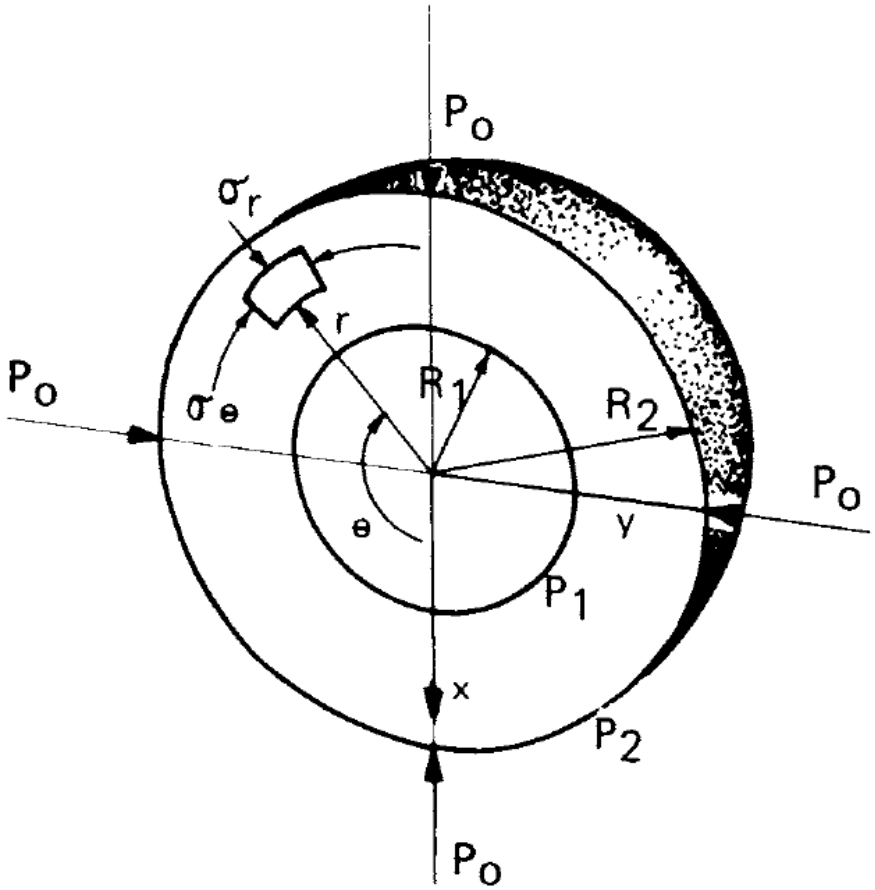

Figure 2.23. Idealized model of sand around a perforation as two hemispherical shells. R1 represents the radius of the perforation and R2 represents the outer radius the reservoir (Bratli & Risnes, 1981).

3 MATERIAL AND TESTING METHODS

3.1 Introduction

This chapter describes the materials and experimental methods used in this study. An array of tests was performed using a purpose-built physical model to study how different parameters affect sanding during CHOPS and,in some cases, to refine and improve the testing methods.

The physical model and initial testing procedures were developed by Pereira (2021), whose work represented the first phase of a longer-term study of CHOPS using a geotechnical centrifuge. Some of the technical details pertaining to different parts of the physical model are discussed in this chapter, but more detailed information can be found in Pereira (2021). Five experiments were reported by Pereira. The last two tests reported by Pereira (2021) correspond to the first two tests reported in this thesis. The focus of these tests, as presented by Pereira (2021), was primarily oriented towards testing and troubleshooting the apparatus (e.g., testing a new wellbore actuator and assessing the functionality of load cells), and the development of testing procedures. The focus of these tests, as presented in this thesis, is on interpretation of the physical significance of the results.New tests reported in this thesis provide additional context to Pereira's work.

The first test reported in this thesis was a validation test (V1 test) which was similar (but not identical) to Vaziri's work (2000; 2003). The next 5 tests involved variations of the materials (sand versus sand and gravel), the type of caprock (simulating with clay instead of steel), and pre-saturating the reservoir with both water and oil. In Table 3.1, the identification of each test is presented including the main objectives of each test.

Table 3.1. Test identification and main changes in each test

Test #	Test ID	Objective
1	V1	Validation test using a dense sandpack
2	G2	Incorporate gravel around sandpack
3	C3	Use synthetic caprock instead of steel plate
4	W4-a	Pre-structuration of sandpack with 2 phases (tap water and canola oil)
5	W4-b	Same as W4-a but with more water drainage
6	W4-c	Repeat of W4-b with proper sealing of load cells

Details pertaining to the six tests included in this thesis are discussed in this chapter. Sections 3.1 to 3.4 provide general descriptions of the testing apparatus, Section 3.5.1 discusses test preparation and assembly procedures for the tests, Section 3.5.2 discusses the general operational procedures during the tests, and Section 2.5.3 discusses the operational procedures used after the tests.

3.2 Geotechnical Centrifuge Experimental Research Facility

The Geotechnical Centrifuge Experimental Research Facility (GeoCERF) operates the only geotechnical beam centrifuge in western Canada located at the University of Alberta in Edmonton. The centrifuge centre was established in the late 2000s and is focused on generating samples and conducting tests to gain insight into tailings behaviour under field conditions in the oil sands industry. Specifications related to this geotechnical centrifuge are provided in Table 3.2, and a photo is shown in Figure 3.1.

Table 3.2. Specification for the geotechnical centrifuge at GeoCERF

Parameter	Description
Rotational speed	5 – 281 RPM
Radius of the swing platform	2 m
Nominal effective radius of payload	1.7
Maximum size of payload	W = 0.6 m L = 0.8 m H = 0.9 m
Maximum payload mass	935 kg
Minimum payload mass	220 kg

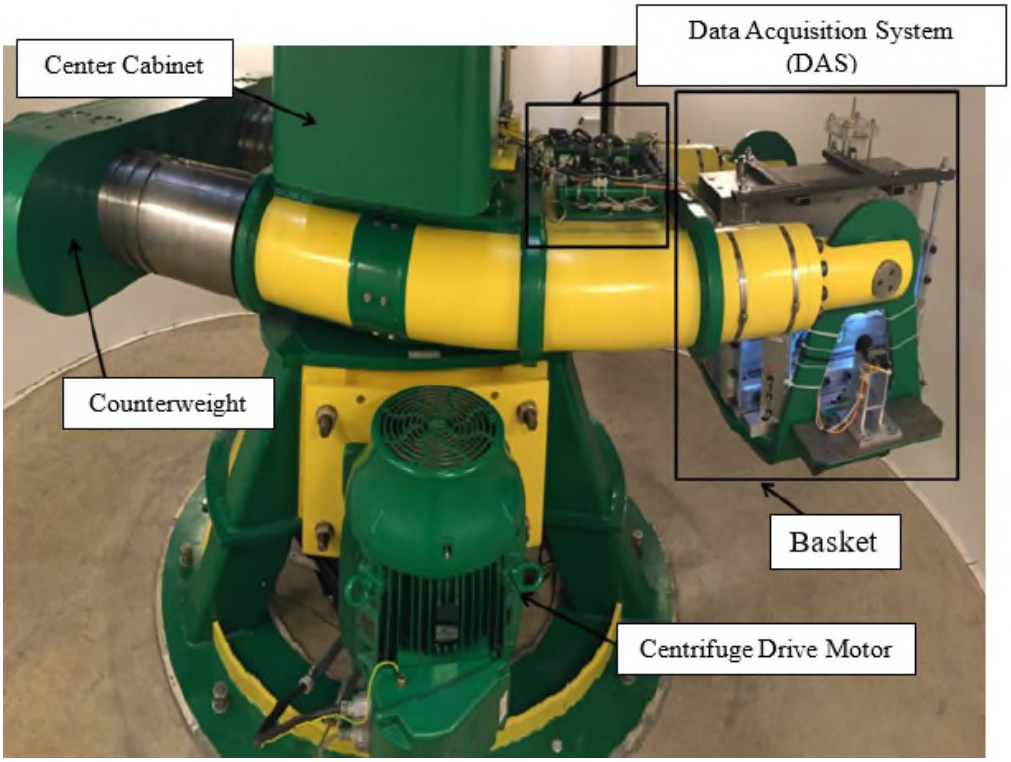

Figure 3.1. Photograph of the GeoCERF geotechnical centrifuge

It should be noted that in typical geotechnical centrifuge investigations, a real-world prototype is usually scaled down and built at the laboratory scale. As such, when the model is scaled-up (in terms of stresses and pressures) in the hypergravity environment which is created by the centrifuge, it represents the prototype. However, it should be noted that the prototype in this work is not a real heavy oil reservoir, and the emphasis on using the centrifuge was to analyze the data in a hyper gravity environment inspired by Vaziri et al. (1998; 2000; 2003).

3.3 Physical Model

3.3.1 Tub

A schematic view of the tub is shown in Figure 3.2. The tub is a cylindrical steel container with an inner diameter of 27.1 cm and height of 52.6 cm, which is where sand is placed in order to represent a heavy oil reservoir. All equipment (i.e., reservoirs, pumps, actuator and etc.) to run each test are mounted on or in the tub. The volume inside the tub consists of three main zones; the sub-reservoir, reservoir and overburden zones. Each of these zones is separated by a steel plate.

The bottom steel plate refers to the base plate located between the sub-reservoir and reservoir, and the upper plate refers to the lid that is placed between the reservoir and the overburden zone.

The sub-reservoir refers to the zone that has been designed for sand collection and is placed below the reservoir. The sub-reservoir only connects with the reservoir through the wellbore. The reservoir refers to a zone in which the sand is placed, and within which most of the major changes occur during a test. The overburden zone was separated from the reservoir with a lid having a radius of 25.7 cm, which results in a gap at its outer extent that allows the overburden to hydraulically communicate with the reservoir. The lid was 20 kg in mass and was placed directly on the sandpack and acted as a caprock. The overburden zone has been designed to provide additional mass on the sandpack and it increases the vertical stress. [Note: After the first two tests reported in this thesis, the steel plate was replaced with a synthetic caprock, as discussed in Section 3.3.3.]

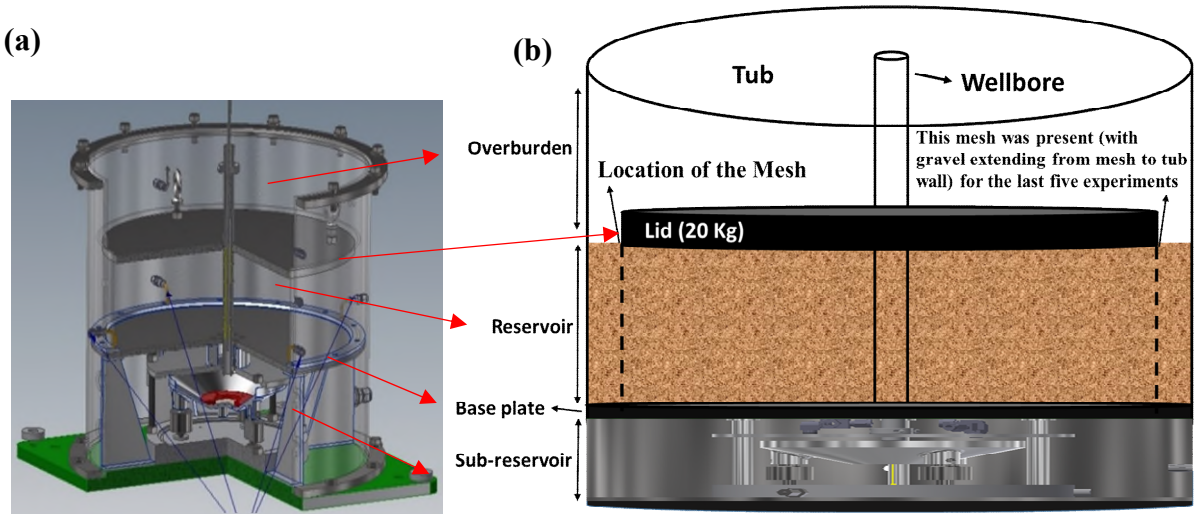

Figure 3.2. (a) Drawing of the tub; (b) Different zones inside the tub (not to scale)

3.3.2 Application of Synthetic Caprock

To study the effect of a flexible caprock, a synthetic caprock was used for some of the experiments (test C3 onward) rather than a steel plate (i.e., the 20 kg lid). The procedures used for casting the synthetic caprock were taken from Jia (2021). The caprock was built on top of an impermeable plastic sheet to make the caprock impermeable to fluid. The mass of the caprock was approximately 17.5 kg with a diameter of 25.7 cm. For each test, a new caprock was cast because during the disassembly stage, the caprock was usually broken.

The material for casting the caprock was a mixture of Kaolin, cement, water and Sil325. The percentage of each material used to cast the caprock is shown in

Table 3.3. Figure 3.3 shows the steps used to prepare a caprock. The lid was removed and a flexible aluminium sheet with length equal to the lid's diameter (90 mm) was attached to cover the lid. This converted the lid to a hollow cylinder where the caprock material could be poured in and allowed it to be dried as shown in Figure 3.3(a). This hollow cylinder was covered with a plastic sheet as shown in Figure 3.3(b). The bushings were installed in the centre to hold the wellbore tight. Next, handles were placed on the lid as shown in Figure 3.3(c). These handles helped the operators to remove the caprock from the top of the sandpack during the disassembly stage. Next, the material was poured into the cylinder as shown in Figure 3.3(d) and it was covered with the same plastic sheet (as shown in Figure 3.3(e)) to allow drying to occur gradually for 20 days. Without using a plastic sheet for drying, the caprock would crack because of losing moisture due to the presence of cement. The casted caprock after drying is shown in Figure 3.3(f). The mechanical property of the caprock is shown in Table 3.4.

Table 3.3. Material and quantity for casting a caprock

Name of the material	Speswhite Kaolin Clay (kg)	Cement (kg)	Water (kg)	Sil325 (38-75µm) (kg)
Values	3.3	2.3	6.7	4.9

Table 3.4. Mechanical properties of the caprock (after Jia 2021)

Triaxial test	Effective Confining Pressure (kPa)	Poisson's Ratio (ν)	Young's Modulus (MPa)	Friction Angle (°)	Cohesion (kPa)
Drained	200	0.25	227.8	28	368
	500	0.25	216.4		
	1000	-	-		
Undrained	200	0.25	423.61	45	256
	500	0.25	419.03		
	1000	0.25	405.5		

Figure 3.3. (a) A hollow cylinder made with tub's lid; (b) The plastic sheet; (c) Placement of handles and the wellbore with its bearings in the center; (d) Hollow cylinder after being filled by the caprock materials; (e) Drying the material for 20 days under plastic sheeting to avoid cracking; (f) The synthetic caprock.

3.3.3 Wellbore

The steel wellbore used in this project had an outer diameter of 2.1 cm with length of 40 cm. Perforations on the wellbore were located at 60-degree increments. There were six rows of perforations for a total of 36 perforations, as shown in Figure 3.4. A diameter of 5 mm was used for these perforations; this number was not chosen based on scaling of heavy oil well perforations but was chosen to provide an opening sufficiently large to enable sand production. With the wellbore placed in the centre of the tub, it passes through the upper part of the tub, the overburden zone, the reservoir, and goes to a depth of approximately 4 cm below the sub-reservoir zone. The perforated wellbore allows fluid and sand to flow from the reservoir downward towards the sandtrap (a component which is described in Section 3.5.5).

To prevent sand production during the early stages of each test, a porous plug comprised of a 3d-printed body filled with steel wool (see Figure 3.5) was initially placed in the wellbore such that it spanned the perforated intervals. When sand production was desired, this plug was moved upward using a DC motor which was mounted on the top of the tub.

(a) **(b)**

Figure 3.4. (a) Steel wellbore with six rows of perforation; (b) Base plate with wellbore in place

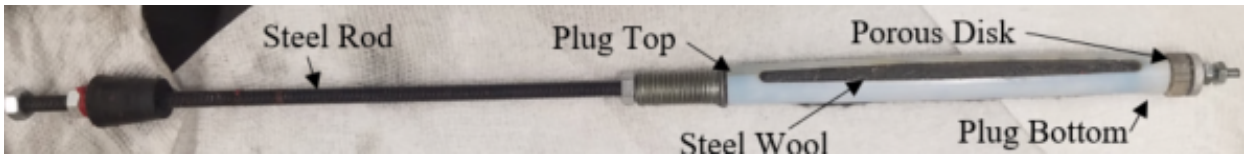

Figure 3.5. 3D printed wellbore-plug filled with steel wool and secured to a steel rod. The whole system moves upward in the wellbore as slowly as possible to avoid erosion in the sandpack and minimize the swabbing effects.

3.3.4 Sandtrap

The sandtrap consists of an aluminium bowl-like dish which was mounted on three load cells as shown in Figure 3.6. The purpose job of this device was to measure the mass of sand produced during the experiments. The oil-sand slurry flowed down the wellbore onto the dish. A disc-shaped filter (Figure 3.7) medium was sat at the base of the dish, which retains sand in the dish while allowing hydraulic communication of oil within and below the dish. The sand, due to its higher density, remained in place while the oil flowed out a port on top of the sand trap to be recirculated, as explained in the following section. To avoid fluid leakage to outside of the sandtrap, a cylindrical plexiglass body (Figure 3.7) was used around the sandtrap and was sealed with o-rings. The fully assembled sandtrap is shown in Figure 3.8.

Figure 3.6. Sandtrap dish mounted on load cells

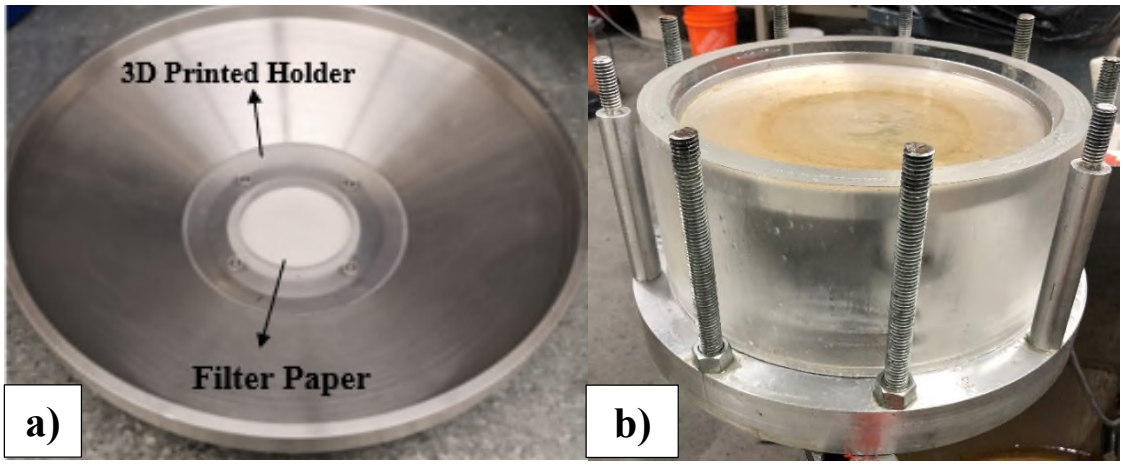

Figure 3.7. (a) Disc-shaped filter paper and its holder; (b) The cylindrical plexiglass that fits around the sandtrap

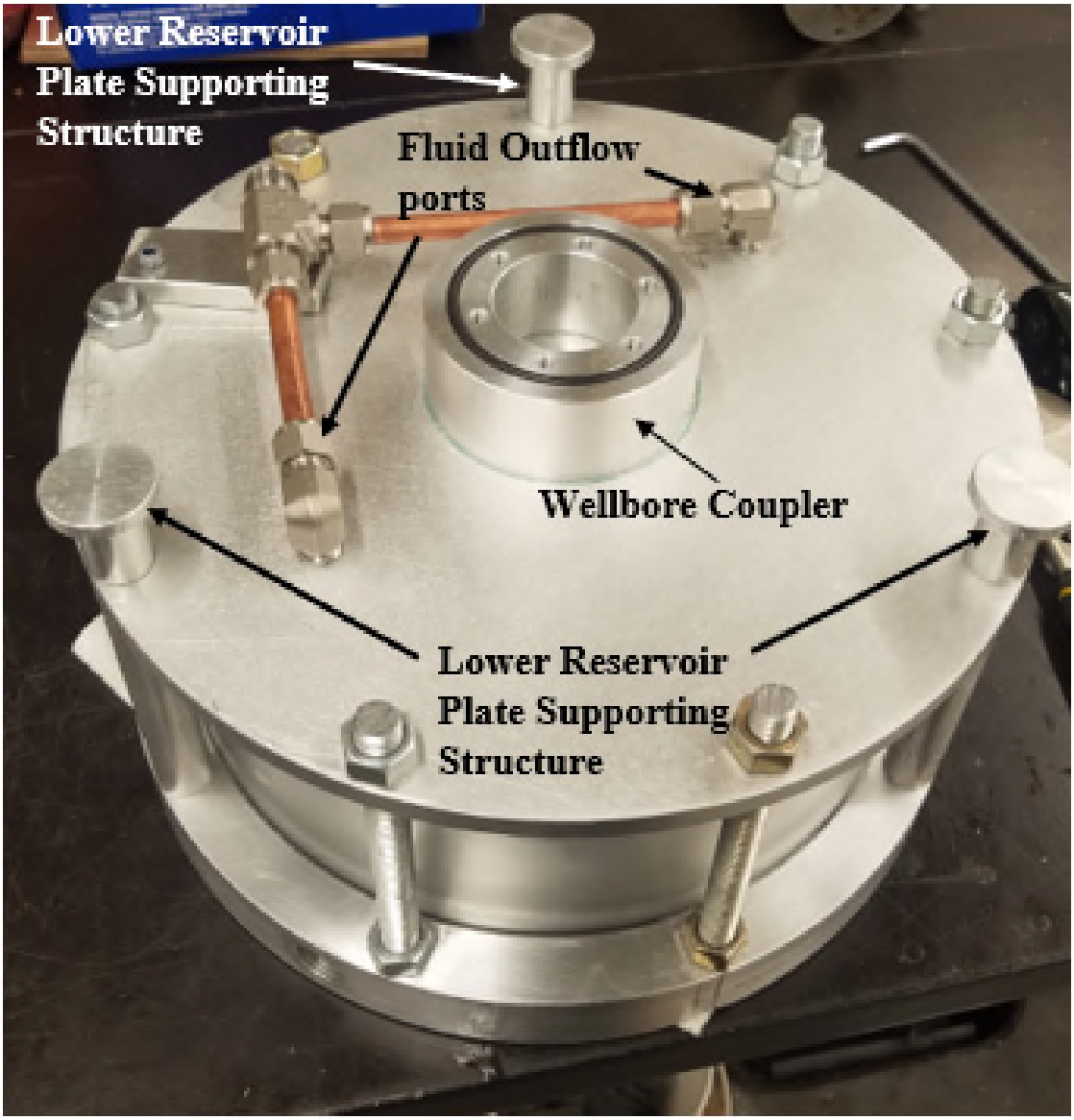

Figure 3.8. A fully assmbled sandtrap with its upper components. The wellbore coupler is used to hold the wellbore inside itself to direct the slurry flow to the sandtrap.

3.3.5 Fluid Circulation System

The fluid circulation system consists of solenoid valves, tanks, a peristaltic pump, pipes, tubes, a head leveling arm, and the sandtrap. The system enables continuous fluid circulation during experiments, based on head differences created by the head leveling arm and the use of the pumping system. T100, T200 and T300 are the tanks that collect fluid during the tests and circulate it through the system. V1, V2, and V3 are the solenoid valves which limit fluid access to different tanks during the experiment.

The leveling arm was designed to move up and down with a help of a DC motor to create head differences with the level of fluid in the tub, hence allowing fluid to flow from the tub to the wellbore and from there to the T100 (Figure 3.9). When the leveling arm is at its maximum height, its elevation is the same as the fluid level in the tub, hence there is no head difference, i.e., no drawdown or fluid flow. As the leveling arm is lowered, a head difference develops, driving fluid flow from the tub (outer perimeter of the sandpack) into the wellbore, through the sandtrap and into T100, assuming valve V1 is open (Figure 3.10). The purpose of V1 is to enable operators to create a massive sudden drawdown, if a maximum driving force for sand production is desired. This can be achieved as follows: 1. Closing V1; 2. Lowering the leveling arm all the way down (maximum range of downward displacement is 16 cm); 3. Opening V1.

There are six pore pressure transducers in the physical model which record and monitor the fluid pressure in different parts of the system (Figure 3.10). The transducer located at the base of T100 was used, in conjunction with knowledge of the density of the fluid in the tank, to determine the fluid level in the tank at any given time. As such, the continuous record of this tank pressure was used during data analysis to determine the rate of slurry/fluid flow into the wellbore/sandtrap system.

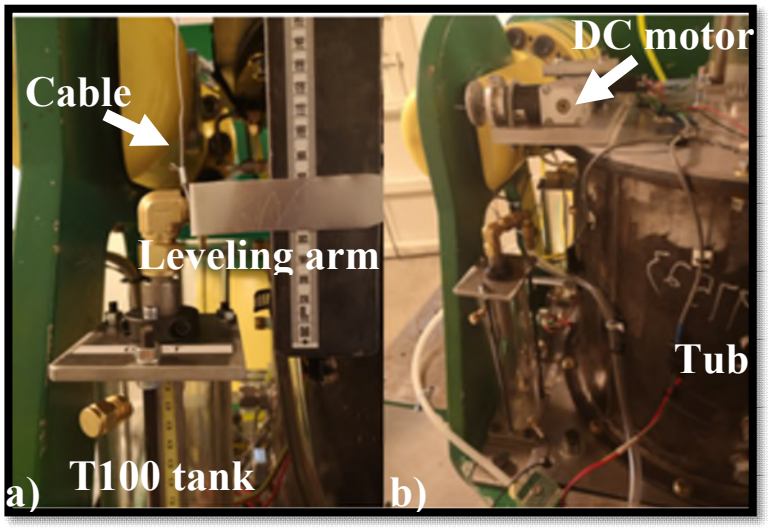

Figure 3.9. a) The leveling arm which sits on top of the T100 tank and can go up and down by the cable that has been attached to it; b) The full view of the leveling arm and the DC motor mounted on the tub.

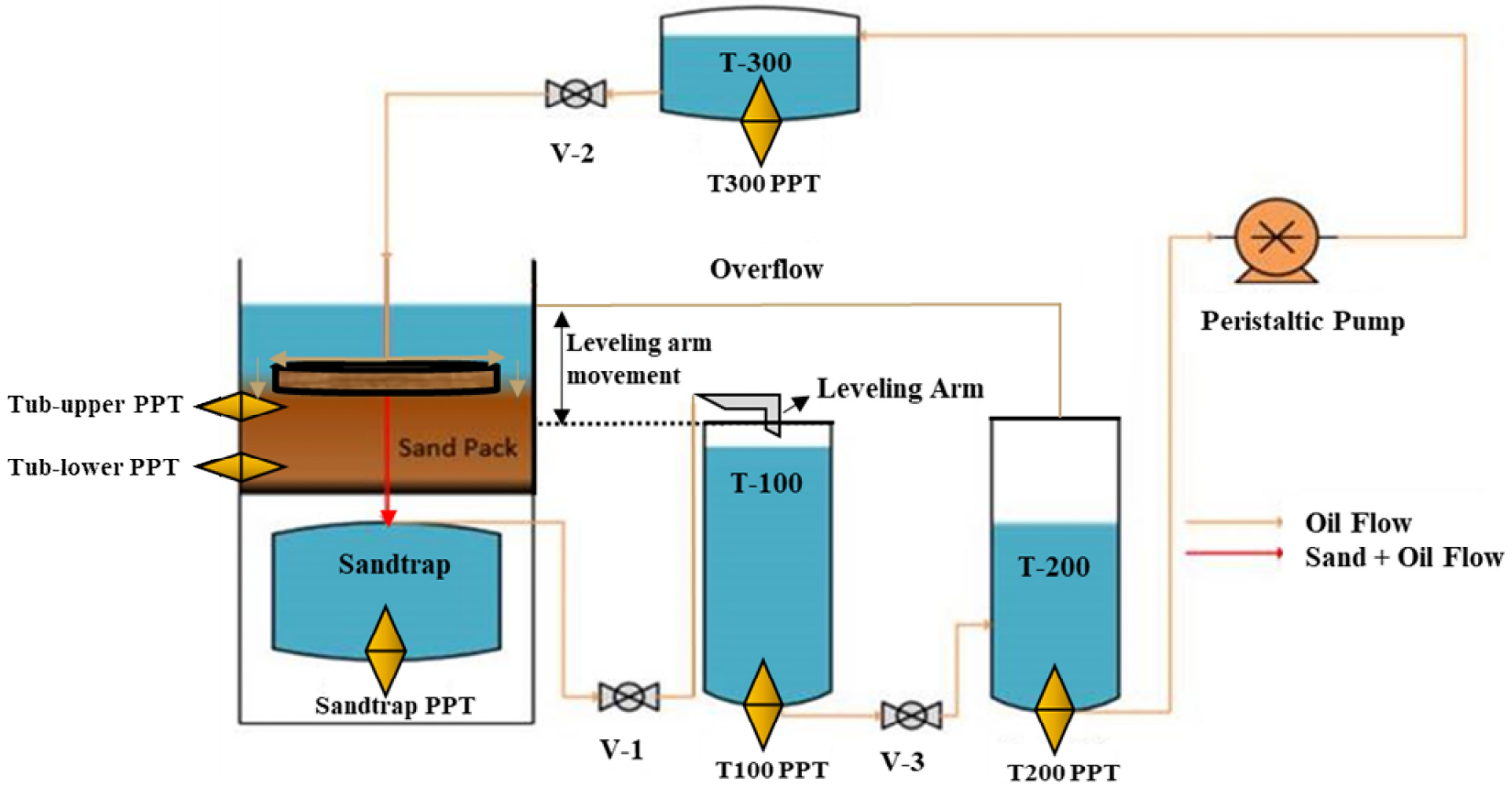

Figure 3.10. Fluid circulation diagram in the physical model (not drawn to scale). The letter T used to denote a tank (fluid reservoir); V denotes a valve; PPT denotes a pore pressure transducer.

3.4 Sand Pluviation

While creating uncemented sandstone reservoirs in this work, it was not feasible to rigorously duplicate a heavy oil reservoir, which would be heterogeneous in terms of grain size distributions, mineralogy, bedding structures, etc. It was deemed reasonable to select a sand with a median grain size (D50) in the range of 100-250 μm for this work. This falls within the range expected for Western Canadian heavy oil reservoirs, as reported by Tremblay et al. (1999). US F-95 sand was purchased from the US Silica Company to cast all the reservoirs in this research. The reason for purchasing a clean sand rather than using the actual produced sand from a real reservoir was that first, the produced sand may have come preferentially from a thin zone, and second, it was challenging to have access to resources to secure a reliable amount of clean sand for running this research. The physical properties of the US F-95 sand are provided in Table 3.5, Table 3.6, and Table 3.7.

A sand pluviation system, as shown in Figure 3.11, was used to to create the sandstone reservoir for all experiments except V1. Use of this pluviation system assists in casting a uniform and high density sandpack for each test by as per the description in Section 3.5.1. The highest achievable drop height for the pluviation system used at GeoCERF was 30 ±2 cm. Using this drop height and plates with 10 mm perforations (Figure 3.12), the expected sand density was 1830 kg/m^3 (Appendix A). However, in practice, it appears that densities actually achieved were somewhat lower (1630 to 1735 kg/m^3).

Table 3.5. Hydraulic conductivity of the US F-95 sand at a low and high sand density (Pereira, 2021)

Initial Soil dry density (kg/m^3)	Average Hydraulic Gradient -	Cumulative Flowrate/ time (m^3/s)	Hydraulic Conductivity (m/s)
1598	1.00	7.07E-7	7.50E-5
1653	1.64	7.67E-7	4.60E-5

Table 3.6. Internal friction of US F-95 sand at low and high dry density (Pereira, 2021)

Initial Soil dry density (kg/m^3)	Confining Stress (kPa)	Void Ratio	Internal Friction Angle
1831	50	0.45	39.9 °
1693	50	0.57	33.7 °

Table 3.7. US F-95 physical properties (Pereira, 2021)

Property	Value
Type	Fine sand
Mineral	Quartz
Color	White
Coefficient of uniformity	2.11
Coefficient of curvature	1.07
D50, μm	163
Specific gravity	2.65
Minimum dry density, kg/m^3	1583
Maximum dry density, kg/m^3	1860

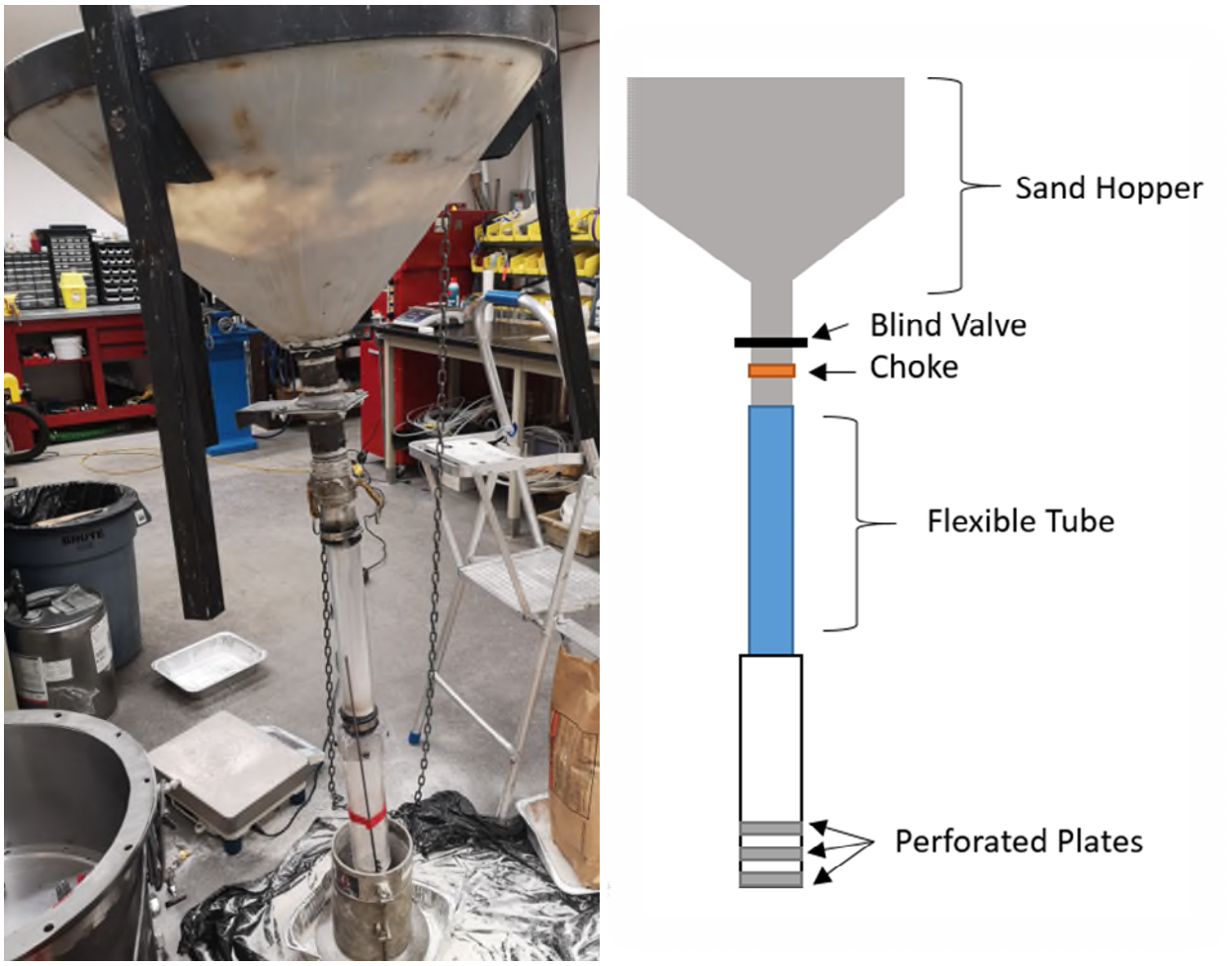

Figure 3.11. Sand pluviation system (left) and schematic of sand pluviation system with its components (right)

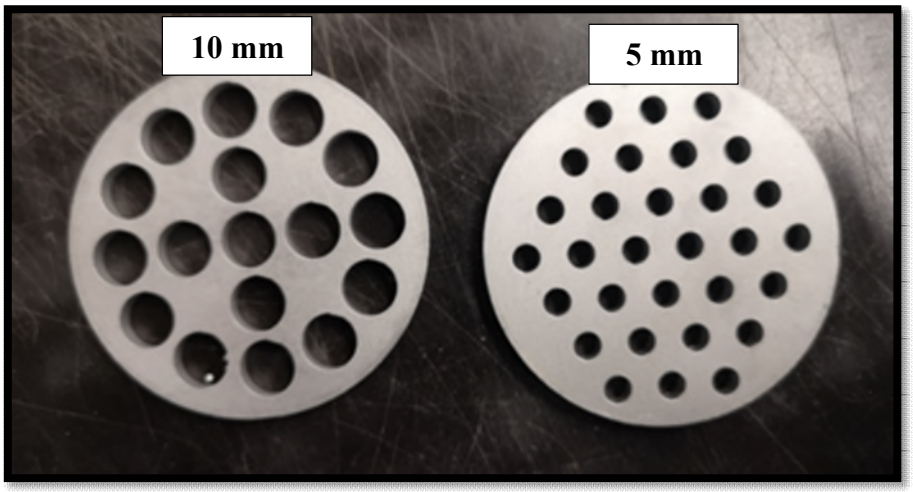

Figure 3.12. Pluviation plates with two different perforation sizes. 10 mm plates were used in this work, as recommended by Pereira (2021).

3.5 Procedures for Centrifuge CHOPS tests

3.5.1 Introduction

This section describes the procedures that were used to set up a sandpack inside the physical model (tub) in different arrangements and explains how data was gathered during and after the tests. It also provides a procedure to pour sand and gravel into the tub and saturate the entire system with canola oil and/or water. Subsequently, key differences in procedures used for other tests (compared to W4-c) are summarized.

Note: The term flight (used below) refers to the spinning of the centrifuge.

3.5.2 Preparation before a Flight

In this section, the preparation of W4-c test is briefly explained. More detailed (step by step) procedures can be found in Pereira (2021). The sandtrap and its copper tubes were placed in the sub-reservoir section of the tub. Then the sub-reservoir was closed by fastening the base-plate onto it. To promote the development of a uniform radial flow through the entire depth of the sandpack, porous gravel was used around the sandpack for all experiments except the first one reported in this thesis. A steel mesh was used to provide structural support for the gravel prior to casting the sandpack. Also, a geotextile material was used on the outer surface of the mesh in order to avoid sand grains from entering the gravel zone. To hold the geotextile in place, mesh clips were used (Figure 3.13). With the mesh in place, a 2 cm gap was provided between tub and the mesh, and the gap was manually filled with gravel (Figure 3.14). The radius of the mesh used in CHOPS experiments from test 2 (G2) onward was 25.7 cm with a height of 16 cm. After placing gravel in the annulus between the mesh and the tub wall, the sandpack was emplaced within the mesh. Next the tubing, fittings, and solenoid valves were installed (Figure 3.15.a).

The wellbore was then placed in the center of the tub. The perforations on the wellbore were temporarily plugged from the outside using plastic wrap and tape. The sandtrap was filled with canola oil by pouring oil down the wellbore. Then the plastic wrap and tape were removed, and the porous plug was inserted into the wellbore to prevent sand displacement into the wellbore and sandtrap during subsequent emplacement of the sandpack. A level was used to ensure the wellbore was vertical (Figure 3.15.b).

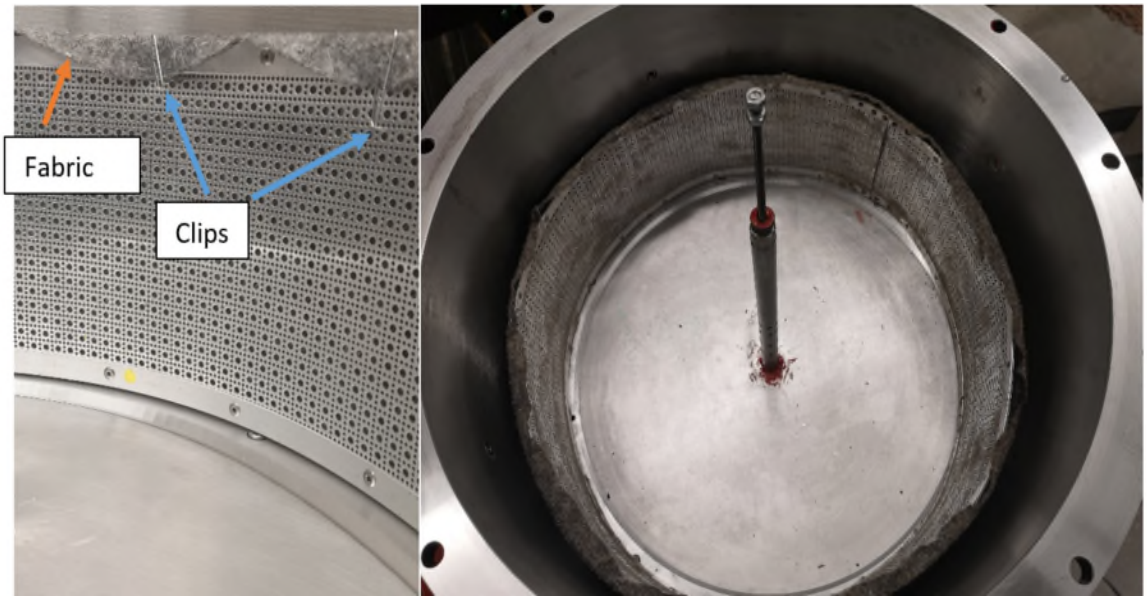

(a) **(b)**

Figure 3.13. (a) Clips holding the geotextile on the steel mesh; (b) Mesh in place in the tub

(a) **(b)**

Figure 3.14. (a) 2 cm gap between the tub and the mesh; (b) Gravel emplaced in the tub-mesh gap

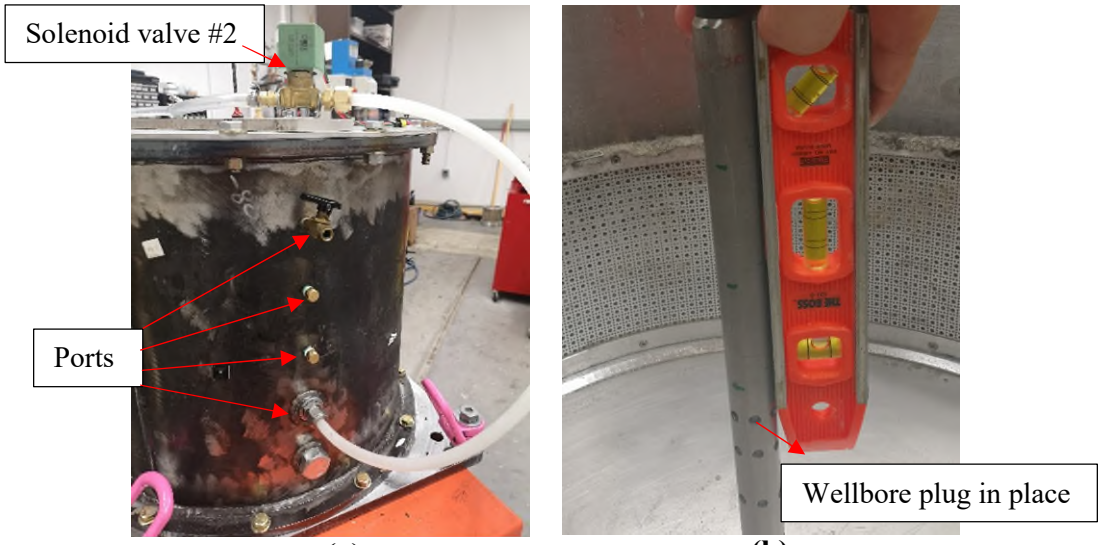

Figure 3.15. (a) Ports where tubes and pore pressure transducers can be added to the tub; (b) The wellbore (porous plug contained within – not visible) and the level used to orient the wellbore vertically

To cast a sandpack in the tub, the pluviation system was lifted by a crane, and the tub was placed beneath the pluviation nozzle (Figure 3.16). Using a ruler, the nozzle was placed 30±2 cm above the height of the surface of the tub. The ruler was adhered to the nozzle to maintain the height from the surface of the pluviated sand so that a consistent sandpack was achieved. Next, the sand was placed in the container of the pluviation system, and it was allowed to pour in the tub. To maintain the 30±2 cm height, the pluviation system was gradually lifted by the crane as the sandpack thickness increased.

The operator needed to manually move the nozzle in the tub doing U-turns to pluviate the sand (Figure 3.17). It usually required 40 kg of silica sand to cast the sandpack. From the C3 test onward (including test W4-c), it was decided to put dye rings at different depths in the sandpack to have a better understanding of the location of sand mobilization. To simplify the set-up, dye rings of different radii were placed manually on the sand layers at different depths. The locations of the rings were as follows:

1. Two rings at the base of the reservoir, creating one ring of radius 40 mm using red dye, and a second ring or radius 60 mm using green dye.

2. Two rings at a height of 50 mm (measured from the base of the sand pack), creating one ring of radius 40 mm using blue dye, and a second ring or radius 60 mm using red dye.

3. Two other rings at a height of 100 mm (measured from the base of the sand pack), creating one ring of radius 40 mm using red dye, and a second ring of radius 60 mm using blue dye (Figure 3.18).

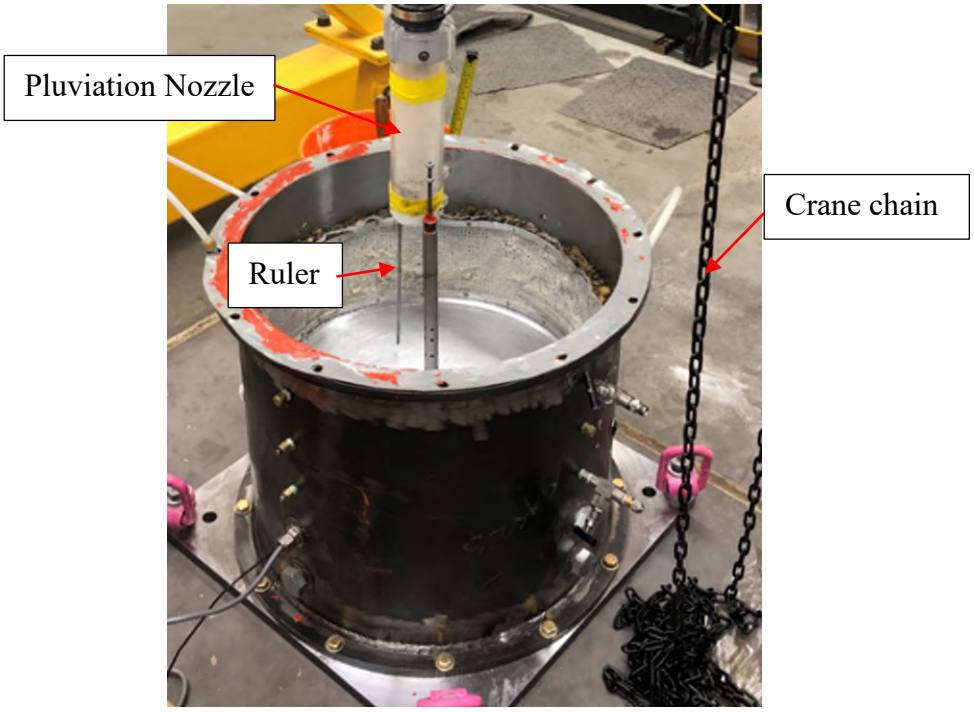

Figure 3.16. Sand pluviation system suspended over the tub

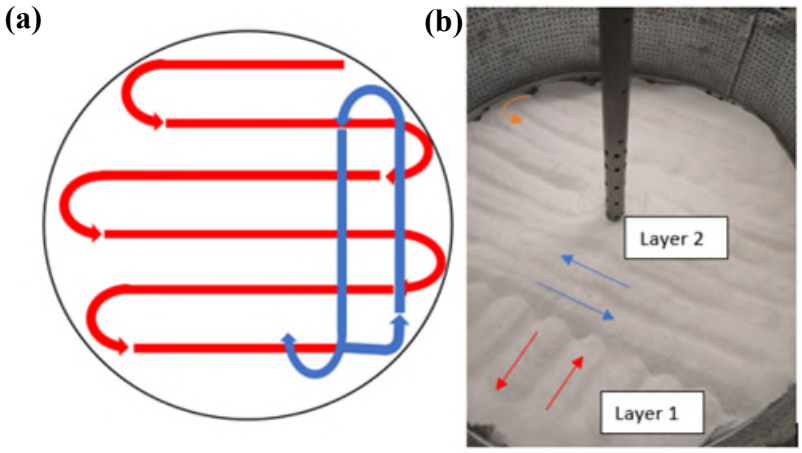

Figure 3.17. (a) Schematic view of U-turn layering of sand; (b) The pluviated sand. In this picture layer 1 has been poured first (red arrows) and then layer 2 (blue arrows) is being poured on layer 1.

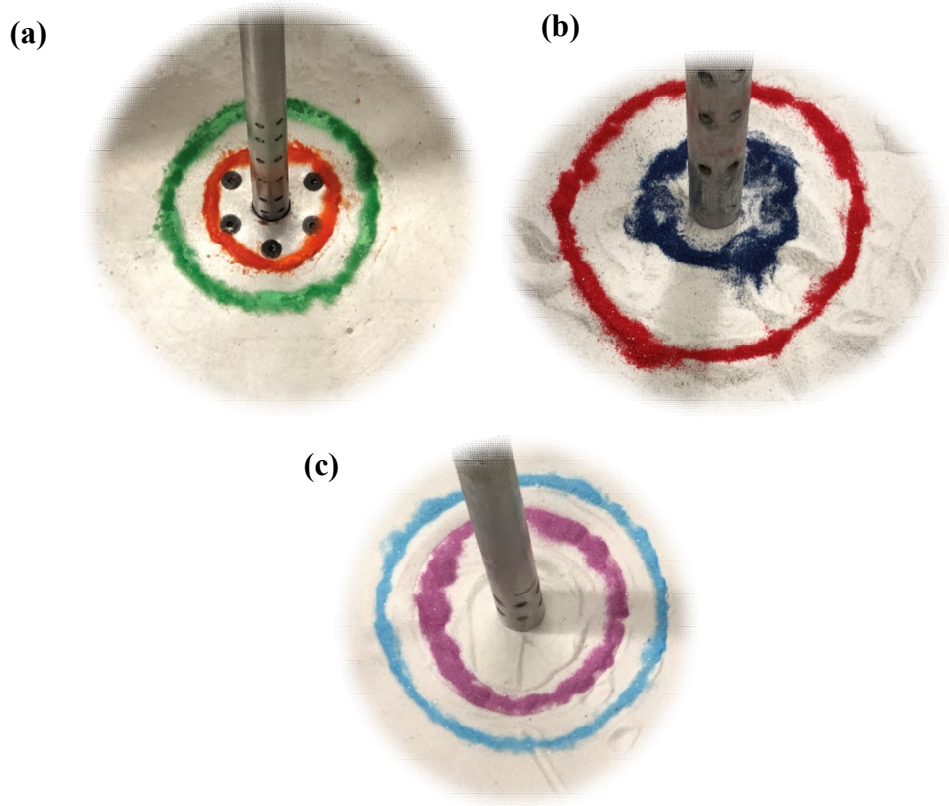

Figure 3.18. (a) Two rings at the base of the sandpack with radii of 40 and 60 mm, respectively; (b)Two rings at height of 50 mm (measured from the base of the sand pack) with radii of 40 and 60 mm, respectively; (c) Two rings at height of 100 mm with radii of 40 and 60 mm, respectively.

After pluviation, the sandpack needed to be saturated. For tests W4-a,W4-b, and W4-c, it was decided to saturate the sandpack with two fluids (Canola oil & tap water); more specifically, to achieve a condition in which the sandpack contains a low water saturation (similar to an oil reservoir at irreducible or connate water saturation), with the balance of the pore volume filled with an oil phase that is mobile. Further to better match field conditions (for a heavy oil reservoir at or above the bubble point pressure), this two-phase condition was chosen for its effect on the geomechanical response of the sandpack. More specifically, the capillary force resulting from two-phase saturation was expected to provide some degrees of cohesion to the unconsolidated sandpack, as per the theory presented in Section 2.9. Early experiments that used single-phase saturations (100% oil) yielded sand production rates that plugged the wellbore and sandtrap, hence

the capillary cohesion derived from two-phase saturation was adopted as a means of reducing the extent of sand production, with the goal of preventing plugging and overflow of the sandtrap.

As demonstrated in Appendix B, it was estimated that a capillary cohesion of roughly 2 kPa could be achieved, and that this would have a notable impact on sand yielding (during sand production) close to the perforations. Details pertaining to saturation procedures used in the different tests are given in Appendix C.

After the saturation stage was completed, the tub had to be opened again (Figure 3.19.a) and additional color rings were placed on top of the sandpack (Figure 3.19.b) for tracking surface effects like surface erosion channels or a cavity around the wellbore. Then the synthetic caprock (wrapped in plastic) was placed on the sandpack (Figure 3.19.c). Next, lead bars with a total mass of 71.2 kg were placed on the caprock to increase the vertical stress exerted on the sandpack (Figure 3.19.d). For the first two tests (V1 and G2) however, gravel was used to stimulate the overburden material. The total vertical stress exerted on the sandpack because due to the combined mass of the caprock and lead bars was estimated to be 115 kPa accounting for the scaling factor of 25 during the test.

Next, the tub was sealed again. The centrifuge was counterbalanced according to the total weight of the physical model (Figure 3.20). Then the physical model was placed on the basket of the geotechnical centrifuge, and it was connected to the data acquisition system (DAS) to enable control of the valves and motors, observe events (via on-board cameras), and collect data during the experiment (Figure 3.21). All other tubes, tanks, valves, and the DC motor were connected to the tub during this stage. This entire process, as described in this section, required approximately one week to complete. Table 3.8 provides a summary of the six tests conducted for this research. Key features and objectives for each of these tests are identified in the table.

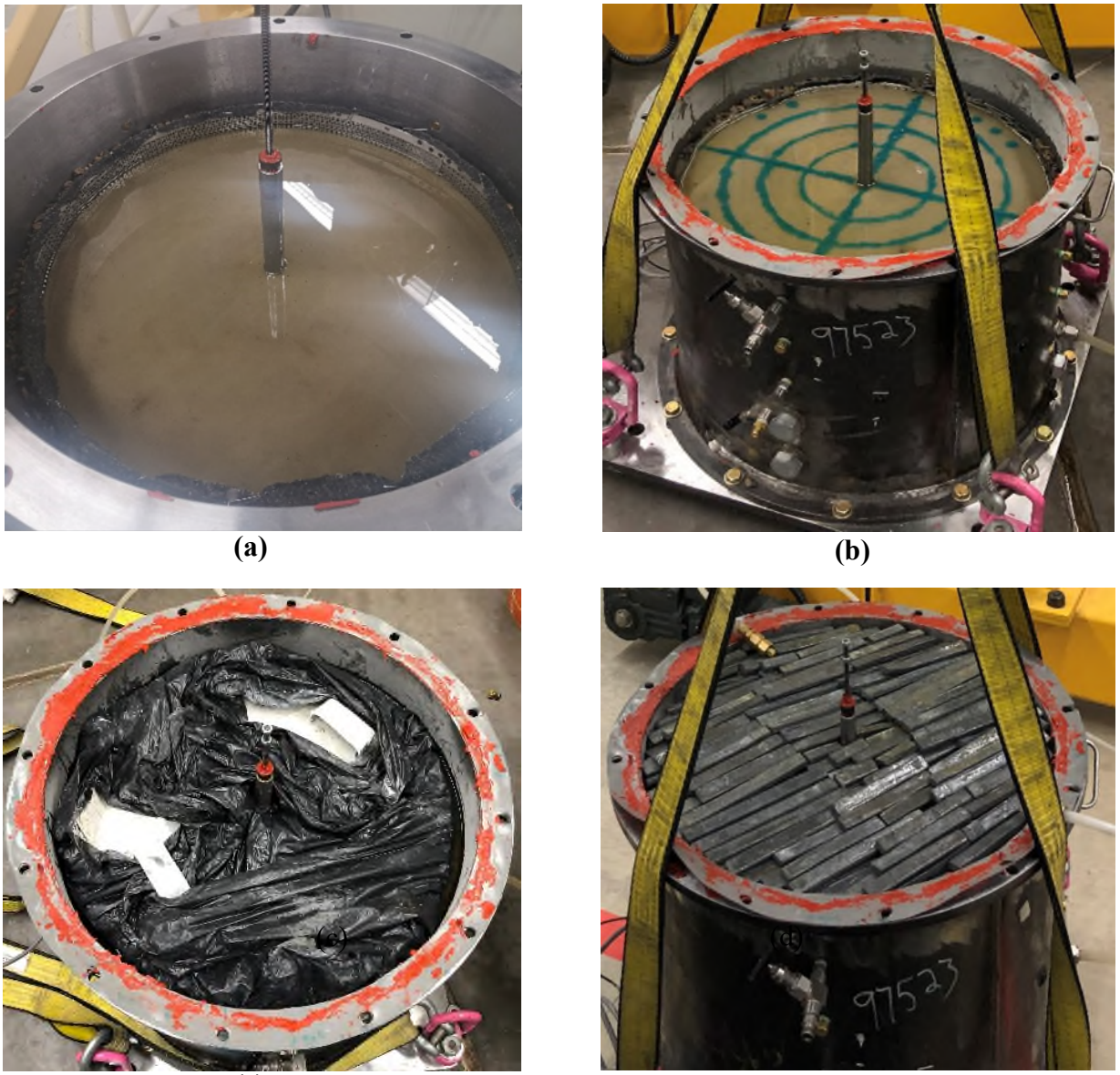

Figure 3.19. (a) The surface of the sandpack after oil saturation; (b) The surface of the sandpack after placing dye rings on the surface; (c) The top of the sandpack after placing the clayey caprock; (4) Top of the caprock after placing the lead bars to model the overburden

Figure 3.20. Total weight of the physical model for one of the experiments using crane scale for counter-balancing the geotechnical centrifuge

Figure 3.21. Physical model placed on the basket of the centrifuge after complete installation of valves, oil tanks, tubing, and all the other wiring and cable works

Table 3.8. Sequence of experimental setups. The letter identifies a distinguishing physical attribute of the test, whereas the number refers to test number.

Test ID	Test description	Schematic of physical model	Objective
V1	**Similar to Vaziri's design:** 1. No mesh/gravel was placed around the sandpack 2. Steel plate was used to represent the caprock 3. Oil was used for saturation 4. For pre-saturation, "revision 0" procedure was used (Appendix C).	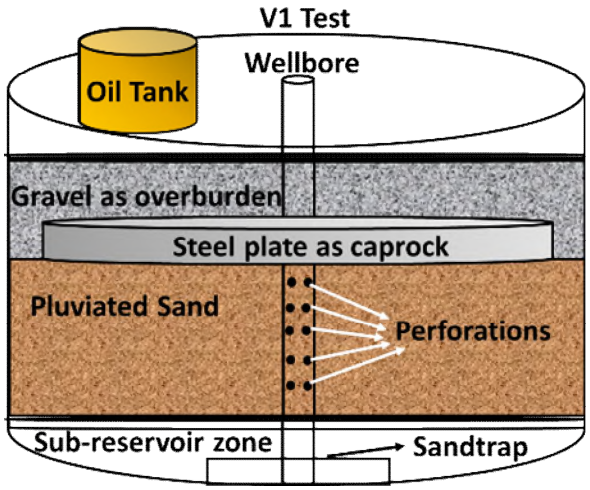	1. To assess the ability of the new apparatus to generated results similar to those reported by Vaziri & Lemoine (2000). 2. To have a base case against which to compare the results of other tests.

Test ID	Test description	Schematic of physical model	Objective
G2	<u>**G**ravel around the sandpack</u> **Similar to V1, except:** 1. Mesh was used to create an annular gap around reservoir which was filled with gravel. 2. For pre-saturation, "revision 0" procedure was used (Appendix C).	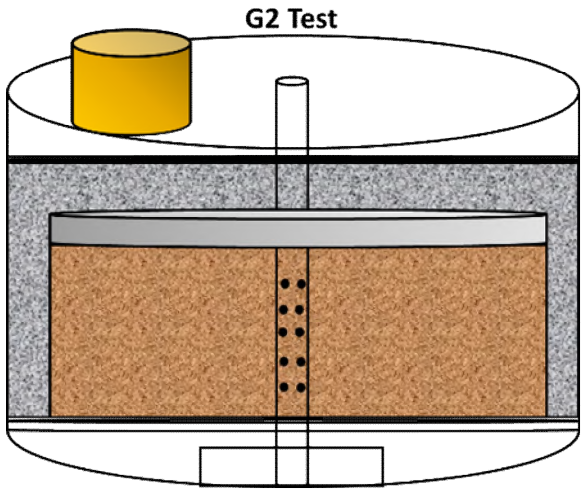	To achieve uniform radial fluid through the entire thickness of the sandpack; to avoid having a zone of relatively high flow velocity immediately below the caprock
C3	<u>Synthetic **C**aprock</u> **Similar to G2, except:** 1. A synthetic caprock was used instead of a steel plate, overlain by lead bars to achieve increased overburden mass. 2. Color rings were placed at different depths of the sandpack to assist post-test interpretation of sand production. 3. For pre-saturation, "revision 0" procedure was used (Appendix C).	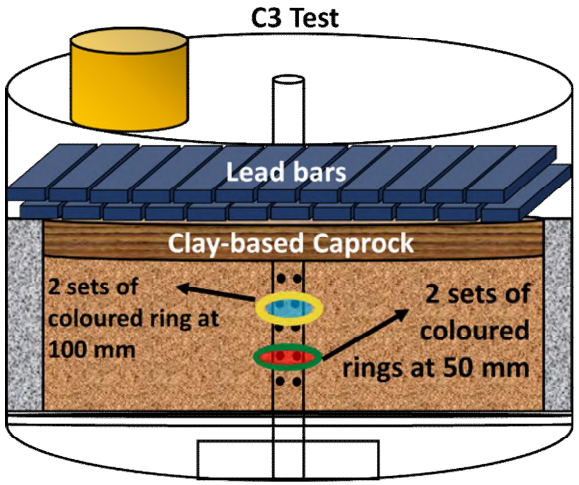	To study the effect of a flexible caprock and its effect on the cavity's growth compared to a steel plate caprock

Test ID	Test description	Schematic of physical model	Objective
W4-a	Two phase (Water-oil) saturation **Same as C3, except:** 1. Sample was pre-saturated with oil and water (9 L of water remained in the sandpack + 2.4 L of oil) 2. For pre-saturation, "revision 1" procedure was used (Appendix C). **Problems:** - Could not reach the desired water saturation using the "revision 1" procedure - Load cells failed during the test due to improper seal against water - Coloured rings were dissolved in water	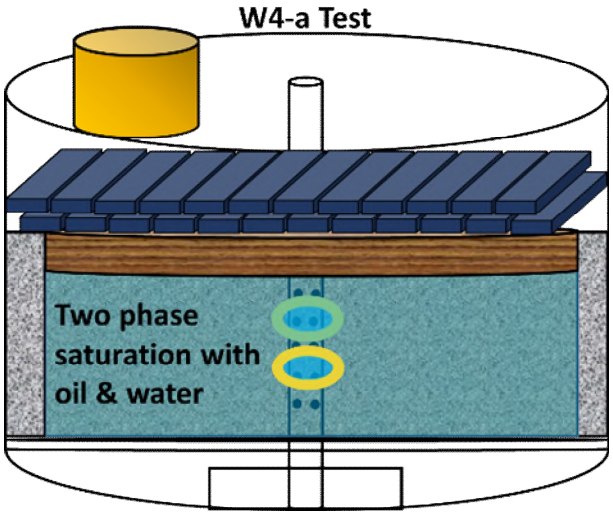	To assess the effect of capillary pressure on sand failure and sand production

Test ID	Test description	Schematic of physical model	Objective
W4-b	**Test W4-a was repeated, except:** 1. Sample was pre-saturated with oil and water (2.4 L of water remained in the sandpack and approximately 9 L of oil) 2. Dye was used to create the coloured rings 3. For pre-saturation, "revision 1" procedure was used (Appendix C). **Problems:** - Air entered the sandpack during the saturation stage - Failed to achieve liquid flow prior to plug removal, perhaps due to air trapped into wellbore plug - Load cells failed during the test due to improper seal against water	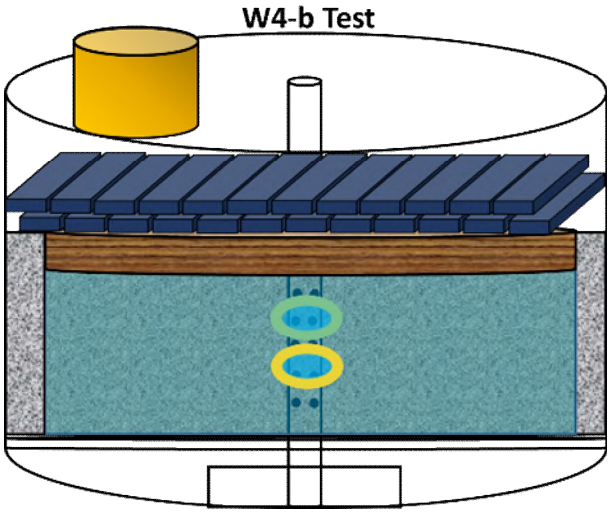	To assess the effect of capillary pressure on sand failure and sand

Test ID	Test description	Schematic of physical model	Objective
W4-c	**Test W4-b was repeated, except:** 1. Sample was pre-saturated with oil and water (1.1 L of water remained in the sandpack and 10.3 L of oil) 2. Additional coloured rings were created at the bottom of the reservoir 3. For pre-saturation, "revision 2" procedure was used (Appendix C). **Problem:** - Air entered the sandtrap and the wellbore during the saturation stage	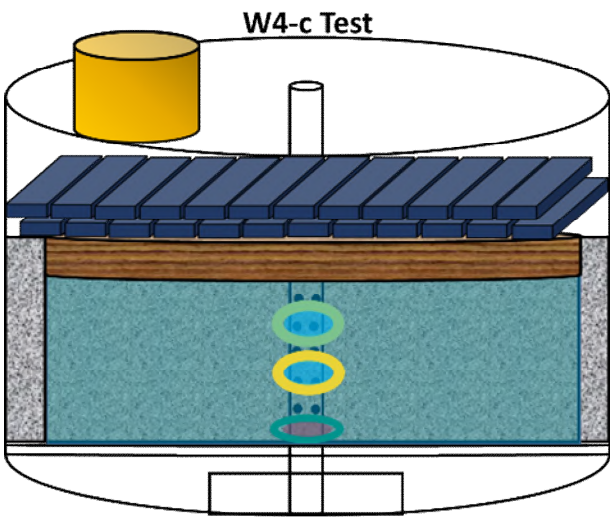	1. To validate the findings of W4-b; to assess the effect of capillary pressure on sand failure and sand 2. To enable the system to achieve liquid flow before plug removal, by preventing accidental air entry into the sandpack 3. To inspect events near the lowest perforations

3.5.3 In-Flight Procedures

After the physical model was fully assembled and fastened on the basket of the centrifuge, the RPM of the centrifuge was set at 111 in order to achieve an enhanced gravity of roughly 25 times earth's gravity (9.81 m/s^2) at one third from the bottom of the physical model according to Section 2.8.7. After starting the test, the operator waited until the system stabilized in terms of load cell and pore pressure transducer readings. Next, it was verified that no overflow of fluid was occurring from the tub to T200 through the overflow port in the tub (Figure 3.10). This was monitored by observing pore pressure at T200. If no overflow was detected, V2 was opened to fill the tub from T300 until overflow occurred. If no overflow was observed and T300 was emptied, the test had to be stopped to refill the T300 with extra oil. After observing overflow, a peristaltic pump that was placed between T200 and T300 (Figure 3.10) was turned on to pump fluid from T200 into T300 and as a result, fluid would go from T300 to the tub by continuous circulation. From this stage to the end of the experiment, V2 remained open, and the peristaltic pump remained on. By opening V3 valve the fluid was flowed into T200 and by having the peristaltic pump which was set at 300 mL/min, the fluid was pumped from T200 to T300.

After stabilization of the sandtrap pore pressure (e.g., see Figure 3.22), a drawdown condition was created in order to promote fluid flow from the tub (i.e., the outer extent of the sandpack) to the wellbore. Drawdown conditions were jointly controlled using valve V1 and by controlling the position of the leveling arm. Figure 3.23 illustrates how the levelling arm position affects drawdown. In scenarios where application of a gradual drawdown was desired, V1 was opened while the leveling arm was in its uppermost (no drawdown or NDD) position, then the arm was gradually lowered as required to achieve the desired drawdown. In scenarios where it was desired to achieve maximum drawdown rapidly, V1 was closed, the leveling arm was moved to its lowermost (maximum drawdown or XDD) position, then V1 was opened.

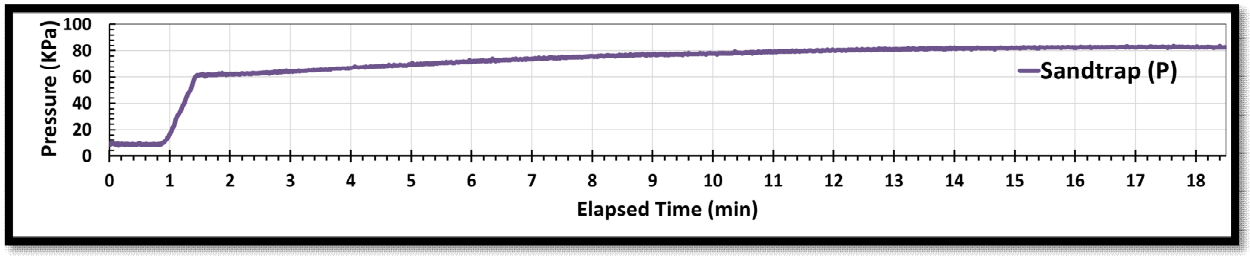

Figure 3.22. Sandtrap pressure early in test. The step increase at ~1 minute corresponds to an increase in beam RPM. Pore pressure was deemed stabilized at ~18 minutes.

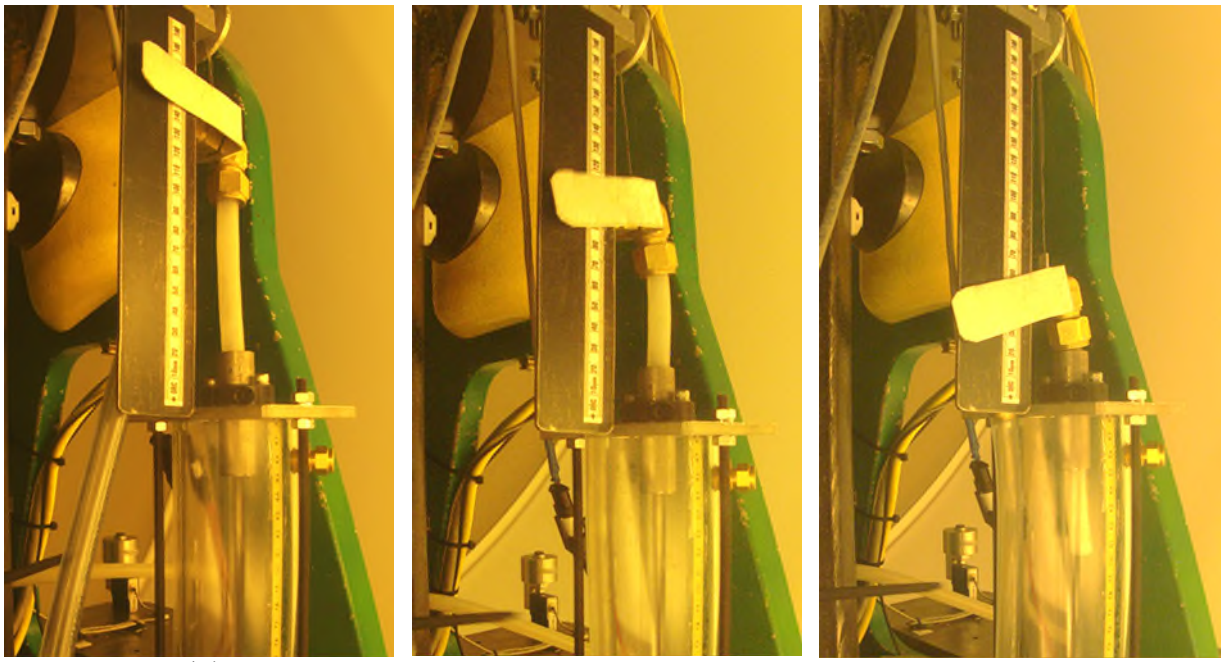

(a) **(b)** **(c)**

Figure 3.23. (a) The leveling arm at its highest location, which creates a no drawdown condition in the tub; (b) The leveling arm at mid height, which creates a medium drawdown (MDD); (c) The leveling arm in its lowest position, which creates the maximum drawdown (XDD) in the tub.

To assess the effect of sand production on flow rate, a baseline maximum flow rate was measured with valve V1 open, in the leveling arm in the XDD position, and the porous plug positioned within the perforated interval of the wellbore. The indicator used to recognize steady state flow conditions was a linear increase in pressure with time for the transducer located at the base of T100. After observing this linear pressure-time response for a period of time, the leveling arm was raised to its origin to create a no flow condition (NDD); to doubly ensure no-flow conditions, valve V1 was also closed. After completion of this stage, the plug in the wellbore was pulled upwards out of the perforated interval using a DC motor. At this stage, it became possible for sand to flow from the sandpack into the wellbore and down into the sandtrap. Measurements used to monitor sand production at this stage were the sandtrap load cells, and pressure increase in T100 (which was proportional to the volume of oil displaced out of the sand trap by the produced sand). At this stage, and throughout the experiment, it was necessary to monitor the pressure in T100 in order to assess if it was becoming too full. In general, if T100 became half full, it was emptied by opening valve V3 and allowing fluid to flow into T200. When doing so, it was critical

to close V3 as quickly as possible because it was not possible to assess flow rate from the sand trap to T100 while this valve was open.

The process of plug removal (PR) required several minutes, as illustrated in Figure 3.24. After PR was complete and all perforated zones were open, the next step was to wait until a stable condition was achieved, e.g., for the sandtrap load cells to reach a plateau, indicating a cessation of sand production. Then, by lowering the leveling arm and opening V1 when desired, a drawdown condition could be created, resulting in the production of oil and sand. Key measurements that were monitored during this time were the sandtrap load cells (indicators of produced sand mass) and T100 pressure (an indicator of oil-sand slurry flow rate). After sand production ceased, the sandtrap capacity reached its maximum capacity, or some other end-point was reached (e.g., the wellbore-sandpack system became plugged, preventing additional slurry flow), the test was terminated. All valves were closed, the pump was turned off, and the centrifuge was then stopped. The events for all tests during flight are provided in Appendix D.

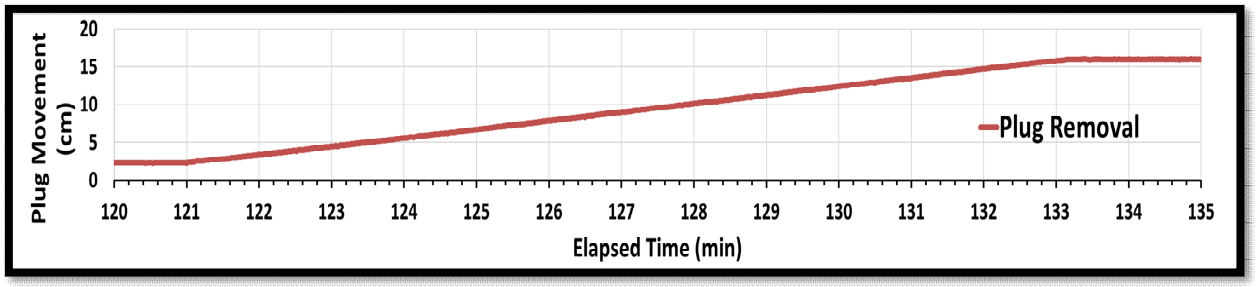

Figure 3.24. The maximum movement of plug in the wellbore was 14 cm upward from the bottom of the wellbore. At 121 minutes, the PR started and at 133 minutes where the slope of the plug reaches to a plateau, this means that the plug has been fully opened all the perforations in the wellbore.

3.5.4 Procedures after C-CHOPS Tests

After the test, the needle valves connected to the ports on the side of the tub were opened to drain fluids while the physical model was still seated on the basket of the centrifuge. Approximately one was required day to drain the physical model fully. Then the tub was detached from the basket and lifted by the crane to the floor from the pit (centrifuge platform). The tub cap and the overburden materials were removed. The remaining oil was removed by napkins or with a syringe. Then the gravel from the annulus between the steel mesh and the tub was removed as much as possible to make the caprock/steel plate loose. Next, the caprock was removed gently. This step usually required crane support. The remaining oil on the surface of the sandpack was also removed. All steps were recorded through photographs. The dimension of the cavity (Figure 3.25) were measured, for tests where a cavity was presented.

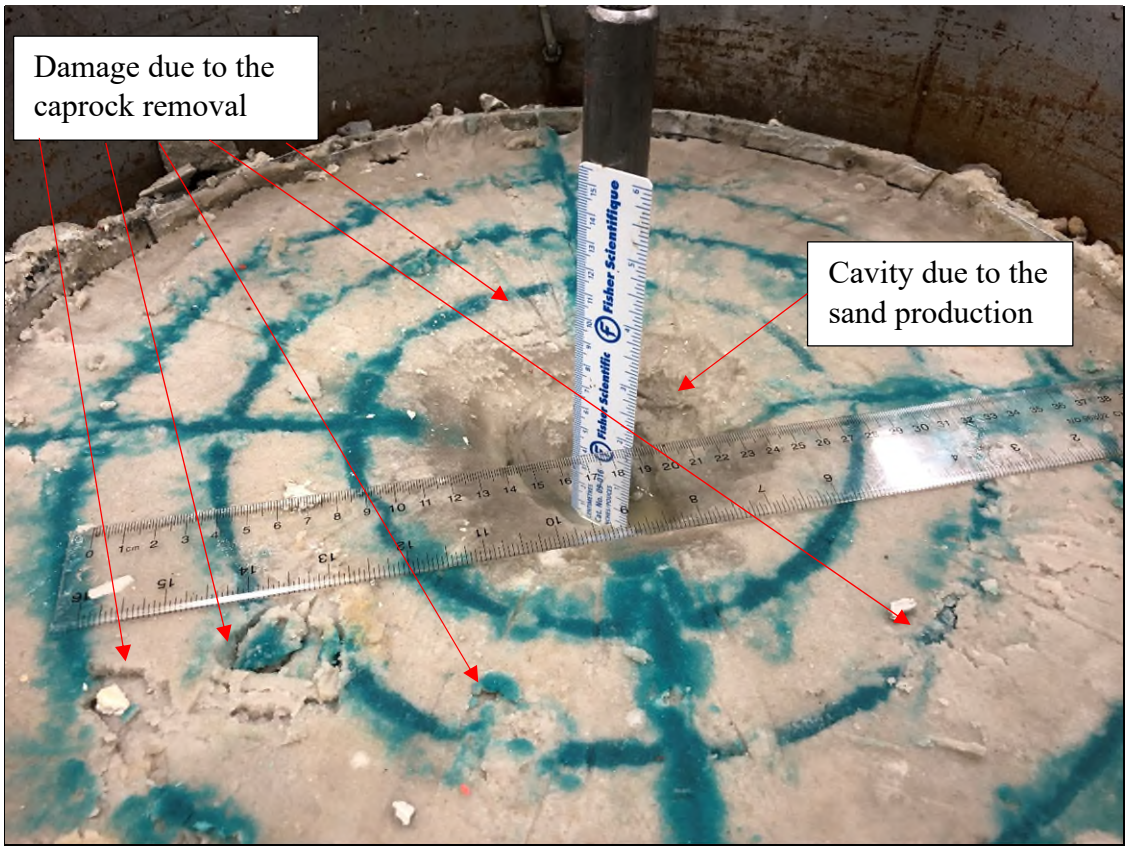

Figure 3.25. The surface of the sandpack after removing the caprock and draining the remaining oil

Before proceeding with the removal of the sandpack, from C3 test onward, three Shelby tubes were inserted into the sandpack prior to the excavation, as shown in Figure 3.26, from test C3 onward. Two were inserted in the vicinity of the wellbore and one near the edge of the sandpack to take samples from parts of the sandpack that were (and were not) affected by sand production. The tubes sampled the sandpack from top to bottom. In general, a density estimate was taken from the upper half and lower half of each tube, based on the measurement of volume and mass of the sample. Next, the sandpack was inspected for any potential wormholes within the sandpack that may have formed during sand production. For this purpose, vertical slabs were created by inserting cutting tools, as illustrated in Figure 3.27.a. Cutting was started at the outer radius of the sand pack and proceeded towards the wellbore, stopping at a radial distance approximately 100 mm from the wellbore. Each slab was cut to a depth that was roughly at mid-depth of the sandpack (6 to 7 cm). After inspection, the slabs were removed from the tub to allow some space for other cuttings (Figure 3.27.b). The cutting process was repeated rotationally around the wellbore, until the outer part (radial distance > 100 mm) of the upper half of the sandpack was excavated. The same procedure was followed for the lower half of the sandpack as shown in Figure 3.28. This provided the maximum space for excavating near the wellbore zone. Again, the remainder of the sandpack was divided into upper and the lower zones for the cutting process. The colored rings during excavation were inspected. The presence or absence of these rings, and their vertical positions (if present) were recorded and used to inform the interpretation of sand production (as described in Chapter 4). Photographs were taken frequently during the excavation process.

(a) (b)

Figure 3.26. (a) The location of the Shelby tubes being inserted for sampling; (b) Height of the sample in the Shelby tube

(a) (b)

Figure 3.27. (a) Vertical slabs cut in order to examine for potential wormholes; (b) Excavation of the upper half of the sand pack

Figure 3.28. Excavation of the lower half of the sandpack at radius about 100 mm from the wellbore.

Next, the base plate was removed to access the sandtrap. The sub-reservoir zone was drained so the wellbore could be disconnected from the sandtrap. It was considered that sand might exist in the wellbore. Therefore, it was important to collect the sand from the wellbore so it could be included in the total mass of sand that had been produced. The next step was to disconnect the sandtrap from the tub as shown in Figure 3.29. Occasionally, so much sand was produced during an experiment that the sandtrap dish capacity was exceeded. As a result, the over-produced sand fell below the dish or out onto the top surface of the sandtrap, as shown in Figure 3.30. All sand was collected and washed with detergents and degreaser, weighed, and then placed in an oven to dry. The total dry mass of the produced sand was calculated for each experiment.

As a final step, sand samples were discarded. Oil and gravel were collected for reuse in those tests that used single-phase (canola oil) saturation; for two-phase tests, the oil and sand were discarded. All equipment was cleaned and stored at GeoCERF at University of Alberta. The results and discussion of all completed tests are provided in Chapter 4.

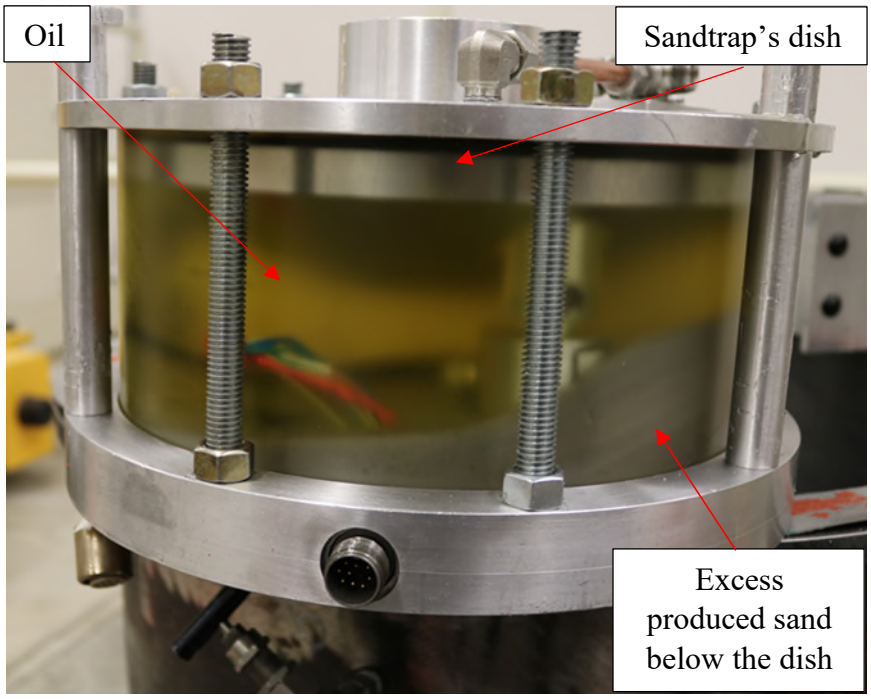

Figure 3.29. Sandtrap after one of the experiments in which an excessive volume of sand was produced, resulting in filling of the dish and an overflow of sand into the lower part of the sandtrap.

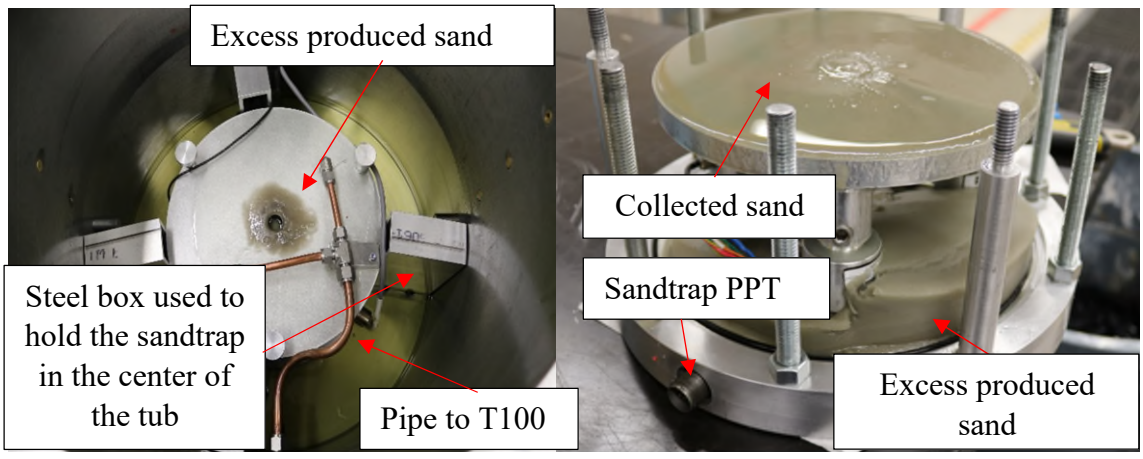

(a) **(b)**

Figure 3.30. Sandtrap after one of the experiments in which an excessive volume of sand was produced. (a) Excess sand accumulated on the top surface of the sandtrap; (b) Excess sand below the dish.

4 RESULTS AND DISCUSSION

4.1 Experiments Results

4.1.1 Summary of In-flight Measurements

As discussed in Section 3.3.7, there were six pressure transducers used in the physical model. Three were located in tanks and used to monitor fluid levels in these tanks, two were located on the edge of the tub and were used to monitor pore pressure at the outer extremity of the reservoir (i.e., reservoir pressure), and one was located in the sandtrap and used to monitor pressure at the centre of the sandpack (i.e., wellbore pressure). All six of these pressures are reported in this section. In addition, hydraulic head in the wellbore and hydraulic head in the reservoir were calculated, to enable easy comparison of conditions in the wellbore and in the reservoir – corrected to a common datum depth. This head is referred to as scaled head, meaning it was calculated using the centrifuge scaling factor such that head could be expressed in a manner that relates directly to fluid levels in the tub. Specifically, scaled hydraulic head was calculated as follows:

$$H = z + \frac{p}{\rho g N} \tag{4.1}$$

Where:

H is scaled hydraulic head (m)

z is elevation above datum (base of sand trap) (m)

p is pressure (Pa)

g is the earth's gravity (9.81 m/s^2)

N is the centrifuge scaling factor (dimensionless)

Scaled head in the reservoir was calculated using equation 4.1, with the pressure measured by the upper tub transducer and an elevation of 0.27 m for this transducer. Scaled head in the wellbore was calculated using equation 4.1, with the pressure measured by the sandtrap transducer and an elevation of 0 m for this transducer.

As discussed in Section 3.3.6, three load cells were placed under the sandtrap dish to monitor the produced sand accumulating in this dish. In principle, it is possible to calculate the mass of

produced sand in the dish using the sum of the loads recorded by these cells, accounting for buoyancy of the sand grains in oil and the enhanced gravity environment (Pereira, 2021). However, quantitative use of the load cell data was hampered by the fact that the load cells also demonstrate a transient response to fluid pressure change in the sandtrap. Regardless, the sum of the load cell responses was qualitatively useful for indicating episodes of sand production (i.e., relatively rapid increase in load).

The position of the porous plug was recorded continuously during each test and is presented in this chapter. A position of 0 cm represents the initial condition, in which the porous plug was positioned within the perforated interval of the wellbore. A position of roughly 16 cm represents a condition in which the base of the plug is position above the uppermost perforations.

As discussed in Section 3.5.3, valve V1 and the head leveling arm are used in combination to control drawdown conditions in the wellbore. Closing valve V1 is effectively equivalent to shutting in a well. If a drawdown condition existed prior to closing the valve, pressure in the sandtrap and wellbore build up until pressure in the well equilibrates with the reservoir pressure (when corrected to a common datum depth), and flow ceases (no drawdown or NDD condition). When valve 1 is open, drawdown (hence flow rate) is controlled by the position of the leveling arm, which can be moved continuously between its highest position (NDD) and its lowest position (maximum drawdown or XDD).

Calculated flow rates are presented in the results that follow. These were calculated based on the rate of pressure increase in tank T100, which is directly proportional to the rate at which oil is being displacement from the sandtrap by produced oil and/or sand. At times when the porous plug was in place, the calculated flow rate represents the oil flow rate. This liquid flow rate was used to calculate the permeability of the sandpack (calculations are provided in Appendix E). Once the porous plug was removed and sand production was possible, the calculated flow rate represents the flow rate of an oil-sand slurry.

4.1.2 Presentation of In-flight Measurements

A complete record of operational events during each experiment is given in Appendix D, and measurements for each individual load cell are available in Appendix F. Plots showing recorded pressures, the calculated sum of the load cells, valve V1 position, plug position, calculated slurry flow rates and calculated scaled heads are shown in Figure 4.1 through 4.6 for experiments V1, G2, C3, W4-a, W4-b and W4-c . Important observations and events for each test are summarized in the following paragraphs. In this summary, the term drawdown head refers to the difference between the scaled head in the reservoir and the scaled head in the wellbore.

Figure 4.1 shows the in-flight measurements for test V1. The centrifuge was not spinning from 0 to 6 minutes, and from 16 to 22 minutes. With the porous plug in-place, a stable drawdown head of roughly 9 cm was applied and a flow rate of 8 cm^3/min was observed from 37 to 54 minutes. Plug removal began at 56 minutes and completed at 64 minutes. A rapid increase in T100 pressure indicated slurry flow immediately after plug removal began. A slurry rate of roughly 150 cm^3/min was observed from 56 to 60 minutes, during which a variable drawdown head between 1 to 3 cm existed. From 60 to 66 minutes, a slurry rate of roughly 30 cm^3/min was observed. Given the lack of drawdown head during this time interval (i.e., NDD condition), this rate is interpreted to represent sand production. This is supported by a steady increase in load cell response over this interval. From 66 to 67 minutes, a relatively high flow rate (287 cm^3/min) was observed; this occurred while a drawdown head of roughly 2 to 3 cm existed and load cell force increased at an accelerating rate, which suggests that both oil and sand were flowing. From 67 to 69 minutes, flow rate reduced to roughly 30 cm^3/min. From 69 minutes onwards, it was not possible to sustain significant flow rates, regardless of the drawdown conditions. After several failed attempts to re-initiate flow by imposing a sudden XDD condition (opening valve V1 with the leveling arm in its lowest position), the test was terminated. One additional observation of interest pertains to the reservoir head behavior between roughly 59 and 75 minutes. Given that this head is governed by the fluid level in the tub, which would normally remain constant at the height of the overflow port, this drop is noteworthy. The subtle drop observed from 59 to 66 minutes might be associated with a swabbing effect resulting from withdrawal of the porous plug and/or a reduction in tub fluid level due to slurry production during the preceding 4 minutes. The more rapid drop from 66 to 69 minutes is associated with an interval of high oil and sand production. It is believed that the fluid

level in the tub dropped at a rate that exceeded the capacity of fluid to flow from T300 into the tub. After slurry production dropped off at 69 minutes, the fluid level was gradually restored, and the reservoir head rebounded to its usual level.

Figure 4.2 shows the in-flight measurements for test G2. The centrifuge reached the target rotary speed in roughly 1 minute then was spun continuously until the end of the test. In the early stages of the test (1 to 16 minutes), a small overbalance pressure was observed (i.e., wellbore head > reservoir head) while valve V1 was closed. This suggests the fluid level in the wellbore had temporarily risen to a height greater than the maximum leveling arm height, and/or the fluid level in the tub was slightly below the overflow port. At 16 minutes, with the porous plug in-place, valve V1 was opened. The levelling arm was then moved to the XDD position, resulting in a drawdown head of roughly 13 cm and a relatively stable flow rate of roughly 10 cm^3/min. Plug removal began at 28 minutes and completed at 36 minutes. An increase in T100 pressure indicated slurry flow immediately after plug removal began. The slurry rate increased then stabilized at roughly 30 cm^3/min from 34 to nearly 40 minutes. At 42 minutes, T100 pressure dropped rapidly because valve V3 was opened momentarily in order to drain tank T100. It appears that limited additional oil was displaced from the sandtrap into T100 from 42 minutes onwards, although the load cell response indicates that sand continued to accumulate in the sand trap until 48 minutes. This suggests that a blockage of some kind existed in the flow system connecting the sandtrap to T100 (via the leveling arm). From 50 minutes onwards, several attempts were made to achieve a slurry flow rate by opening valve V1 with the leveling arm in the XDD position. However, it was not possible to achieve a significant flow rate; an observation consistent with the aforenoted interpretation of a blockage in the flow system. The test was terminated at 216 minutes because of the inability to achieve flow.

Figure 4.3 shows the in-flight measurements for test C3. Due to a data acquisition error, load cell measurements were only available from 69 to 128 minutes for this test. The centrifuge reached the target rotary speed in roughly 1 minute then was spun continuously until the end of the test. After some initial adjustments to fluid levels and pressures, target values were achieved at roughly 70 minutes. At 77 minutes, with the porous plug-in place, a drawdown condition was created by opening valve V1 with the leveling arm positioned in the XDD position. Following a short-lived transient drawdown that occurred while the tubing between the sandtrap and levelling arm filled,

a stable drawdown head of roughly 13 cm was achieved and a flow rate of 6 cm^3/min was observed between 77 to 96 minutes. Valve V1 was then closed to create a NDD condition, and valve V3 was opened briefly to empty tank T100. Plug removal began at 119 minutes and completed at 126 minutes. A sudden increase in load cell response at 119 minutes suggests that sand production initiated immediately upon plug removal. Counter to experience in the previous two experiments, T100 pressure did not show an increase during plug removal in this test because valve V1 was closed rather than open. The sudden increase in load cell response at 120 minutes does suggest that sand was being produced during plug removal, which is consistent with the previous experiments. At 139 minutes, an XDD condition was created by opening valve V1 with the leveling head in its lowest position. This resulted in a sudden increase to a maximum slurry rate of roughly 430 cm^3/min, after which rates declined steadily and reached 0 cm^3/min by 146 minutes. This suggests that a blockage had developed in the flow system. The test was terminated at 151 minutes because of the inability to achieve flow.

Figure 4.4 shows the in-flight measurements for test W4-a. This was the first test that used both water and oil as the pore fluids. The estimated water saturation was roughly 77%. The irreducible water saturation was unknown at the time, and it was expected to be approximately 20%, hence there was mobile water present in the sandpack. No load cell measurements were obtained for this test because the load cells failed. The centrifuge reached the target rotary speed at roughly 46 minutes then was spun continuously until the end of the test. After some initial adjustments to fluid levels and pressures, target values were achieved at roughly 60 minutes. At 63 minutes, with the porous plug in-place, a drawdown condition was created by opening valve V1 with the leveling arm positioned in the XDD position. From 63 to 94 minutes a relatively stable flow rate in the 80 to 120 cm^3/min range was observed. At 94 minutes, the leveling arm was raised roughly 3.2 cm, resulting in a slight reduction in drawdown head (i.e., from roughly 12 to 10 cm). As expected, from 94 to 132 minutes a relatively stable but slightly lower flow rate (50 to 75 cm^3/min) was observed. The pronounced sawtooth pattern observed in T100 pressure from 64 to 132 minutes is a result of the need to repeatedly open valve V3 to drain tank T100 during this relatively long interval of sustained, high flow rates. At 132 minutes a NDD condition was created by raising the leveling arm to its highest position, then from 139 to 152 minutes the porous plug was removed. Though no load cell data were available, the steady rise in T100 pressure suggests

that sand was being produced, hence displacing oil and/or water from the sandtrap into tank T100. Slurry flow rates calculated during and shortly after plug removal were in the 40 to 75 cm^3/min range. However, counter to expectations, lower flow rates (roughly 10 to 20 cm^3/min) were subsequently achieved when valve V1 was opened, and progressively larger drawdowns were imposed by lowering the leveling arm from its highest position downwards in a stepwise fashion. A possible explanation for this unexpected behaviour became apparent during post-flight analysis of this test and is discussed in Section 4.3. The test was terminated at 175 minutes because of the unexpectedly low flow rates.

Figure 4.5 shows the in-flight measurements for test W4-b. This was the second test that used both water and oil as the pore fluids; the estimated water saturation was roughly 18% in this test. However, camera footage in T100 during the test showed some accumulation of water in the lower part of the tank. Hence, the 18% was slightly greater than the irreducible water saturation. No load cell measurements were obtained for this test because the load cells failed. The first 110 minutes of data did not yield any useful quantitative data. During the time interval, the fundamental problem was the fact that a measurable flow rate could not be achieved while the porous plug was in place. Various measures (e.g., stopping and starting the centrifuge, operating at increased rotary speeds, emptying tanks, opening-closing valves, shifting the entire leveling arm mechanism downwards slightly, partially removing the porous plug) were attempted, but all failed. Thus, it was not possible to obtain a baseline flow rate for the calculation of sandpack permeability and for comparison against post-sand production flow rates. Having abandoned attempts to achieve a baseline flow rate, target pressures were achieved at roughly 110 minutes, and the porous plug was removed from 122 to 132 minutes. Valve V1 was open continuously during plug removal and for roughly 45 minutes afterwards. The leveling arm was in a high position during plug removal and onwards to 145 minutes, resulting in a drawdown head of roughly 2 cm. A steady slurry rate of roughly 40 cm^3/min was observed during plug removal. Calculation of flow rate in the time interval immediately following plug removal is problematic because valve V3 was opened during much of this interval, in order to drain tank T100. Given that flow rate can only be calculated when valve V3 is closed (hence T100 pressure is rising), it was only possible to calculate flow rate for a brief interval between 136 and 137 minutes. Based on calculated rates in the 80 to 200 cm^3/min during this short interval, supplemented by the fact that ongoing drainage of tank T100 was required, it is

inferred that flow occurred continuously from 132 to 146 minutes. The average slurry flow rate curve shown in Figure 4.5 was estimated based on this assumption. From 146 to 179 minutes, the leveling arm was lowered in a series of small (roughly 2.7 cm) steps. As expected, with each increase in drawdown head an increase in slurry flow rate was observed (with the exception of an anomalous interval from 150 to 154 minutes where constant T100 pressure suggests that no flow occurred). The test was concluded with two cycles during which XDD conditions were achieved, by closing then opening valve V1 with the leveling arm in its lowest position. Near-identical slurry rates of roughly 360 cm^3/min were achieved during each of these XDD cycles. With no load cell measurements, it was not known if sand production was occurring during these cycles. Given that the rates were nearly the same, and sand production is expected to result in increased rates, it was suggested that sand production might have ceased. The experiment was terminated at 202 minutes in order to investigate the status of the sandpack and the sandtrap.

Figure 4.6 shows the in-flight measurements for test W4-c. This was the third test that used both water and oil at the pore fluids; the estimated water saturation was roughly 10% in this test, and it is suggested that only immobile (residual) water was present in the sandpack. Similar to test W4-b, the first 310 minutes of data did not yield any useful quantitative data because a measurable flow rate could not be achieved while the porous plug was in place, in spite of various remedial measures that were attempted. Having abandoned attempts to achieve a baseline flow rate, target pressures were achieved at roughly 310 minutes, and the porous plug was removed from 317 to 332 minutes. Valve V1 was closed during plug removal, hence a NDD condition existed. The load cell response shows that sand production occurred during plug removal. Further, the calculated wellbore head during plug removal reached a value several cm more than the reservoir pressure, which suggests the influx of sand lead to an increase of fluid level in the wellbore. At 333 minutes, valve V1 was opened while the leveling arm was in its uppermost position. This allowed the excess fluid level in the wellbore to flow into tank T100, at a calculated rate of roughly 300 cm^3/min. From 333 to 363 minutes, the leveling arm was lowered in a stepwise fashion (roughly 2 cm for four steps and a 2.6 cm step for the last step). For the first three steps, the flow rate increased slightly from one step to the next, as expected, reaching a peak of roughly 486 cm^3/min at a drawdown head of roughly 2 cm. For the last two steps, the flow rate reduced slightly, with a flow rate of roughly 336 cm^3/min observed at a drawdown of roughly 3.6 cm. Based on the load cell

response, it appears that sand production was occurring at a steady rate once valve V1 was opened at 333 minutes. Valve V1 was closed at 362 minutes, after which flow, and sand production ceased. The experiment was terminated at 368 minutes in order to investigate the status of the sandpack and the sandtrap.

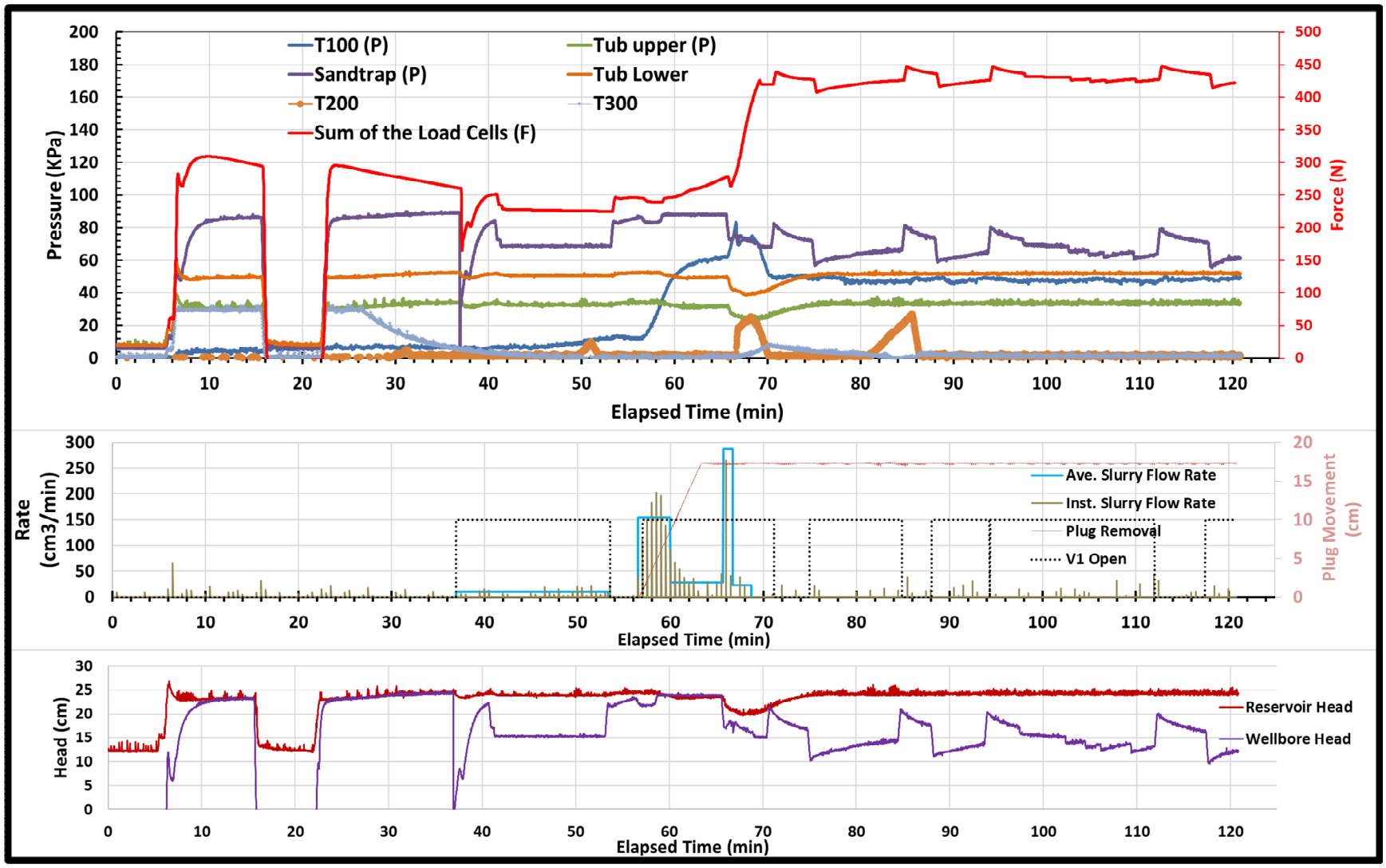

Figure 4.1. Recorded pressures, load cell sum, operational status (porous plug position, valve V1 status) and interpreted parameters (flow rates, scaled heads) for test V1. The centrifuge was not spinning between 0 to 6 minutes, and between 16 and 22 minutes.

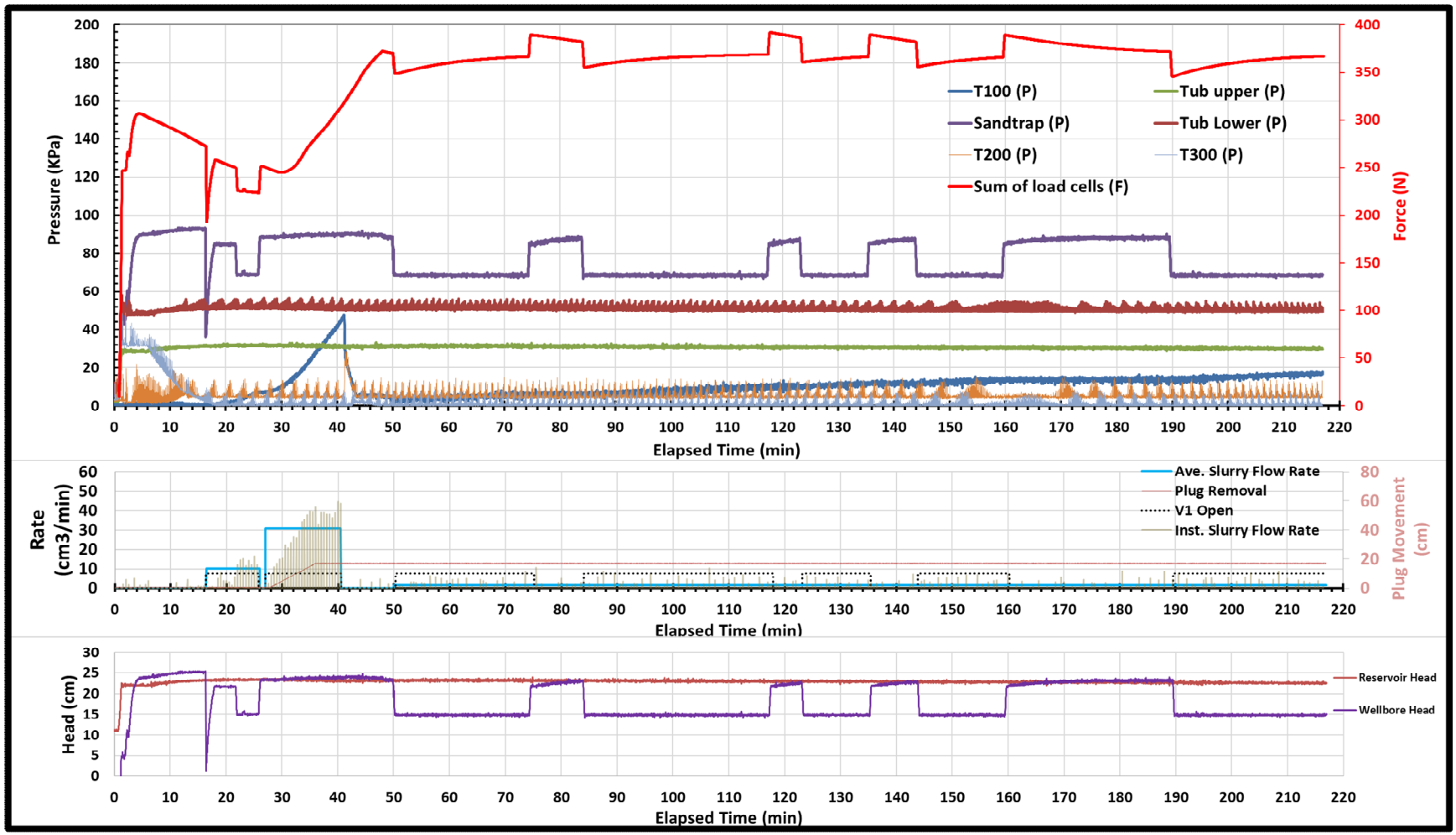

Figure 4.2. Recorded pressures, load cell sum, operational status (porous plug position, valve V1 status) and interpreted parameters (flow rates, scaled heads) for test G2.

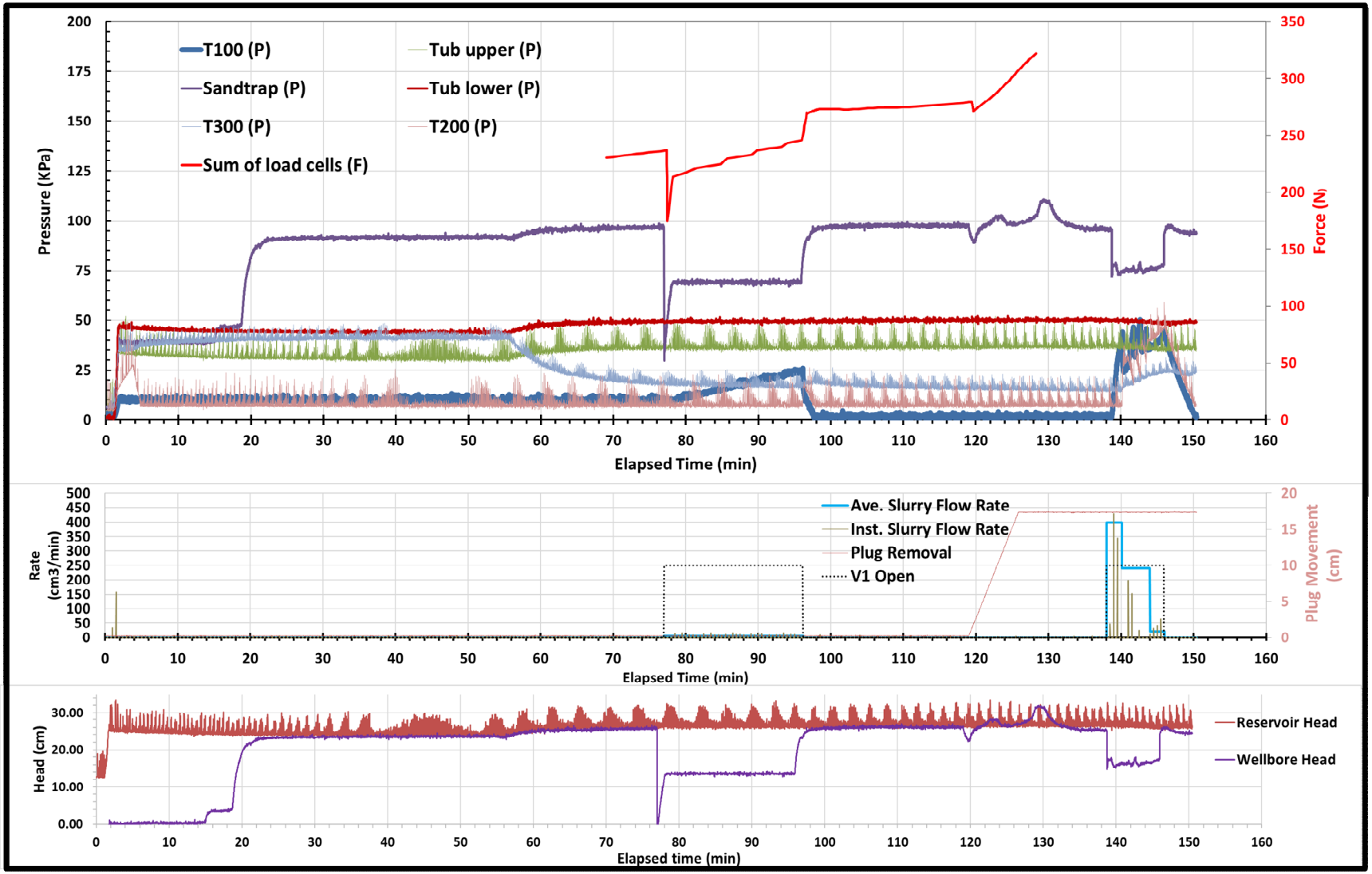

Figure 4.3. Recorded pressures, load cell sum, operational status (porous plug position, valve V1 status) and interpreted parameters (flow rates, scaled heads) for test C3. Early and late-time recordings of the load cell data were lost due to a problem with the data acquisition system.

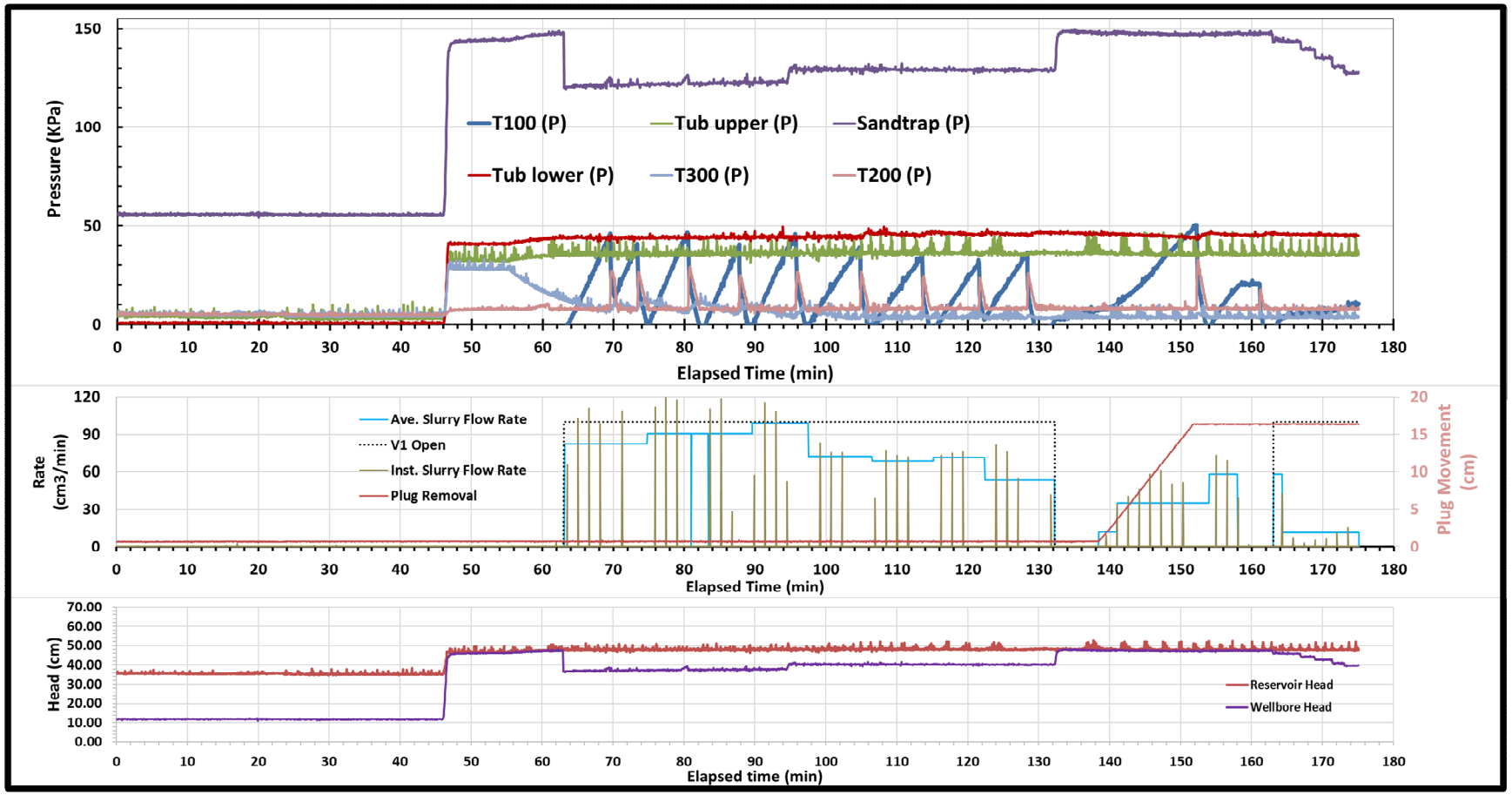

Figure 4.4. Recorded pressures, load cell sum, operational status (porous plug position, valve V1 status) and interpreted parameters (flow rates, scaled heads) for W4-a test. No load cell measurements were recorded due to an equipment failure.

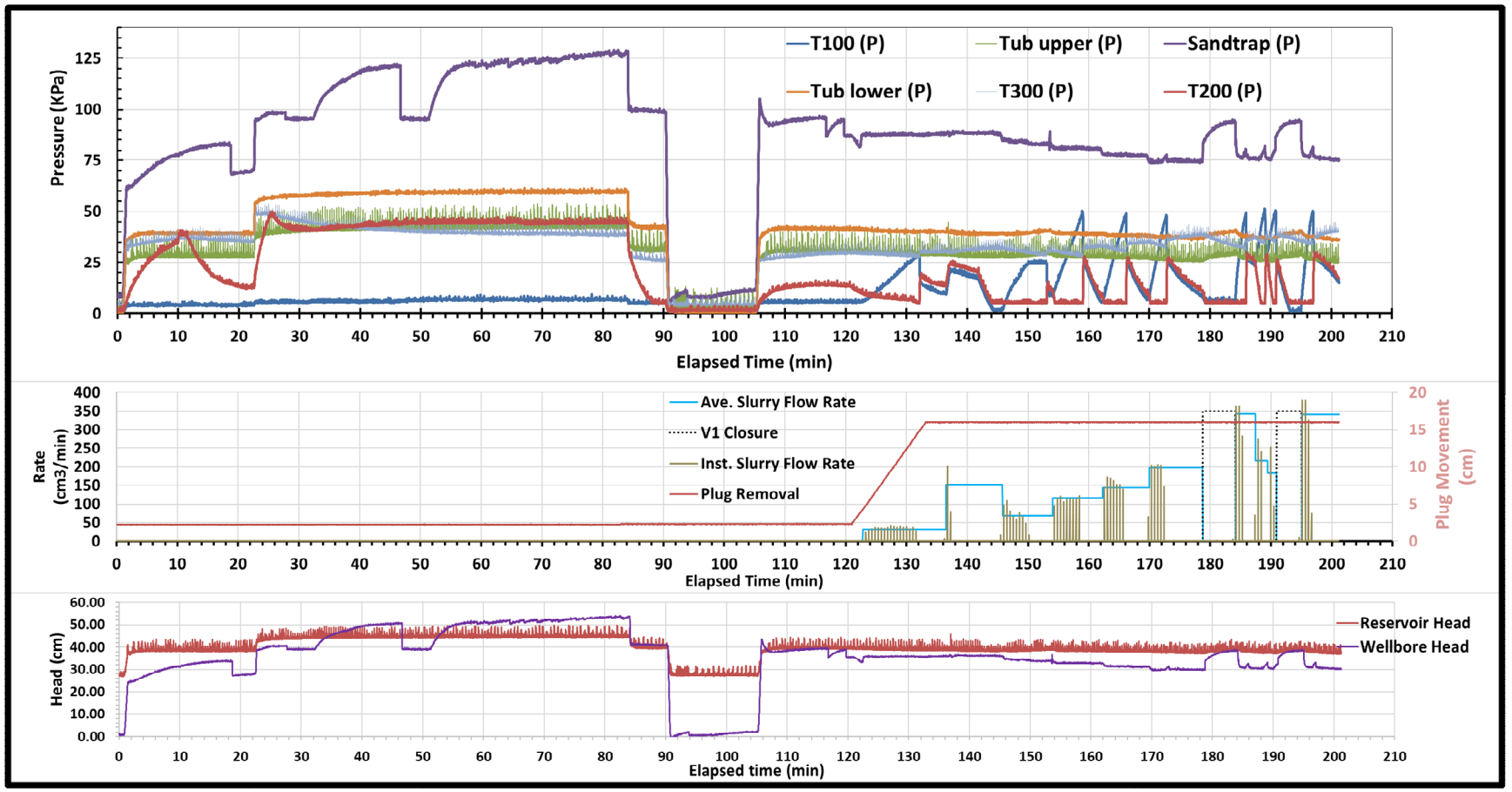

Figure 4.5. Recorded pressures, load cell sum, operational status (porous plug position, valve V1 status) and interpreted parameters (flow rates, scaled heads) for test W4-b. The centrifuge was not spinning between 90 and 106 minutes. Calculated heads from 34 to 46 minutes and 54 to 84 minutes are not accurate because the centrifuge was temporarily operating at increased rotary speed during these time intervals. No load cell measurements were recorded due to an equipment failure. Note that instantaneous flow rate can only be calculated when valve V3 is closed, and T100 pressure is increasing. For intervals where valve V3 is opened in order to drain tank T100, it is assumed that flow continues at a rate equal to the average rate calculated for the minutes preceding valve closure.

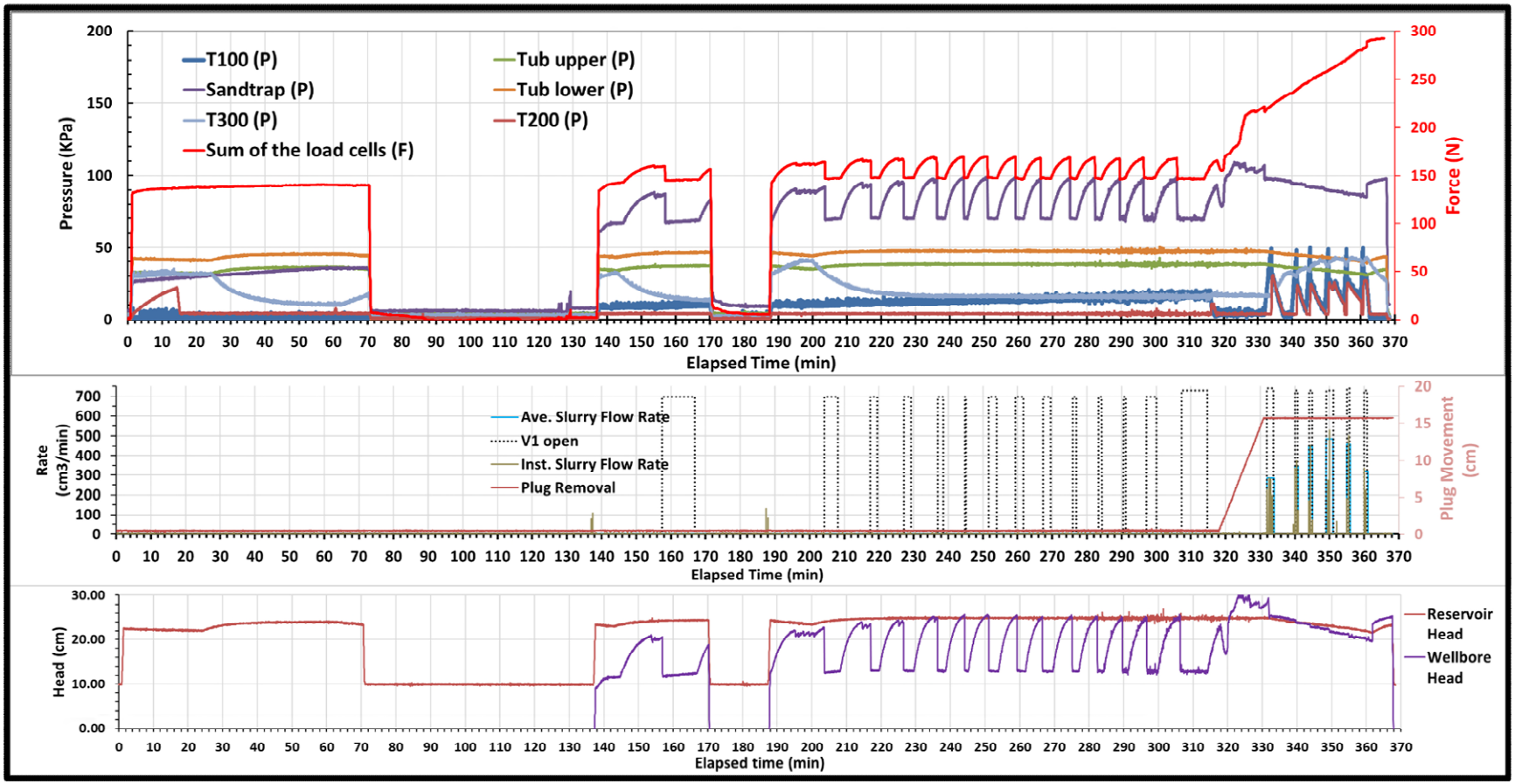

Figure 4.6. Recorded pressures, load cell sum, operational status (porous plug position, valve V1 status) and interpreted parameters (flow rates, scaled heads) for test W4-c. The centrifuge was not spinning between 70 and 13 minutes, and between 170 and 187 minutes.

4.1.3 Post-Flight Observations

Various post-flight observations and measurements made after disassembling the physical model are reported in this section. Photographs showing to top of the sandpacks after each test are shown in Figure 4.7, Figure 4.8, Figure 4.9, Figure 4.10, Figure 4.11 and Figure 4.12. The top surface of the sandpacks showed almost symmetrical cavities near the wellbore in all tests. Cross-sectional drawings of these cavities, based on averaged dimensions and slope angles measured for each test, are shown in Figure 4.13. The pink zones that are shown for tests V1 and W4-c represent estimates of the cavities that developed early in the test (i.e., upon removal of the porous plug). These predictions were based on the mass of sand initially produced as determined from calibrated load cell data, converted to a volume assuming densities measured after each of these tests, and assuming that the early cavities had the same geometries as the cavities that were observed at the end of these tests.

Test V1 is the only experiment for which erosion channels were observed on the top surface of the sandpack, extending from the perimeter of the cavity to the perimeter of the sandpack (see Figure 4.11). These were distinguished from other surface features (e.g., disturbance resulting from post-test removal of the caprock, gravel falling onto the sandpack from the top of perimeter of the tub, wrinkles imprinted by the plastic sheet separating the sandpack from the caprock for tests C3 onwards) by the localised absence of the blue dyed rings that had been emplaced on top of the sandpack prior to the experiment. These erosion channels are similar to features observed during early tests using the equipment (Pereira 2021). Reasons for the absence of these features in test G2 and all later tests are discussed in Section 4.2.

Test W4-b is the only experiment in which a feature resembling a wormhole was observed, as shown in Figure 4.11. The tip of a tube-like cavity was observed near the upper edge of the cavity. To the naked eye, it seems that it did not penetrate more than several mm into the sandpack. The Technician excavating this sandpack did not record any observations of and extension of this feature extending from the cavity to the outer perimeter of the sandpack. As such, it is unknown if this tip represents the beginning of a wormhole that was in the early stages of growth when the experiment was terminated, or whether it had been fully developed yet collapsed when the experiment terminated. Either way, there is evidence that the feature served as a preferential

conduit for flow during the experiment, based on the path of the erosion channel extending from the feature to the wellbore. More specifically: this channel had developed post-test, it would have followed a straight path from the wormhole tip to the wellbore, following the maximum slope of the cavity surface. However, the curved shape of the channel suggests that fluid flowed out of this tip while the centrifuge was spinning, resulting in a curved shape due to the Coriolis effect.

The post-test locations and conditions of coloured rings emplaced within the sandpack in tests C3, W4-b and W4-c are shown and discussed in Table 4.1. The rings emplaced for test W4-a were not effective because they dissolved in the water added to the sandpack for this test. For tests W4-b and W4-c, non water-soluble coloured sand (Activa Scenic Sand) was used for the rings.

Densities measured on Shelby tube samples taken at various locations from test C3 onward are summarized in Table 4.2. These densities were measured on the samples in their post-test condition, after gravity drainage of the sandpack at 1×G. The samples appeared to be nearly saturated, but this was not verified. The greatest value of these samples was to allow a relative comparison of densities throughout the sandpack. The results consistently suggest near-well densities roughly 100 kg/m^3 (5%) less than densities measured near the outer boundary of the sandpack.

A compilation of key experimental results recorded for all tests is given in Table 4.3

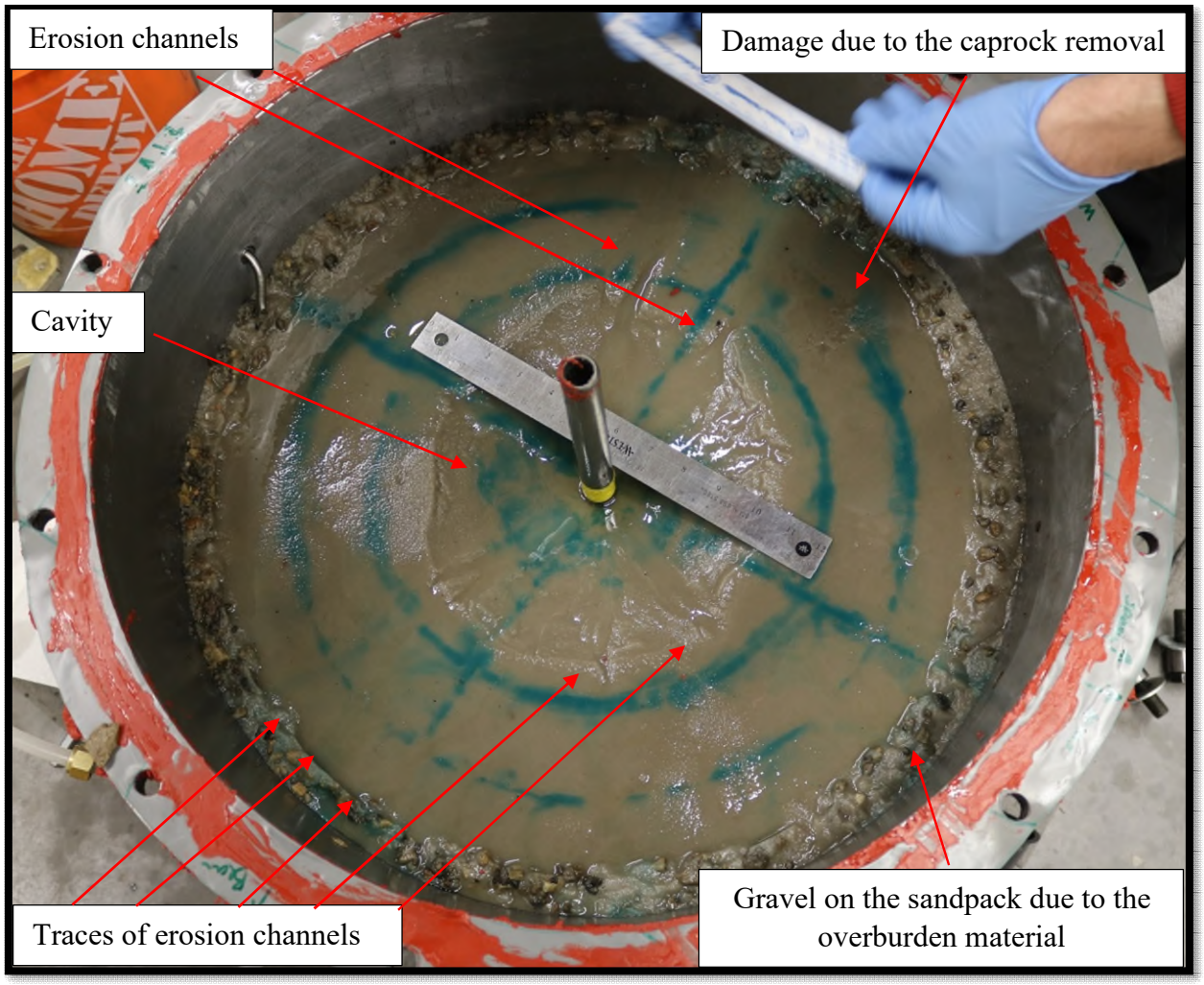

Figure 4.7. The top of the sandpack following test V1. The top diameter of the cavity was measured at 24 cm (average) with a depth of 4.6 cm. The mass of produced sand recovered in and above the sandpack was measured to be 1.4 kg, after drying the sand.

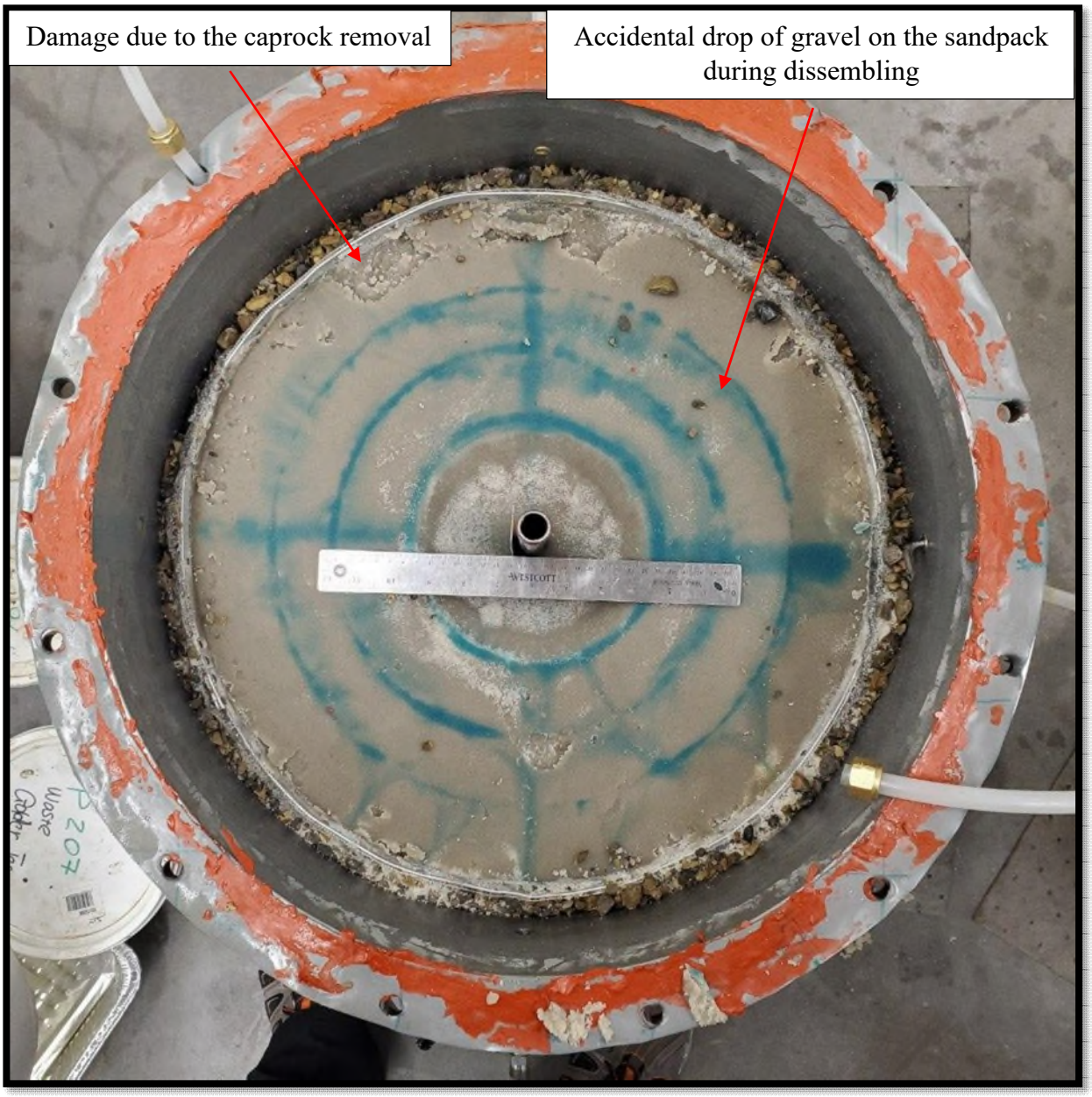

Figure 4.8. The top of the sandpack following test G2. The top diameter of the cavity was measured at 17 cm (average) with a depth of 5.5 cm. The mass of produced sand was not recorded.

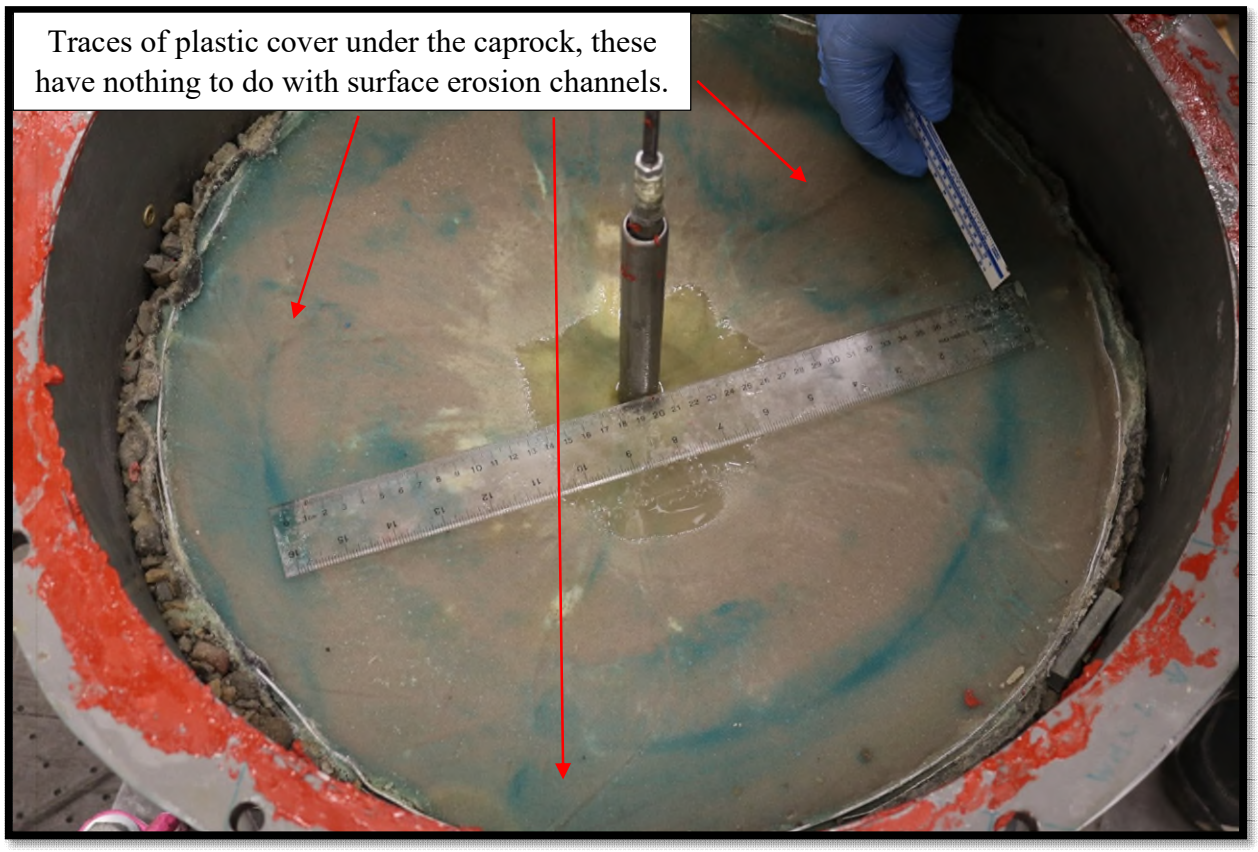

Figure 4.9. The top of the sandpack following test C3. The top diameter of the cavity was measured at 13 cm (average) with a depth of 3 cm. The dry mass of produced dry sand was 3.6 kg.

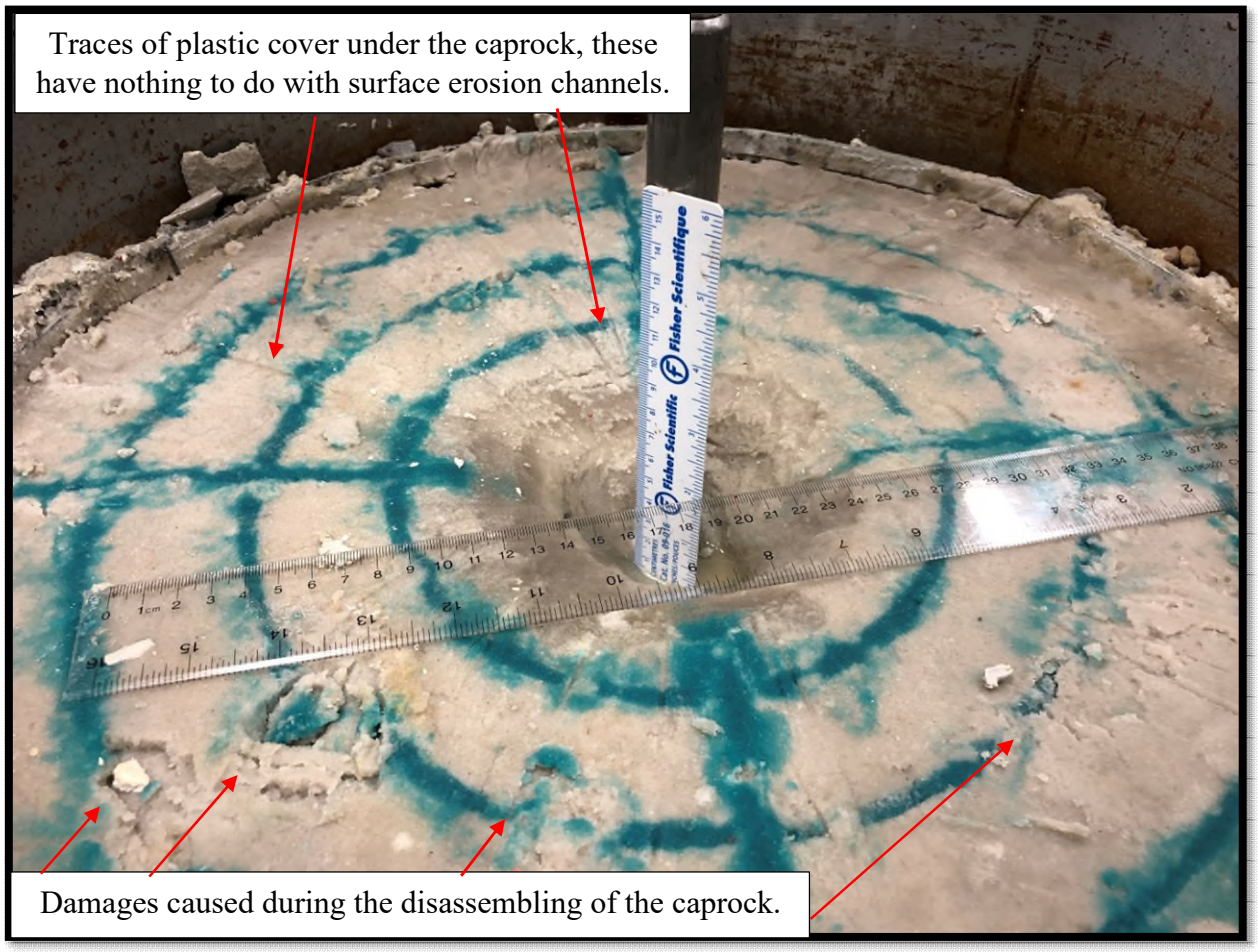

Figure 4.10. The top of the sandpack following test W4-a. The top diameter of the cavity was measured at 13 cm (average) with a depth of 4.8 cm. The dry mass of produced sand was 0.43 kg.

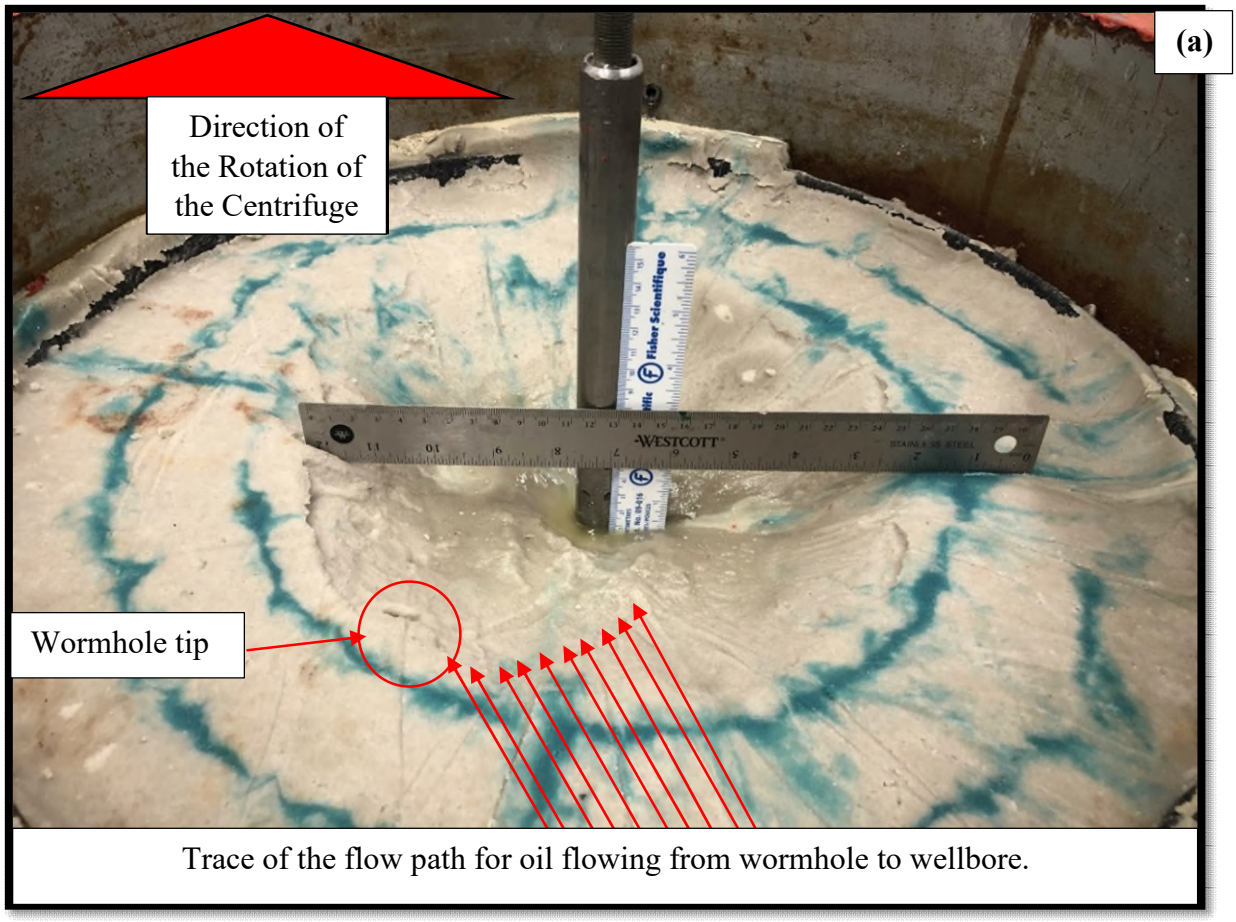

Trace of the flow path for oil flowing from wormhole to wellbore.

Figure 4.11. (a) The top of the sandpack following test W4-b. The top diameter of the cavity was measured at 28 cm (average) with a depth of 5.7 cm. The dry mass of produced dry sand was 3.5 kg. (b) Front view of the wormhole tip observed for this test.

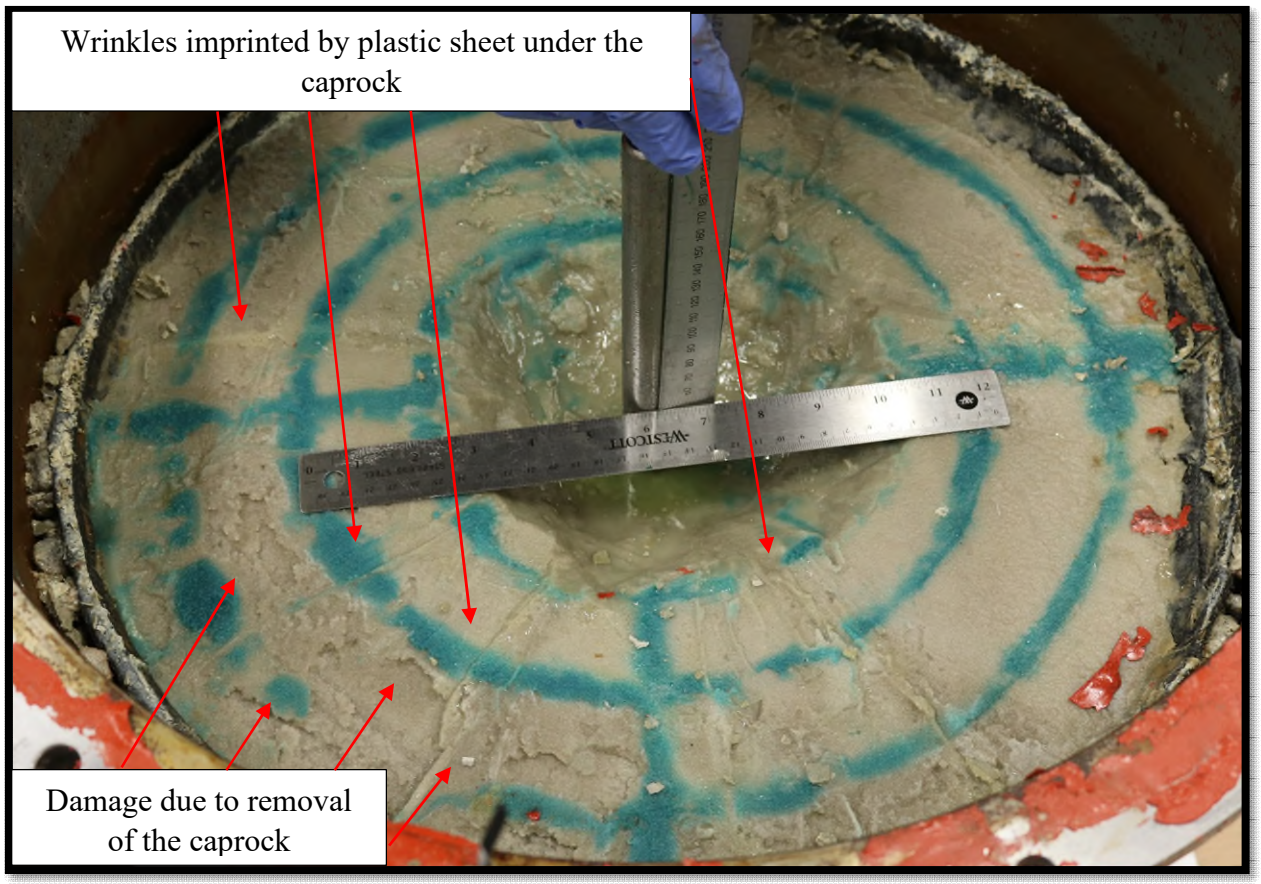

Figure 4.12. The top of the sandpack for test W4-c. The top diameter of the cavity was measured at 18 cm (average) with a depth of 5 cm. The dry mass of produced sand was 1.8 kg.

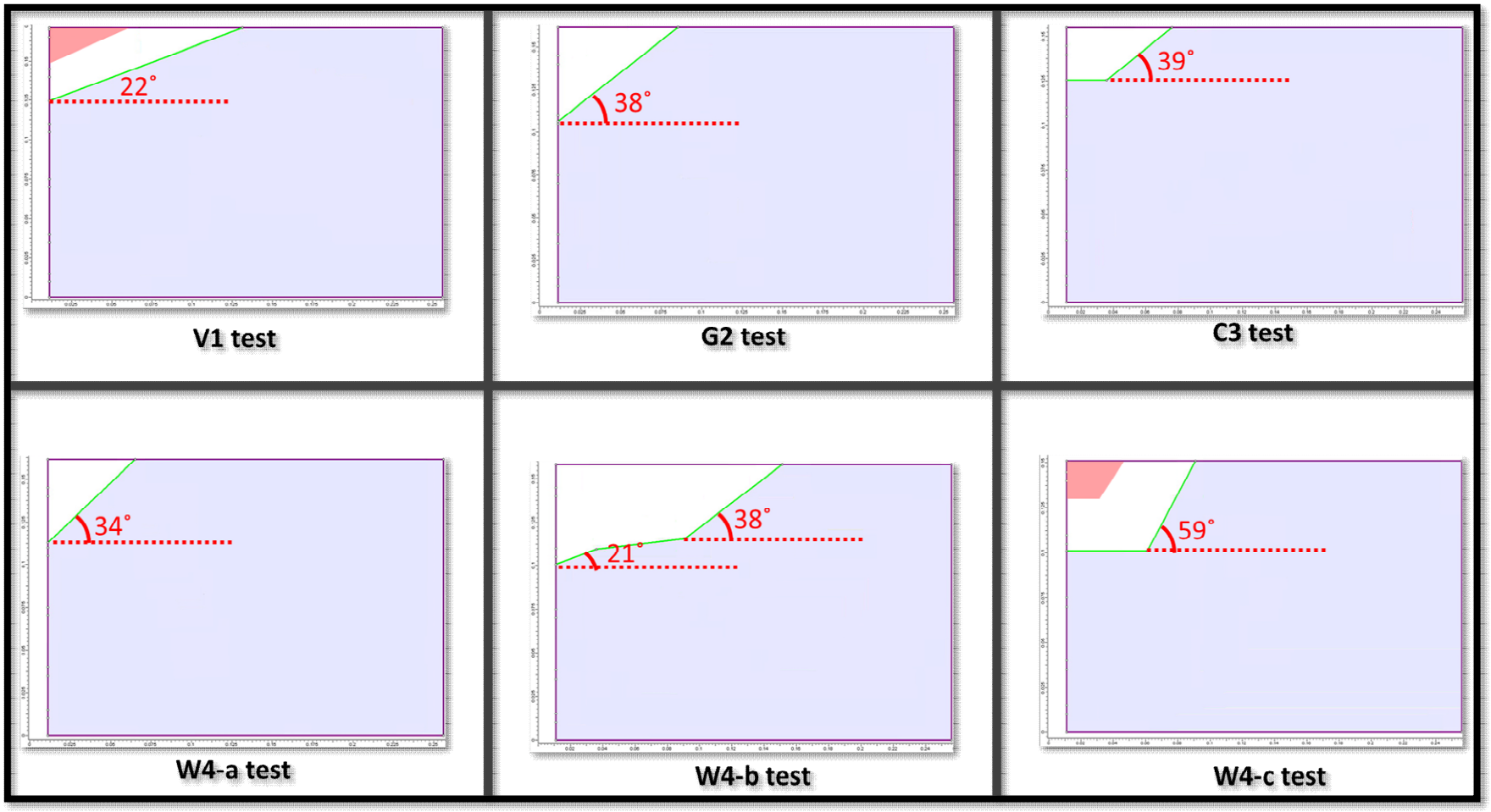

Figure 4.13. Scaled drawings of average cavity geometries for all the tests, generated using the model-builder in RocScience RS2.

Table 4.1. Location of coloured rings observed during sandpack excavation

Test ID	Observation	Photo
C3	The red and green rings that were placed 50 mm above the base of the sandpack were absent. The blue ring that was placed 100 mm above the base of the sandpack, with a radius of 40 mm, was absent. The yellow ring originally placed 100 mm above the base of the sandpack, with a radius of 60 mm, was present. However, it had shifted over 50 mm downwards and some distance radially inwards. This suggests large-scale sand production in the lower part of the sandpack and near-well sand production in the middle part.	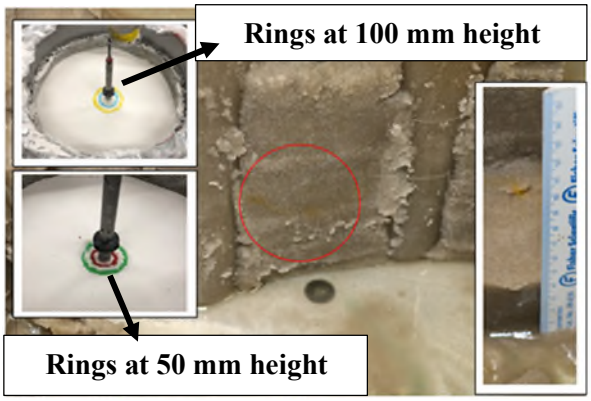
W4-b	The dark blue ring (50 mm height, 60 mm radius) and red ring (100 mm depth, 60 mm radius) were not displaced or disturbed. The orange ring (50 mm height, 40 mm radius) was also not displaced or disturbed. However, the green ring (100 mm height, 40 mm radius) was absent. This suggests that sand production was localized to the near-well area at mid to upper heights in the sandpack.	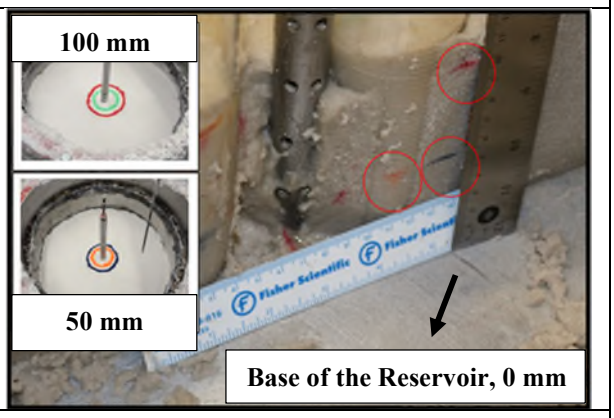
W4-c	Effectively same results as test W4-b, although different colours were used. Both outer rings (red-lower, light blue-upper) were undisturbed and undisplaced, as well as the inner & lower (dark blue) ring. The inner & upper (red) ring was absent. Additionally, orange and green rings were placed at the base of the sandpack for this test, and both were undisturbed and undisplaced. As shown in Figure 4.12, the blue rings on the top of the sandpack were largely present (though displaced downwards, following the cavity surface), which suggests the cavity initially developed by subsidence downwards into space vacated by sand production near perforations at mid-upper heights.	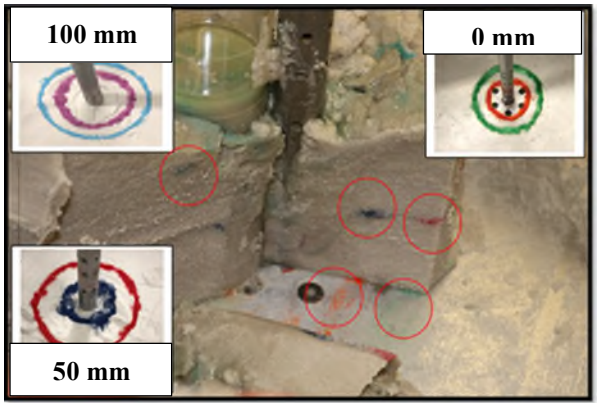

Table 4.2. Summary of the bulk densities recorded post-test from test C3 onward.

Test ID	Average Density after Sand Production kg/m^3			Locations of Shelby Tubes
	Shelby Tube I	Shelby Tube II	Shelby Tube III	
C3	2114	2174	2277	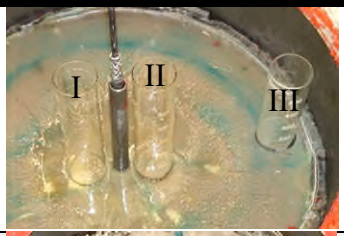
W4-a	1795	1802	1880	
W4-b	1808	1820	1904	
W4-c	1841	1875	1972	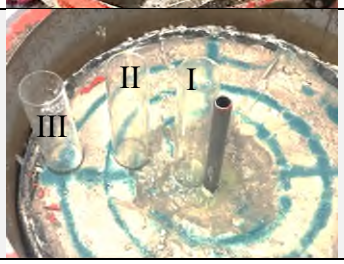

Table 4.3. Key experimental results for C-CHOPS tests

Data	V1	G2	C3	W4-a	W4-b	W4-c
Height of Sand after Pluviation, cm	17.4	16.2	17.4	16.1	16.7	16.0
Dry Sand Density, kg/m^3	1705	1715	1725	1668*	1638	1445*
Density after Saturation, kg/m^3	1870	1840	1870	2082*	1810	1755*
Oil Density, kg/m^3	923	923	923	923	923	923
Porosity, %	36	37	35	37*	38	45*
Downward Movement of Leveling Arm during Max Flow Rate, cm	16	0	16	0	16	2
Reservoir Head, m	0.24	0.24	0.24	0.24	0.24	0.24
ΔH during Max Flow Rate, m	0.13	0	0.13	0	0.13	0.01
Water Saturation, %	0	0	0	77*	18	10*
Max Liquid Flow Rate before PR, cm^3/min	8	10	6	99	N/A	N/A
Max Ave. Slurry Rate after PR, cm^3/min	287	31	400	58	345	485
Permeability before PR, D	1.1	1.9	1.5	0.21	N/A	N/A
Dry Mass of Produced Sand, kg	1.4	N/A+	3.6	0.43	3.5	1.8
Estimated Dry Mass of Sand from Cavity using Dry Density, kg	1.2	0.7	0.21	0.3	1.9	0.7
Cavity Present	Yes	Yes	Yes	Yes	Yes	Yes
Erosion Channel(s) Present	Yes	No	No	No	No	No
Wormhole(s) Present	No	No	No	No	Yes	No
Cavity Depth, cm	4.6	5.5	3	4.8	5.7	5
Cavity Diameter, cm	24	17	13	13	28	18
Max Side Slope of the Cavity, º	22	38	39	34	38	59
Min Side Slope of the Cavity, º	22	38	0	34	21	0
Location of Sanding during PR	N/A	N/A	Bot.	N/A	Bot.	Bot.
Location of Sanding after PR^	N/A	N/A	Bot.	N/A	Top	Top
Mass of Overburden on the Caprock, kg	24	24	71.5	89	74.5	84
Mass of Caprock, kg	20	20	17.5	17.5+	17.5+	14.5
Wellbore/sandtrap Blockage During Sand Production	Yes	Yes	Yes	No	No	No

*Density measurement reported by technical staff has some degree of error which has impacted the porosity and water saturation values

+Mass was not recorded by technical staff

^Based on tracking the color rings embedded in the sandpack.

4.2 NUMERICAL MODELLING

To provide some context to support the interpretation of experimental results, RocScience RS2 was used to conduct some numerical modelling of selected CHOPS experimental scenarios. RS2 is a 2-dimensional finite element program capable of stress analysis and seepage analysis. Given the challenges of modelling the complex, transient processes occurring during sand production, the models were constructed to represent conditions prior to sand production, and conditions at the end of an experiment. More specifically, the two scenarios considered were the following:

1. Stress analysis to characterize conditions immediately upon removal of the porous plug; i.e., prior to the onset of sand production. No fluid flow was occurring at this stage of the experiment; hence seepage analysis was not included in this modelling;

2. Seepage analysis to characterize flow conditions at the end of an experiment. Stress analyses for this late-test condition were attempted, but the results were not helpful. In part because stresses and sandpack stability at this stage are extremely sensitive to boundary conditions at the caprock-wellbore interface, which is poorly defined in the physical model; also, because most post-cavity stress-analysis models were unable to converge due to acute stress concentrations near the edges of the cavity. In spite of this limitation, stand-alone seepage analyses were possible and yielded results that were helpful for interpreting the physical modelling results.

The model inputs were compiled based on test W4-c because of the relatively complete dataset for this experiment, and because it included all of the testing innovations included in this research (i.e., a sandpack surrounded by gravel, a flexible caprock, and two-phase fluid saturation).

The results presented here were generated using a numerical model with a spatial domain that matched the dimensions of the physical model, using mechanical and hydraulic boundary conditions that also match the physical model, and specific weights for the sandpack and canola oil that were adjusted to account for the hypergravity environment. Numerical models representative of the prototype were also developed and generated similar results (e.g., in terms of yielding, and stress and pore pressure distributions); however, these results are not shown here. The main motivation for the numerical modelling was to provide results that could be compared to the physical model, and provide insights on selected mechanisms underlying its performance.

Assumptions which are common to both models were as follows:

1. Axisymmetric geometry, as illustrated in Figure 4.16;
2. Homogeneous, isotropic and continuous material properties;
3. A 25×G hypergravity environment exists through the entire model domain.

Major assumptions specific to the pre-sanding stress analysis are:

1. The material model is linear elastic – perfectly plastic;
2. Hydraulic head is uniform throughout the model domain (i.e., no-flow condition); with no coupling between pore pressures and mechanical deformation;
3. Deformation and yielding are governed by effective stresses;
4. Effective stress = total stress – pore (oil) pressure (the effects of capillary pressures are accounted for as apparent cohesion and apparent tensile strength, rather than including capillary pressures in the representation of effective stress);
5. Porous plug removal is instantaneous, and does not generate any pressure reduction (swabbing effect) in the wellbore;
6. Given the axisymmetric nature of the model, perforations are represented as slits (i.e., openings that extend around the entire perimeter of the wellbore).

Major assumptions specific to the post-sanding seepage analysis are:

1. Steady state, single-phase flow conditions;
2. Density, porosity and hydraulic conductivity for the W4-c test are the same as test C3, because these parameters were either unavailable or of poor quality for test W4-c;
3. The cavity geometry during the flowing, hypergravity stage of the experiment was the same as the geometry observed when the test was terminated and dismantled at 1×G conditions.

Additional details regarding model input parameters, boundary conditions and simplifying assumptions can be found in Appendix G (stress analysis) and Appendix H (seepage analysis).

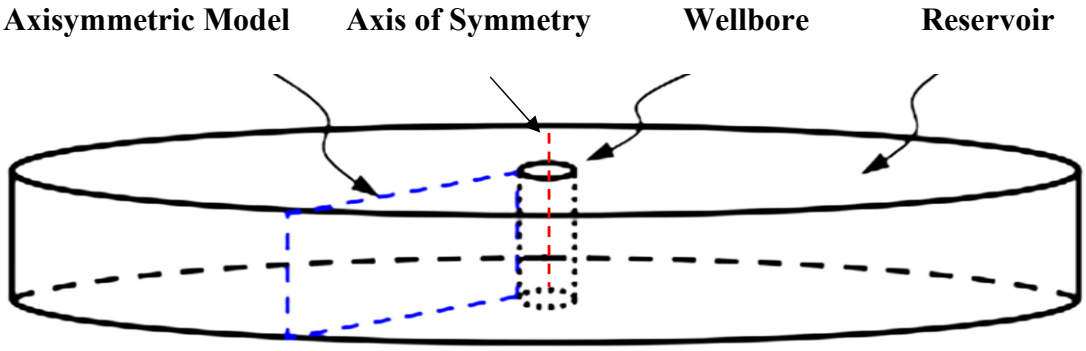

Figure 4.14. Axisymmetric model after Choi (2011)

4.2.1 Stress Analysis Before Drawdown

The objectives of this modelling were to investigate stresses and yielded zones in the sandpack at the beginning of an experiment, and to assess how a 2 kPa capillary cohesion affects the yielded zones. To this end, one model with cohesion (2 kPa) and another model without cohesion (0 kPa) were built. [For additional consideration of the effects of capillary cohesion, see the analytical model presented in Section 2.10.2 and implemented in Appendix B.]

Predicted maximum plastic shear strains for both models are shown in Figure 4.15. Though there is a subtle difference in the results, both scenarios show that there is significant shear displacement and of the sand close to the perforations, in addition to a well-defined shear band of greater radial extent near the top of the sandpack. These zones of high shear strain are deemed likely to be disturbed and prone to sand production. Figure 4.16 is the same as Figure 4.15, with the addition of yielded elements being denoted with a red X. Interestingly, the shapes of the yielded zones in the upper part of both models are similar to the cavities seen in CHOPS tests. Also, from these figures, the radius of the yielded zone on top of the sandpack is much smaller in the scenario with cohesion (115 mm) compared to the one without cohesion (187 mm).

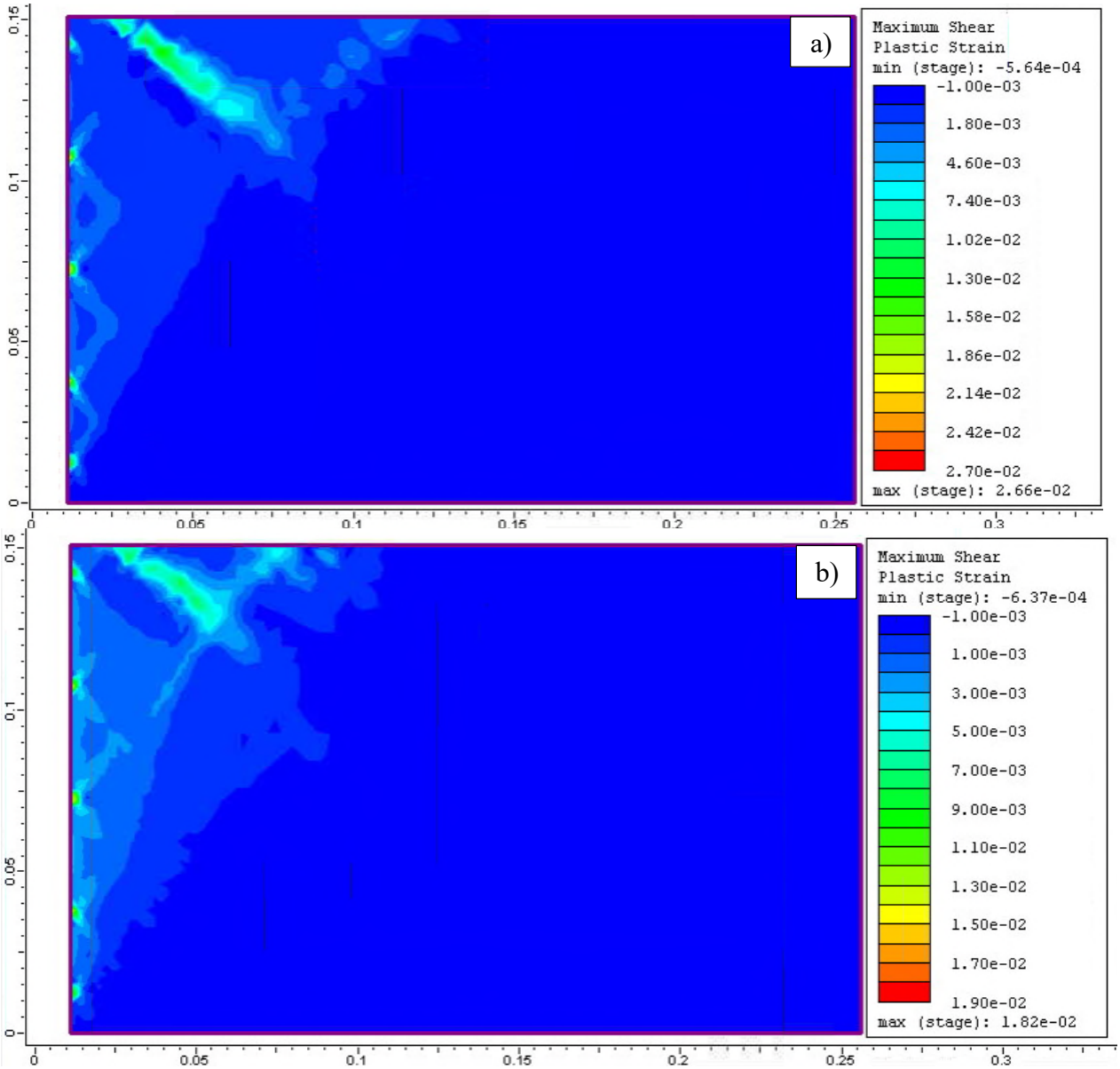

Figure 4.15. Maximum shear plastic strain for a) 0 kPa cohesion model b) 2 kPa cohesion model. Bright spots along the wellbore (left edge of model) correspond to perforations.

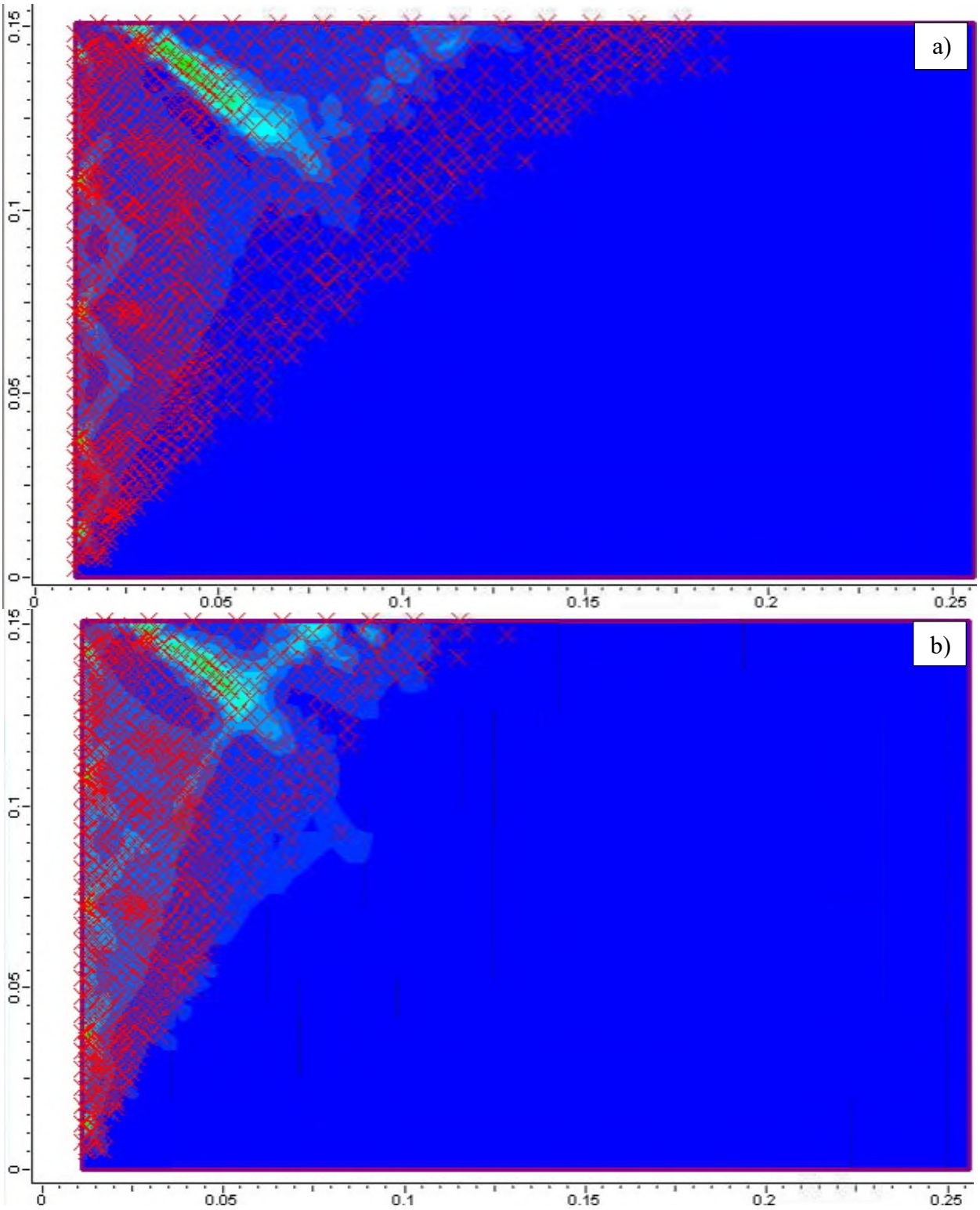

Figure 4.16. Predicted yielded elements (denoted with a red X) for a) 0 kPa cohesion model; and b) 2 kPa cohesion model.

4.2.2 Seepage Analyses After Cavity Development

The objective of this modelling was to study whether altered hydraulic conductivity of the yielded (i.e., remolded) zones around the wellbore/cavity have an important effect on high flowrates that were observed after sand production in test W4-c. Two scenarios were considered for this modelling as follows:

1. A remolded zone with increased hydraulic conductivity exists near the wellbore, due to dilation of sand near the perforations. See "Remolded Zone I" in Figure 4.17;
2. An additional zone with increased hydraulic conductivity exists over a broader area beneath the cavity (where stresses will be lower due to the lack of direct transfer of vertical stresses from the caprock to the sandpack) and around the cavity (due to dilation of sand in this zone of high shear stress) See "Remolded Zone II" in Figure 4.17.

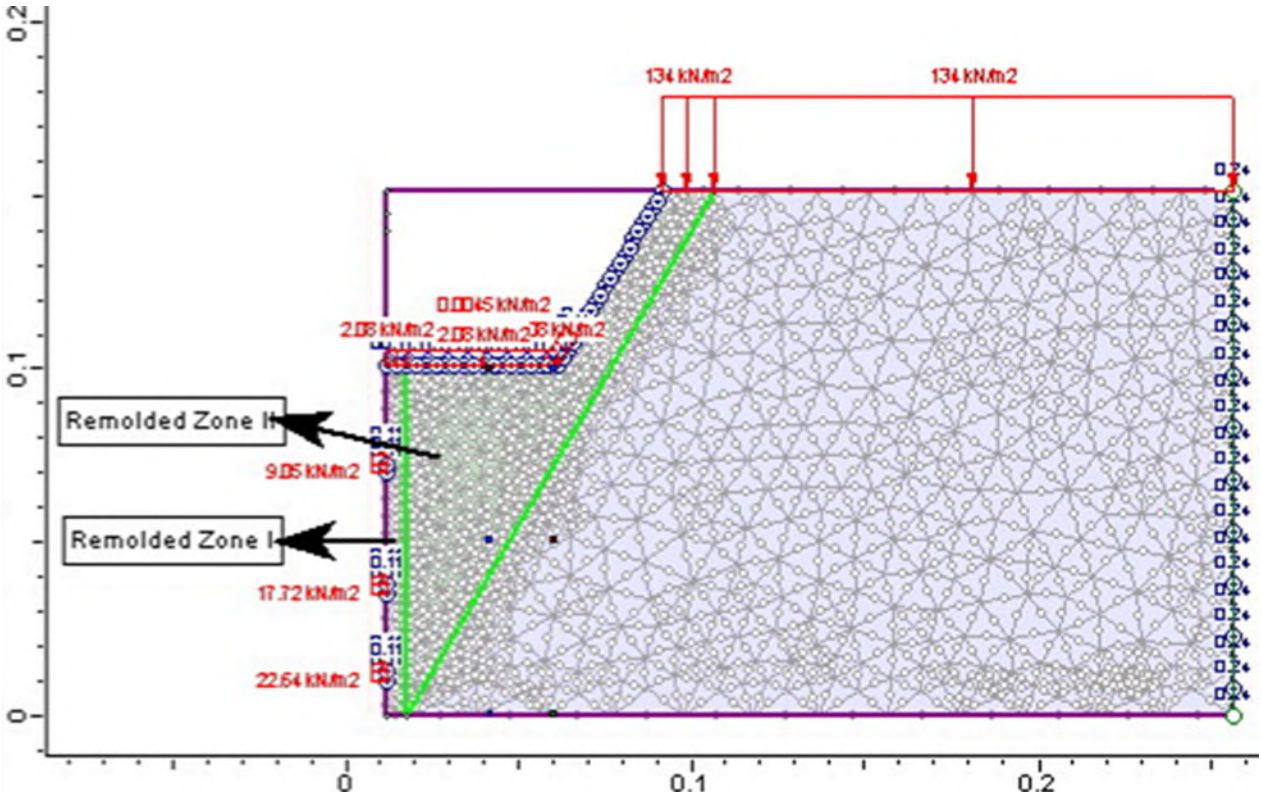

Figure 4.17. The modified model with remolded zones for W4-c test

It was assumed that the hydraulic conductivity of rest of the reservoir is similar to the condition before sand production, and that hydraulic conductivity might increase in the remolded zones due to dilation during yielding.

Figure 4.18 show the results of both scenarios, for a series of simulations where hydraulic conductivities of the remolded zones were progressively increased. These results show that it was impossible for either scenario to match the observed experimental flowrate for test W4-c, regardless of the assumed hydraulic conductivity in the remolded zones. This suggests that additional factors influence (enhance) flow rate during these experiments; potential factors will be discussed in Section 4.3.

The seepage analysis conducted in this research was also useful for confirming flow paths that develop in the presence of a cavity. More specifically, consistent with expectations and with the seepage analyses presented by Pereira (2021), flow preferentially occurs towards the cavity (see Appendix H). This occurs because the flow path from the outer perimeter of the sandpack to the cavity is short relative to flow paths towards the lower parts of the wellbore that are surrounded by sand (even if the near-well sand has enhanced permeability due to shearing and dilation).

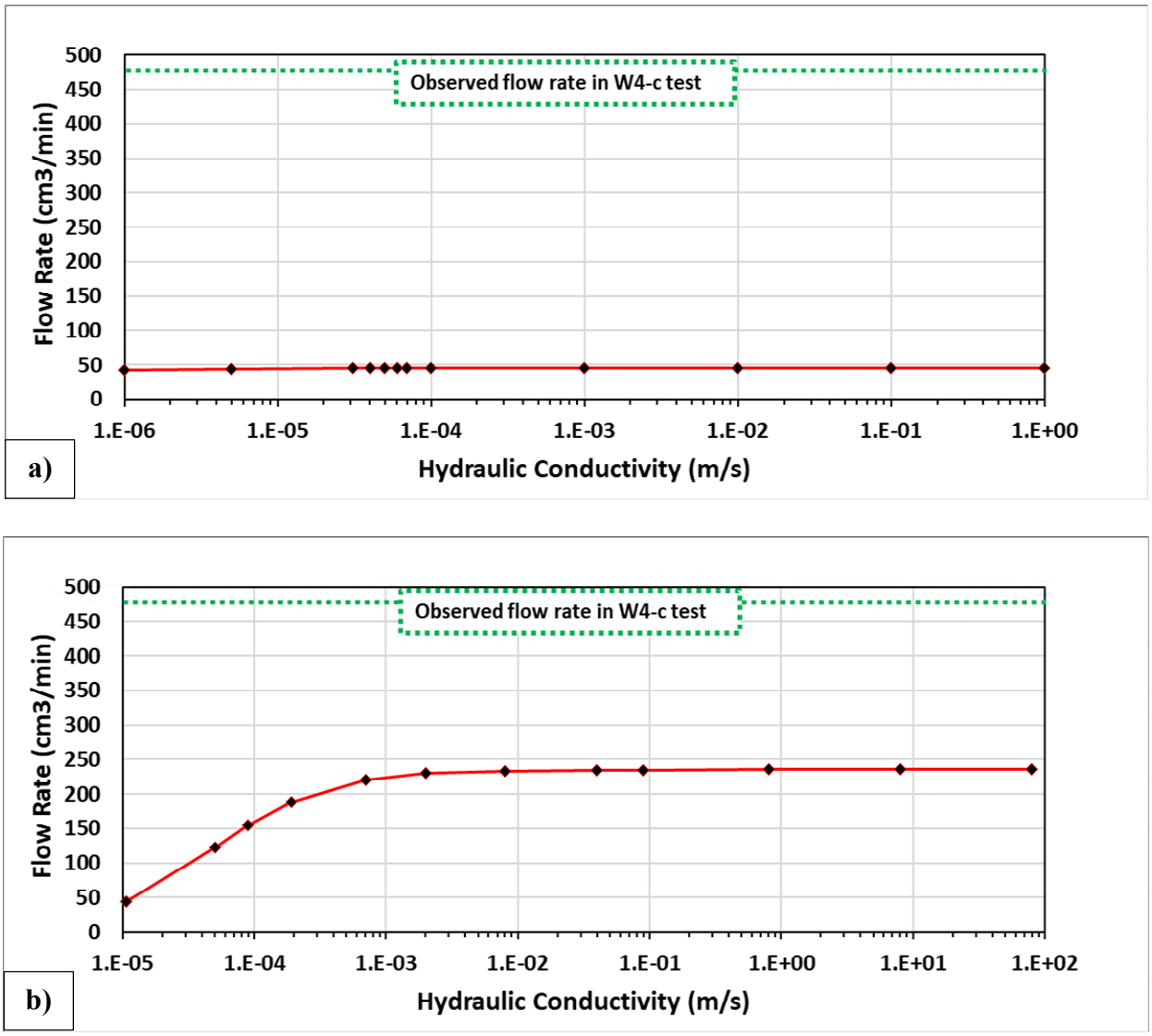

Figure 4.18. Predicted oil flow rates as a function of remolded zone hydraulic conductivity for scenarios with: a) Remolded zone I alone has altered hydraulic conductivity b) Remolded zones I and II have altered hydraulic conductivities. For comparison purposes, the observed flow rate for test W4-c is shown, and it is observed to be hundreds of cm^3/min greater than any of the model scenarios.

4.3 Discussion

4.3.1 Conceptual Model

A general conceptual model based on the experimental and numerical modelling results is presented in this section, then subsequent sections discuss the results of each specific test in the context of this conceptual model. The conceptual model is illustrated in Figure 4.19, and the various stages presented in this figure are explained as follows:

a. Prior to spinning the centrifuge, wellbore plug in place and no drawdown. Stresses are relatively low. Effective vertical stress at any point is due solely to the weight of overlying materials (→ total vertical stress) and weight of overlying pore fluid (→ pore pressure). Effective horizontal stresses are isotropic; i.e., a fraction of the effective vertical stress estimated assuming rigid lateral boundaries for sandpack (at-rest lateral earth pressure coefficient).

b. Wellbore plug still in place and no drawdown created, but centrifuge is spinning to create hypergravity environment. Similar to conditions at stage a, but effective vertical stresses increased due to hypergravity, and effective horizontal stresses increased proportionally according to lateral earth pressure coefficient.

c1. Same as stage b, but the wellbore plug has been removed. The rigid support formerly provided by the plug is replaced by lesser and compliant support provided by fluid pressure in the wellbore. The effective stress acting in the radial direction becomes relatively small and the effective stress acting in the plane tangent to sand-face becomes relatively large, resulting in plastic shearing and dilation. Some of this yielded sand flows into the wellbore, resulting in sand production.

c2. Same as stage c1, after some sand has been produced into the wellbore. Due to the force of hypergravity acting towards the base of the sandpack, near-wellbore sand from the upper part of the sandpack will displace downwards (subsidence) as underlying sand flows into the wellbore. This results in the development of a cavity. Sand production might cease by arching or bridging mechanisms, depending on the residual strength of the yielded sand. Because no drawdown pressure (or head) has been created,

no seepage forces are acting. With sufficient arching/bridging, a stable condition might be achieved; otherwise, sand production and subsidence might continue, and the cavity will continue to grow.

d. A drawdown condition is created by reducing the fluid pressure (or head) in the wellbore. This promotes seepage-induced failure, and additional sand production. Fluid will flow preferentially towards the cavity because this is the path of least resistance (shortest flow path) to the wellbore. Seepage-induced failure will be greatest where mean stresses are relatively low and fluid velocities are relatively high, hence sand production will occur preferentially around the cavity, resulting in cavity growth. High shear stresses along the sloping surface of the cavity may exist and enhance the seepage-induced failure.

e. During the late stage of the test, most of the flow is directed towards the cavity in the upper part of the reservoir. Whether the cavity has stabilized (or would have continued growing) at the end of the experiment is a complex function of the mechanical interaction of the caprock with the sandpack, and the magnitude and nature of seepage-induced forces. The term nature is used to denote the difference between relatively homogeneous flow conditions, hence uniformly distributed seepage forces, versus a condition in which most of the flow occurs along localized flow path(s) such as wormholes or erosion channels. More specifically, cavity growth may be mitigated if localized flow path develops, hence reducing the seepage forces acting on the full surface-area of the cavity.

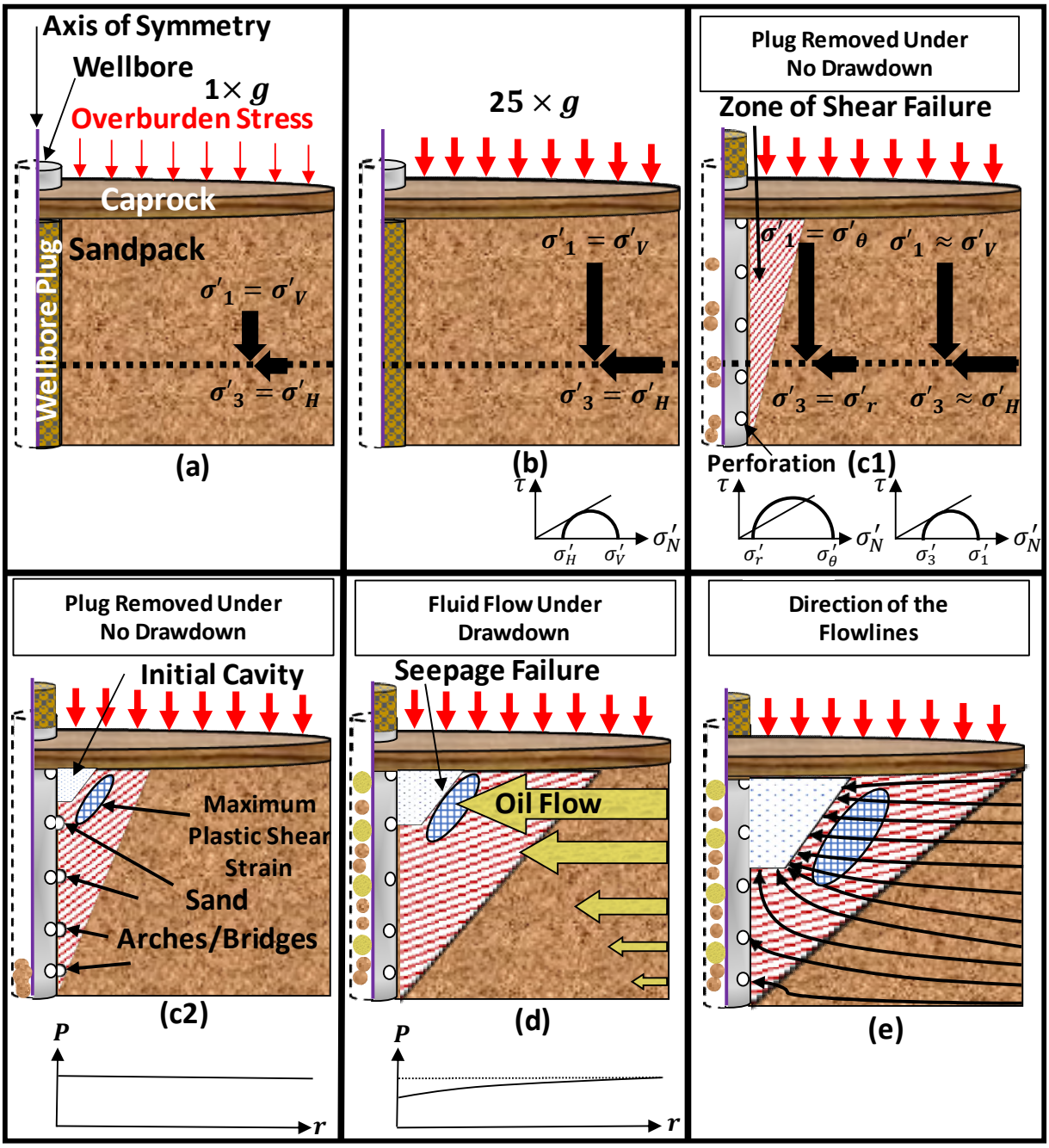

Figure 4.19. Conceptual model illustrating mechanical and flow processes occurring during C-CHOPS experiments. σ'_r and σ'_θ in (c1) denote effective radial and tangential stresses that develop in the sandpack adjacent to each perforation.

4.3.2 V1 Test

The sand production in this test increased slurry flowrate from 8 cm^3/min (prior to sanding) to 287 cm^3/min, which supports the idea that sand production increases production rates in heavy oil reservoirs in weak sands. Significant sand production occurred during plug removal (PR) and based on the load cell it appears that sand production was ongoing when drawdown conditions were created. After creating a drawdown, the aforenoted maximum rate was achieved, but flow rapidly tapered off to zero; not because of conditions in the sandpack, but because the flow system became blocked. These observations are consistent with the conceptual model, for a scenario in which sand strength was too low to develop pseudo-stable arches around the perforations. The relatively low sand strength is consistent with the absence of capillary cohesion in this test, which used single-phase (oil) saturation.

This is the only experiment in which erosion channels developed at the caprock-sandpack interface. This may be explained by the fact that this was the only experiment that did not use a gravel pack around the perimeter of the sandpack. As such, from the outset of this experiment fluid would have flowed preferentially near the top of the sandpack. This initial predisposition for preferential flow, enhanced by the development of a broad cavity (the second-largest cavity diameter observed, with test W4-b being the largest), resulted in high flow velocities. Sandpack zones in this upper area that possessed subtle heterogeneities (slightly greater porosities and hydraulic conductivities) likely experienced flow velocities that exceeded the critical velocity for seepage failure. Once this threshold had been crossed channel growth became a self-amplifying process.

Another notable aspect of test V1 is the cavity slope angle of 22°, which was more than 10° less than the maximum slope angle observed in all other tests. Assessment of stable slope angles in the C-CHOPS environment is challenging. As mentioned in Section 4.2, attempts at stress analysis via numerical modelling failed to converge. Following the approach presented in Pereira (2021), a simple analytical solution for estimating the stable slope angle for an infinite, planar surface for saturated (submerged) sand was used; modified to account for the hypergravity environment. As shown in Appendix I, depending on the friction angle of the sand, stable slope angles in the 20° to 25° were calculated. At face value, this seems to compare favourably with the observed angle of 22° for test V1. However, the calculation does not account for the conical shape

of the cavity surface, which would result in a greater slope angle due to stress arching effects; nor does it account for seepage forces, which would result in a lesser slope angle. In a relative sense, it seems reasonable to suggest that the lower angle observed in V1 was impacted by greater seepage forces acting the upper part of the sandpack.

4.3.3 G2 Test

In this test, like test V1, significant sand production occurred during and immediately after PR. In fact, it appears the rapid onset of sand production blocked the flow system even before a drawdown condition was created. As such, insignificant flow rates were achieved under drawdown conditions, hence it was not possible to assess the effects of sand production on oil production rates, nor was it possible to assess the effects of seepage forces on sand failure. Massive initial sand production is, like test V1, consistent with the absence of capillary cohesion, hence the inability to establish pseudo-stable arches around the perforations.

As a result of the observed sand production, a uniform cavity was formed around the wellbore. As per the conceptual model, this cavity likely developed due to subsidence resulting from sand production into perforations in the lower and middle part of the sandpack. No surface erosion channels were observed in this test. This is consistent with the fact that significant flow rates (hence seepage forces) were never achieved in this test. It is suggested that the addition of a high-permeability annulus of gravel around the sandpack might also have mitigated preferential flow in the upper part of the sandpack in the early stages of the experiment, hence mitigating the driving forces for erosion channel development. The higher slope angle of the cavity observed in test G2 (38°, compared to 22° for test V1) is consistent with lower seepage-induced forces in this test.

4.3.4 C3 Test

In this test, tank T100 was isolated from the wellbore and sandtrap (valve V1 was closed) during PR. However, load cell measurements were available during plug removal, and these indicate that sand production was occurring. However, because load cell data were lost shortly after PR, it was not possible to determine if sand production had ended prior to creating drawdown condition. If it did continue, though, it was not sufficient to block the flow system. A high slurry rate of 400 cm^3/min (compared to an oil rate of 6 cm^3/min prior to PR) when maximum drawdown (XDD) was imposed. This seems reasonable to suggest that the oil rate was likely greater than 6

cm^3/min, hence flow was enhanced due to sand production; however, it is not possible to prove this.

As noted in Table 4.1, the absence of and/or displaced positions of the coloured rings within the sandpack suggest that large-scale sand production occurred in the lower part of the sandpack, and near-well sand production occurred in the middle part.

Within a few minutes of achieving the afore-noted maximum slurry rate, rates dropped quickly, and the experiment was terminated. As such, it was not possible to assess what final conditions might have been achieved after long-term, sustained flow. However, unlike test G2, it was possible to interpret the test results knowing that seepage forces had existed in the late stages of the experiment. This fact makes it especially interesting that no surface erosion channels were detected around the cavity in this test. Compared to test V1, two differences in test C3 that could explain the lack of erosion channels are the gravel-filled annulus which distributed the initial fluid flow more uniformly with depth, and the use of a flexible caprock which altered the mechanical interaction between the top of the sandpack and the base of the caprock.

The slope angle of the outer part of the cavity for test C3 was similar to G2 (39° and 38°, respectively. The difference was the presence of the synthetic caprock in C3. The effect of caprock flexure is complex and was not explored in this research. Despite the unknowns pertaining to synthetic caprock effects, this type of caprock was used for all remaining tests because it was deemed more representative of in-situ (shale) caprocks.

Test C3 also differs from G2 in the presence of an inner zone with low angle (sub-horizontal) slope in the cavity. The instrumentation available, it is not possible to assess if this zone existed during the experiment, or whether it developed after the test was completed. It is suggested that sand transported into the cavity during late-stage, seepage-induced cavity enlargement settled to the bottom of a deeper cavity when the test was terminated, resulting in a relatively flat infilled-zone at the base of the cavity.

A final observation of interest for this test (and all others using synthetic caprock) is the fact that the caprock remained intact, hence shielding the underlying cavity from stresses and affecting its stability. The results obtained here are therefore deemed representative for reservoirs possessing relatively thick and competent shale caprocks.

4.3.5 W4-a Test

This test was conducted using an initial water saturation (77%) much greater than intended. As such, the results are not directly applicable to a CHOPS scenario, but the test was conducted to assess the consequences of testing with a flowing fluid of lower viscosity. In this test, relatively high flow rates (80 to 100 cm^3/min) were achieved while the porous plug was still in place. This is consistent with the fact that water viscosity is roughly 78 times less than canola oil viscosity, and water was likely the predominant flowing fluid at this stage of the experiment. Though no load cell data were available, it is clear from pressure data that sand production occurred during plug removal; more specifically, slurry rates in the 40 to 60 cm^3/min range were observed during plug removal. Immediately following plug removal, similar slurry rates were observed for roughly 10 minutes while a NDD condition existed. When small, then incrementally larger drawdowns were applied, flow continued, but at lesser rates (10 – 20 cm^3/min). The experiment was terminated on the presumed basis that flow system blockages might have accounted for the reduced rates.

After excavation, a relatively narrow cavity was found, with a diameter of 13 cm, depth of 4.8 cm, and a uniform slope angle of 34°. No erosion channels or wormholes were observed. The mass of the produced sand (0.43 kg) was significantly less than all other tests. Importantly, from an operations and test interpretation perspective, there was no evidence that the wellbore, sandtrap, or any other component of the flow system had become blocked.

The capillary cohesion resulting from the saturation state would have been smaller than intended, hence it is not clear if two-phase saturations played a role in the relatively small mass of produced sand. Regardless, it is suggested that the lesser mass of sand production might have been a consequence of the lower viscosity (hence lower drag force) of the flowing fluid. It is unclear why the slope angle was a few degrees lower than the maximum value observed for test C3.

It is suggested that the relatively low flow rates observed in the late stages of the experiment (compared to rates observed before plug removal) may be a consequent of several factors, including: an increase in the viscosity of the flowing fluid (given that canola oil from tank T300 flowed into the sandpack during the test); a relatively small increase in produced sand mass (hence a lesser permeability increased compared to other tests); and failure to lower the leveling arm to the XDD condition before deciding to terminate the test.

The result of this test was interesting in terms of the effect of water on the CHOPS process; i.e., the flow-enhancement achieved by sand production is lesser for a lower-viscosity fluid.

4.3.6 W4-b Test

This test was problematic in some aspects; e.g., during the saturation stage of test set-up, some air entered into the wellbore (and perhaps the sandpack) as water was being drained and replaced by oil; the initial water saturation was much lower than test W4-a, but at least some mobile water remained in the sand pack when the test was initiated; a baseline flow rate could not be achieved before plug removal (possibly due to air being present in the wellbore plug and blocking its pores); and the failure of the load cells. Regardless, the test did yield some novel and important results.

During removal of the porous plug, a slurry rate of roughly 30 cm^3/min was observed. Valve V1 was open and a small drawdown head was applied as the plug was removed. The fact that a relatively small slurry rate was observed (compared to 150 – 200 cm^3/min in test V1, for example), in spite of a drawdown condition (which would enhance sand production) suggests that the capillary cohesion was sufficient to reduce yielding and production of sand. Another important outcome of this test was the fact that progressively greater slurry rates were achieved with progressively higher drawdown heads, and the flow system did not suffer a blockage through the duration of the test.

As indicated in Table 4.1, and in sharp contrast to the finding for test C3, the coloured rings suggest that sand production was localized to the near-well area at mid to upper heights in the sandpack for test W4-b. This supports the notion that capillary cohesion was effective for reducing yielding near the perforations and/or improving the stability of sand arches near the perforations.

It is suggested that the formation of the cavity increased oil flow rates, but because there was no fluid flow before PR, this cannot be proven or quantified. The development of a stable wormhole tip in test W4-b was significant. Like test V1, which developed erosion channels, the radius of the cavity was large. As such, these two tests should have had the largest fluid flow velocities, hence the greatest driving force for erosion. Though erosion channels developed at the caprock-sandpack interface for test V1, the localized erosional feature (wormhole) developed slightly below this interface for test W4-b. It is suggested that this might be due to greater resistance to grain displacements at the caprock-sandpack interface, due to the softer nature of this

interface (synthetic caprock underlain by a plastic sheet). This suppressed erosion at the interface, so erosion occurred slightly below, where flow rates were near their highest values and stresses were near their lowest values, and the sand grains were more easily dislodged.

Although the wormhole was not visible deeper into the sandpack after the test, it is suggested that it might have extended to the outer edge during the test but collapsed when the experiment was terminated. This suggestion is supported by the numerical modelling presented in Section 4.2, which suggests that permeability enhancement of some kind (beyond dilation near the wellbore and around the cavity) must be present in order to account for the relatively high flow rates observed in some of these experiments (W4-b and W4-c, most importantly). The fact that the wormhole remained open near the cavity face may be due to the fact that vertical stress was lower there, compared to the outer parts of the sandpack.

Post-test analysis revealed that the flow system had not become plugged during this test, although a relatively large mass of sand was produced and the sandtrap had exceeded its capacity and overflown. This suggests that more gradual sand production, due to increased sand strength, may result in lower potential of wellbore or flow system blockage.

The maximum slope angle in test W4-b (38°) was intermediate to the values observed in tests C3 and W4-a (39° and 34°, respectively). It is unknown if the lesser slopes observed closer to the wellbore existed during the experiment (e.g., low-angle slope due to seepage forces that were distributed over the face of the cavity prior to wormhole development), and/or if they developed as produced sand from the outer portion of the cavity was deposited at the base of the cavity at the end of the test.

4.3.7 W4-c Test

This test was a success in the sense that the objective of achieving a residual water saturation was reached (i.e., 10% water saturation, and no apparent water observed in tank T100 during the test). The test was also an improvement on W4-b because the load cells had been repaired and sealed more effectively, hence they functioned throughout the test. Challenges encountered during the test were inaccurate pre-test density measurements that affected porosity and saturation calculations, and the fact that flow could not be achieved prior to plug removal. Despite measures taken to improve the sandpack saturation procedures, it appears some air may have entered the wellbore and blocked pores within the porous plug. Alternatively, water may have blocked the pores, though further investigation (or a new plug design) is recommended for future researchers using this equipment.

Based on the load cell data, it is evident that sand production occurred during plug removal. However, two notable improvements are noted here, both of which are attributed to the benefits of capillary cohesion according to Figure 4.20: (1) sand production ceased when plug removal stopped, suggesting that stable arches developed; and (2) as shown in Figure 4.15, the total mass of sand produced was markedly reduced compared to test G2, which had no capillary cohesion.

In this experiment, the flow system did not clog, and as a result, it was possible to achieve flow through the duration of the experiment. Very high flow rate (300 – 500 cm^3/min) were achieved under relatively small drawdown heads. One minor issue noted during this interval of extended, high-rate flow was the fact that reservoir pressure (head) reduced slightly, as tank T300 could not replenish the fluid level in the tub at a rate that matched the rate of slurry production. Sand production occurred steadily while drawdown conditions existed, but stopped once the NDD condition was restored at the end of the test. This suggests that all of the sand production after plug removal was seepage-induced.

As indicated in Table 4.1, and similar to test W4-b, the coloured rings suggest that sand production was localized to the near-well area at mid to upper heights in the sandpack for test W4-c. This supports the notion that capillary cohesion was effective for reducing yielding near the perforations and/or improving the stability of sand arches near the perforations. Additional coloured rings were added at the base of the sandpack for test W4-c, and there were found in-lace and undisturbed at the end of

the test. This suggests that preferential flow did not occur at the base of the sandpack. Similarly, there were no erosional features observed at the top of the sandpack, indicating that preferential flow had occurred there. As such, given the discrepancy between observed flow rate and modeled flow rate, as presented in Section 4.2, it appears that preferential flow paths might exist within the sandpack during the experiment, even though they are not visible after the experiment. Further investigation of this is recommended for future research; e.g., CT-scanning of the sand-pack after a test in order to seek evidence of collapsed wormholes (which should possess lower densities that the surrounding sand.)

The slope angle of the outer part of the cavity for test W4-c was anomalously high (59°), compared to all other experiments. Possible explanations include: enhanced capillary cohesion due to the presence of air; seepage forces affecting the slope were minor due to very small drawdown heads used and/or redirection of most of the flow through undetected wormholes.

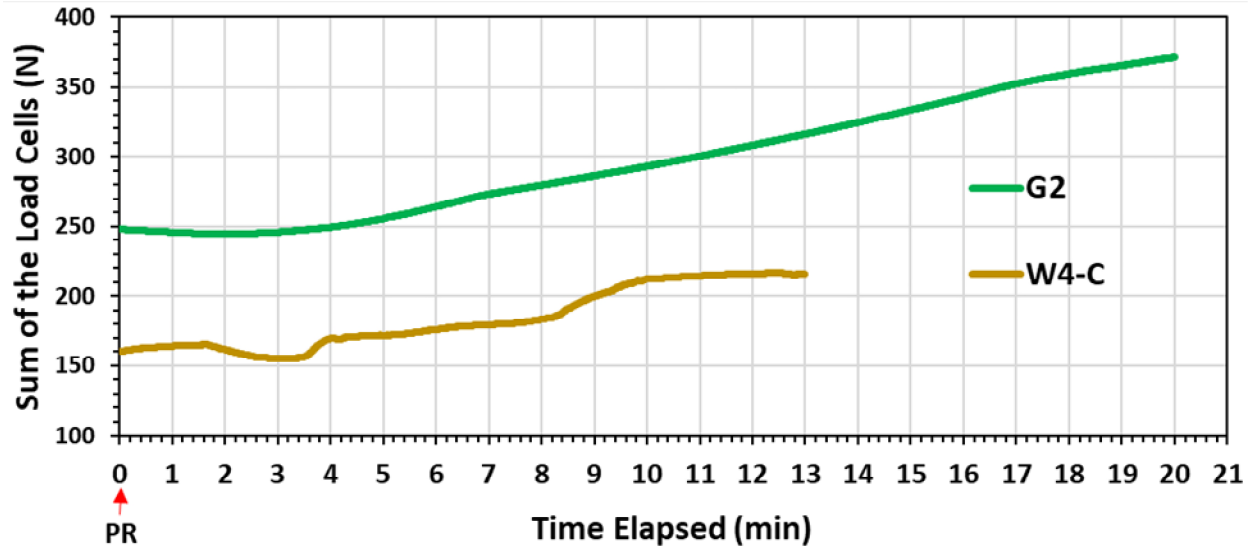

Figure 4.20. Comparison of load cell response (proportional to produced sand mass) for tests G2 and W4-c. The x-axis shows time since porous plug removal was initiated.

5 CONCLUSIONS AND RECOMMENDATIONS

5.1 Conclusions

The thrust of this research was to design and implement a laboratory system using a geotechnical centrifuge to study the shape of voids that form during sand production within an uncemented sand reservoirs in a 25×G hypergravity environment. Shear failure and/or seepage forces within these reservoirs can dislodge a portion of the formation solids and carry them into the wellbore. Studies have shown that removal of solids from a low strength reservoir will enhance oil & gas production by several fold, but only if a competent caprock is present. The experiments performed in this work did not rigorously represent all mechanisms at play in a heavy oil reservoir, but they can explain the role of certain mechanisms that can increase productivity as observed in field operations and provide guidance on the implementation of post-CHOPS enhanced recovery operations.

Due to the removal of sand during the sand production from the near wellbore zone, effective horizontal stress reduces, and therefore causes yielding and lateral dilation adjacent to the wellbore. This dilatation is shown to be one of the responsible factors for the increase in productivity of wells operating under CHOPS by increasing porosity and hydraulic conductivity locally in the plastic/yielded zone, though the results of this research did not enable explicit investigation of dilation-related effects on flow rates.

Also, results of tests that had two-phase fluid saturation indicate that capillary pressure supplied by the wetting phase (water) can increase effective strength of sand grains in the reservoir, which can diminish the sand failure, especially in lower part of the reservoir.

The results for one experiment suggest that a potential mechanism for an increase in productivity can be related to high permeability wormholes that form due to seepage forces. The wormhole is formed locally in low stress parts of the reservoir and may extend from the cavity towards the edges of the reservoir. The wormhole observed in this work had a minimal impact on the overall density of a column of sand in the reservoir and did not occur at the reservoir/caprock interface. Depending on in-situ stresses condition in the reservoir, the wormhole may have collapsed and faded with minimal/no trace in the reservoir once the seepage stopped. Formation of surface erosion channels can be related to the magnitude of flow rate. In cases where the flow

rate is high at the interface of the reservoir/caprock, this can erode the solids in these zones by overcoming the grains' frictional forces. In contrast, using a flexible caprock has shown that it can increase frictional strength between sand grains at the caprock-reservoir interface, and with the presence of high permeable material which can distribute fluid flow uniformly, these can significantly reduce the flow rate which is required for initiation of surface erosion channels.

Lastly, results of one experiment showed that the presence of low viscosity fluid in the sandstone reservoir may reduce sand production by lowering the impact drag forces caused by the seepage. This can inform the operators in fields to take reasonable measurements to avoid water coning which may cause detrimental effects in oil production.

Another practical implication from this research may be possible to improve enhanced recovery operations if heated fluids/solvents are injected into the deeper, less disturbed part of the reservoir, in order to avoid premature breakthrough (production) of these injected fluids.

5.2 Recommendations

For better results in future research, the recommendations to modify the physical model/procedures/designs are given based on this research:

1. To study the effect of heterogeneity on void geometries in the reservoir on the CHOPS process, create a sandpack using various sizes and/or types of sedimentary materials (e.g., layers or channels of finer and coarser-grained sand or clay);
2. To avoid entrance of air into the sandtrap, which has shown to be a potential factor in interrupting flow rate prior to sand production, develop new procedures and/or a new porous plug design;
3. Install a camera targeting the sandtrap's dish to monitor sand production during the experiment in conjunction with the load cells;
4. To study the effect of brine (i.e., NaCl and tap water) on cohesion and tensile strength resulting from capillary pressures;
5. Redesign/modify the current sandtrap in a way that increases its capacity;
6. Develop a modified or new apparatus that can enable study of the effect of anisotropic stresses in the reservoir and its effect on void geometries and productivity.

7. Develop a modified or new apparatus that can enable study of the effect of live oil; i.e., to run the experiments such that gas comes out of solution and foamy oil flow occurs once a drawdown pressure is applied.
8. To conduct imaging (e.g., CT scanning) of the sandpack after tests in order to assess the geometry of low-density zones that might represent dilated, high-permeability zones and/or collapsed wormholes.

6 REFERENCES

Beier, N. A. (2015). Development of a tailings management simulation and technology evaluation tool, doctoral thesis, University of Alberta, Canada.

Bratli, R. K., & Risnes, R. (1981). Stability and failure of sand arches. Society of Petroleum Engineers Journal, 21(02), 236-248, SPE-8427-PA.

Choi, J. W. (2011). Geomechanics of subsurface sand production and gas storage. [Unpublished PhD thesis], Georgia Institute of Technology.

Clearly, M. P., Melvan, J. J., & Kohlhaas, C. A. (1979). The effect of confining stress and fluid properties on arch stability in unconsolidated sands. In SPE Annual Technical Conference and Exhibition, SPE-8426-MS.

Daneshy, A., Valkó, P., Norman, L., Economides, M. J., Watters, L. T., & Dunn-Norman, S. (1998). Well Stimulation. Chapter 17 in: Petroleum Well Construction. Edited by M. Economides. Wiley, 506.

De Lazzer, A., Dreyer, M., & Rath, H. J. (1999). Particle− surface capillary forces. Langmuir, 15(13), 4551-4559.

Du, Z., Zeng, F., & Chan, C. (2015). An experimental study of the post-CHOPS cyclic solvent injection process. Journal of Energy Resources Technology, 137(4).

Diaz, B. M., Sawatzky, R., & Kuru, E. (2010). Sand on demand: An approach to improving productivity in horizontal wells under heavy oil primary production-part II. In SPE Western Regional Meeting. SPE-133500-MS.

Elkins, L. F., Morton, D., & Blackwell, W. A. (1972, October). Experimental fireflood in a very viscous oil-unconsolidated sand reservoir, SE Pauls Valley Field, Oklahoma. In Fall Meeting of the Society of Petroleum Engineers of AIME. SPE-174050-MS.

Geilikman, M. B. (1999). Sand production caused by foamy oil flow. Transport in Porous Media, 35(2), 259-272.

Gomes, R. D., Adissi, M. O., da Silva, T. A., Lima Filho, A. C., Spohn, M. A., & Belo, F. A. (2015). Application of wireless sensor networks technology for induction motor monitoring in industrial environments. In Intelligent Environmental Sensing (pp. 227-277). Springer, Cham.

Han, G., & Dusseault, M. B. (2002, January). Quantitative analysis of mechanisms for water-related sand production. In International Symposium and Exhibition on Formation Damage Control. Society of Petroleum Engineers, SPE-73737-MS.

Han, G. , Bruno, M. , & Dusseault, M. B. (2007). How much oil you can get from CHOPS. Journal of Canadian Petroleum Technology, 46(04), PETSOC-07-04-02.

Hill, P. (2017). Hydrocarbon distribution in the Mannville Waseca Member, Edam oil field, west-central Saskatchewan. Summary of Investigations, Saskatchewan Geological Survey, 2017-4.

Islam, M. R., & George, A. E. (1989, April). Sand control in horizontal wells in heavy oil Reservoirs. In SPE California Regional Meeting. SPE-18789-MS.

Istchenko, C. M., & Gates, I. D. (2014). Well/wormhole model of cold heavy-oil production with sand. SPE Journal, 19(02), 260-269, SPE-150633-PA.

Jia, S. (2021). Beam centrifuge modelling of caprock integrity, doctoral thesis, University of Alberta, Canada.

Kutter, B. L. (1992). Dynamic centrifuge modeling of geotechnical structures. Transportation research record, (1336), ISSN: 0361-1981.

Lambe, T. W., & Whitman, R. V. (1991). Soil mechanics (Vol. 10). John Wiley & Sons.

Liu, Y., Wan, R. G., & Jian, Z. (2008). Effects of foamy oil and geomechanics on cold production. Journal of Canadian Petroleum Technology, 47(04), PETSOC-08-04-55.

Ma, H., Huang, D., Yu, G., She, Y., & Gu, Y. (2017). Combined cyclic solvent injection and waterflooding in the post-cold heavy oil production with sand reservoirs. Energy & fuels, 31(1), 418-428.

Madabhushi, G. (2014). Centrifuge modelling for civil engineers. CRC Press.

Mahmud, H. B., Leong, V. H., & Lestariono, Y. (2020). Sand production: A smart control framework for risk mitigation. Petroleum, 6(1), 1-13.

McCormack, M. E. (1988). Mechanisms of sand retainment by wire-wrapped screens. In 4th UNITAR/UNDP Conference on Heavy Crude and Tar Sands, Edmonton, Alberta, Canada (pp. 7-12).

McPhee, D., & Pemberton, S. G. (1994). Sequence stratigraphy of the lower Cretaceous Mannville Group of East Central Alberta, Canadian Society of Petroleum Geologists Conference, Calgary, Canada, Extended Abstract, Pages 27-28.

Menzel, W., & Schreiner, W. (1989). Geochemical aspects for the establishment and the operation of gas cavern stores in salt formations of the GDR. In International conference on storage of gases in rock caverns (pp. 115-120).

Metwally, M., & Solanski, S. C. (1995). Heavy oil reservoir mechanisms, Lindbergh and Frog Lake Fields, Alberta Part I: Field Observations and Reservoir Simulation. In Annual Technical Meeting. PETSOC-95-63.

Meza-Díaz, B., Sawatzky, R., & Kuru, E. (2012). Sand on demand: a laboratory investigation on improving productivity in horizontal wells under heavy-oil primary production—part II. SPE Journal, 17(04), 1012-1028, SPE-133500-PA.

Meza, B., Tremblay, B., & Doan, Q. (2002). Visualization of sand structures surrounding a horizontal well slot during cold production. In SPE International Thermal Operations and Heavy Oil Symposium and International Horizontal Well Technology Conference, SPE-79025-MS.

Meza Diaz, B., Ron, S., & Kuru, E. (2010). Sand on demand for horizontal wells: tracking

behaviour with the CT scanner. In SPE Annual Technical Conference and Exhibition, SPE-134493-MS.

Miller, K. A., Carlson, J. E., Morgan, R. J., Thornton, R. W., & Willis, K. (2003). Preliminary results from a solvent gas injection field test in a depleted heavy oil reservoir. Journal of Canadian Petroleum Technology, 42(02), PETSOC-03-02-05.

Miller, W. G. (1994). Sand flow mechanisms at well casing perforations, Master of science thesis, University of Alberta, Canada.

Oldakowski, K., & Sawatzky, R. P. (2018). Direction of wormhole growth under anisotropic stress. In SPE Canada Heavy Oil Technical Conference, SPE-189734-MS.

Orr, R. D., Johnston, J. R., & Manko, E. M. (1977). Lower Cretaceous geology and heavy-oil potential of the Lloydminster area. Bulletin of Canadian Petroleum Geology, 25(6), 1187-1221.

Pan, Y., Chen, Z., Sun, J., Bao, X., Xiao, L., & Wang, R. (2010, May). Research progress of modelling on cold heavy oil production with sand. In SPE Western Regional Meeting, SPE-165541-MS.

Penberthy, W. L., & Shaughnessy, C. M. (1992). Sand control. Henry L. Doherty Memorial Fund of AIME, Society of Petroleum Engineers.

Pereira, M. (2021). A physical model to assess sand production processes during Cold Heavy Oil Production with Sand, master of science thesis, University of Saskatchewan, Canada.

Rangriz Shokri, A., & Babadagli, T. (2012). An approach to model CHOPS (Cold Heavy Oil Production with Sand) and Post-CHOPS applications. In SPE Annual Technical Conference and Exhibition, SPE-159437-MS.

Riediger, C. L., Fowler, M. G., Snowdon, L. R., MacDonald, R., & Sherwin, M. D. (1999). Origin and alteration of lower Cretaceous Mannville Group oils from the Provost oil field, east central Alberta, Canada. Bulletin of Canadian Petroleum Geology, 47(1), 43-62.

Risnes, R., Bratli, R. K., & Horsrud, P. (1982). Sand arching-a case study. In European Petroleum Conference, SPE-12948-MS.

Sawatzky, R. P., Lillico, D. A., London, M. J., Tremblay, B. R., & Coates, R. M. (2002). Tracking cold production footprints. In Canadian International Petroleum Conference, PETSOC-2002-086.

Senden, M. M. G., & Verkooijen, A. H. M. (Eds) (1983), The role of practice interactions in powder mechanics, International symposium, Eindhoven Vol. 28.

Smith, G. E. (1988). Fluid flow and sand production in heavy-oil reservoirs under solution-gas drive. SPE Production Engineering, 3(02), 169-180, SPE-15094-PA.

Squires, A. (1993, March). Inter-well tracer results and gel blocking program. In 10th Annual Heavy Oil and Oil Sands Technical Symposium, Calgary, Alberta, Canada (Vol. 9).

Taylor, R. E. (Ed.). (1995). Geotechnical centrifuge technology, Geotechnical Engineering

Research Center, City University, London.

Terry, R. E., Rogers, J. B., & Craft, B. C. (2014). Applied petroleum reservoir engineering. Pearson Education.

Terzaghi, K. (1936). Stress distribution in dry and in saturated sand above a yielding trap-door, 1st International Conference on Soil Mechanics and Foundation Engineering, Cambridge, USA, pp 307-311.

Tortike, W. S., & Ali, S. M. (1991). Prediction of oil sand failure due to steam-induced stresses. Journal of Canadian Petroleum Technology, 30(01), PETSOC-91-01-08.

Townsend, F., Shiau, J.-M. & Pietrus, T. (1987) Piping susceptibility and filter criteria for sands. ASCE Geotechnical Special Publication no. 10, Symposium on Engineering Aspects of Soil Erosion, Dispersive Clays, and Loess, Atlantic City, USA, 46-66.

Tremblay, B., Sedgwick, G., & Vu, D. (1998, April). CT imaging of wormhole growth under solution-gas drive. In SPE/DOE Improved Oil Recovery Symposium, SPE-39638-MS.

Tremblay, B., Sedgwick, G., & Vu, D. (1999, August). A review of cold production in heavy oil reservoirs. In IOR 1999-10th European Symposium on Improved Oil Recovery, European Association of Geoscientists & Engineers, cp-80-00007.

Tremblay, B. (2009). Cold flow: a multi-well cold production (CHOPS) model. Journal of Canadian Petroleum Technology, 48(02), 22-28.

Tremblay, B., & Oldakowski, K. (2003). Modeling of wormhole growth in cold production. Transport in Porous Media, 53(2), 197-214.

Tremblay, B., Sedgwick, G., & Forshner, K. (1997). Simulation of cold production in heavy-oil reservoirs: Wormhole dynamics. SPE Reservoir Engineering, 12(02), 110-117, SPE-35387-PA.

Tronvoll, J., Skj, A., & Papamichos, E. (1997). Sand production: mechanical failure or hydrodynamic erosion?, International Journal of Rock Mechanics and Mining Sciences, 34(3-4), Pages 291.e1-291.e17.

Vardoulakis, I., Stavropoulou, M., & Papanastasiou, P. (1996). Hydro-mechanical aspects of the sand production problem. Transport in Porous Media, 22(2), 225-244.

Vaziri, H., Barree, B., Xiao, Y., Palmer, I., & Kutas, M. (2002, September). What is the magic of water in producing sand?. In SPE Annual Technical Conference and Exhibition, SPE-77683-MS.

Vaziri, H. H., Xiao, Y., Islam, R., & Lemoine, E. (2003). Physical modeling study of the influence of shale interbeds and perforation sequence on sand production. Journal of Petroleum Science and Engineering, 37(1-2), 11-23.

Vaziri, H. H., Lemoine, E., Palmer, I. D., McLennan, J., & Islam, R. (2000, October). How can sand production yield a several-fold increase in productivity: experimental and field data. In SPE Annual Technical Conference and Exhibition, SPE-63235-MS.

Vaziri, H.H., & Lemoine, L. (2000). Pacific rocks 2000 : 'Rock around the rim' : proceedings of the fourth North American Rock Mechanics Symposium, NARMS 2000, Seattle, Washington, USA,

Vaziri, H. H., Jalali, J. S., & Islam, R. (2001). An analytical model for stability analysis of rock layers over a circular opening. International journal of solids and structures, 38(21), 3735-3757.

Vermeer, P. A. (1998). Non-associated plasticity for soils, concrete and rock. In Physics of dry granular media (pp. 163-196). Springer, Dordrecht.

Wolski, W. (1965). Model tests on the seepage erosion in the silty clay core of an earth dam. In Soil Mech & Fdn Eng Conf Proc/Canada/.Wong, R. C. K. (2003). Sand production in oil sand under heavy oil foamy flow. Journal of Canadian Petroleum Technology, 42(03), pp 583-587.

Xiao, L., & Zhao, G. (2017). Estimation of CHOPS wormhole coverage from rate/time flow behaviors. SPE Reservoir Evaluation & Engineering, 20(04), pp. 0957-0973, SPE-157935-PA.

Yim, K., Dusseault, M. B., & Zhang, L. (1994, August). Experimental study of sand production processes near an orifice. In Rock Mechanics in Petroleum Engineering, SPE-28068-MS.

Zaitlin, B. A., & Shultz, B. C. (1984). An estuarine-embayment fill model from the lower Cretaceous Mannville Group West-central Saskatchewan, Symposium on the Mesozoic of Middle North America, Calgary, Alberta, Canada — Memoir 9, 455-469.

Zhao, D. W., Wang, J., & Gates, I. D. (2014). Thermal recovery strategies for thin heavy oil reservoirs. Fuel, 117, 431-441.

APPENDIX A. Pluviation Callibration Data

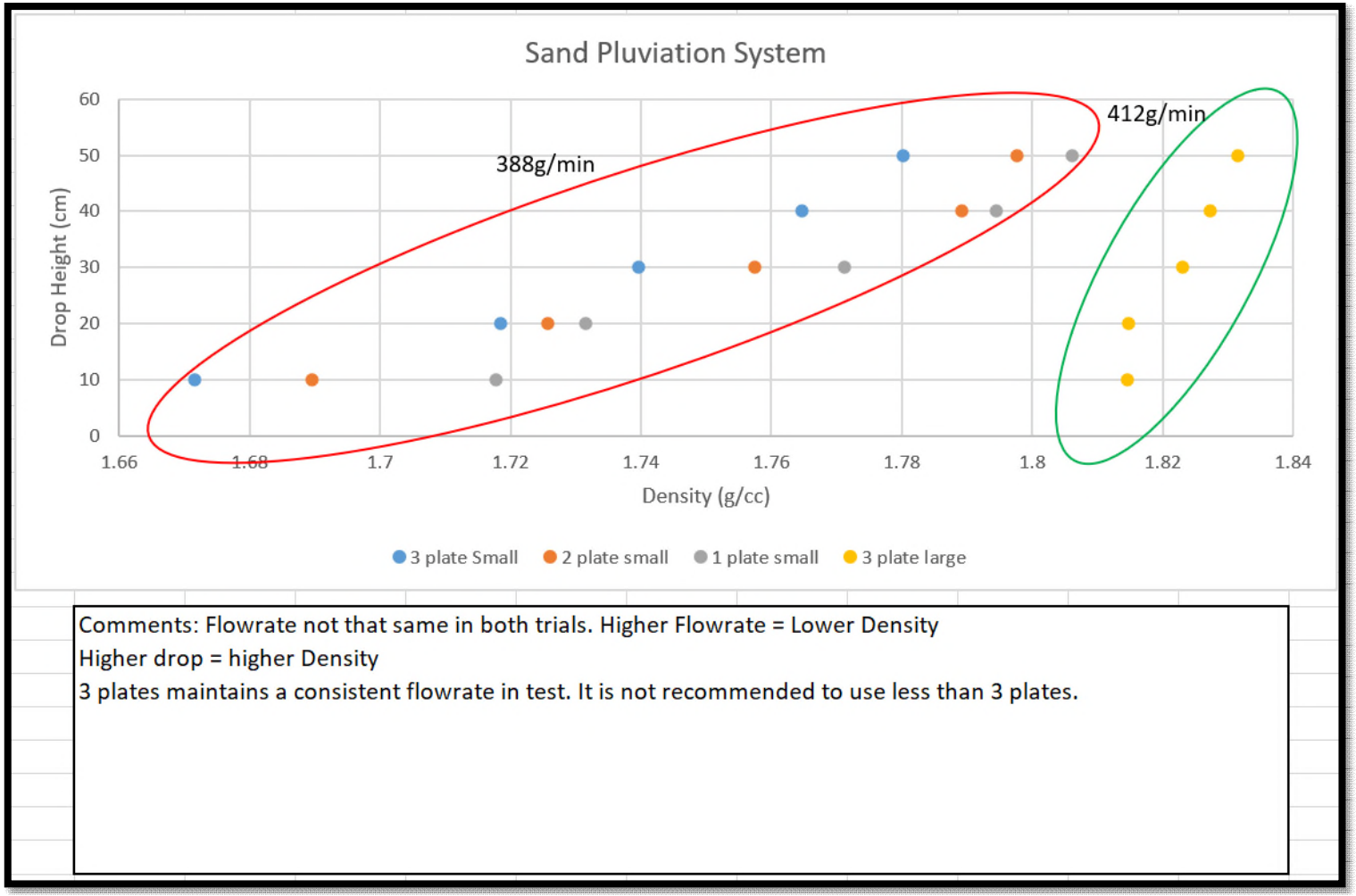

(Pereira, 2021)

APPENDIX B. Capillary Cohesion Calculations

W4-c Test:

Based on the grain size of the sand which is being used in this project (0.0000815m), the 35% porosity of the sandpack obtained from sand pluviation in W4-c test, and friction angle of 40°, water saturation of the sandpack by 10% would result in approximately 2.21 kPa of cohesion which is a result of water capillary force.

In W4-c test, 1.1 L of residual water remained in the sandpack. To calculate the residual water saturation the following equation was used:

$$S_{wr} = \frac{V_{water}}{(V_{sand} - V_{wellbore}) \times \varphi} \times 100 \quad \text{(B1)}$$

Radius of Sandpack	Height of Sand Before Flight	Outer Diameter of Wellbore	Volume of Sand (including wellbore)	Volume of Well	Sand Volume	Sand Porosity	Volume of Water in Sandpack	Residual Water Saturation Target
m	m	m	m3	m3	m3	fr.	L	%
0.257	0.158	0.008	0.033	3.098E-05	0.033	0.35	1.1	10

To calculate the capillary cohesion obtained by 10% residual water saturation first, the water angle needs to be determined using the graph showed below. Then by using equations 2.7 – 2.13, the cohesion can be calculated as follow:

α water angle	R Grain Size	ɣ Surface Tension	n Porosity	φ Friction Angle	θ Contact Angle	Xp	r	ΔP	F°c Capillary bond (capillary pressure)	Fs capillary bond (ɣ)	Fc	σ UCS	Cohesion
degree	m	N/m	-	Radians	-	m	m	Pa	N	N	N	KPa	KPa
0.6	8.15E-05	0.023	0.35	0.70	0	4.60E-05	1.72E-05	-844.585	-5.62E-06	3.80E-06	9.42E-06	9.48	2.21
	Oil/W 20C	0.023											

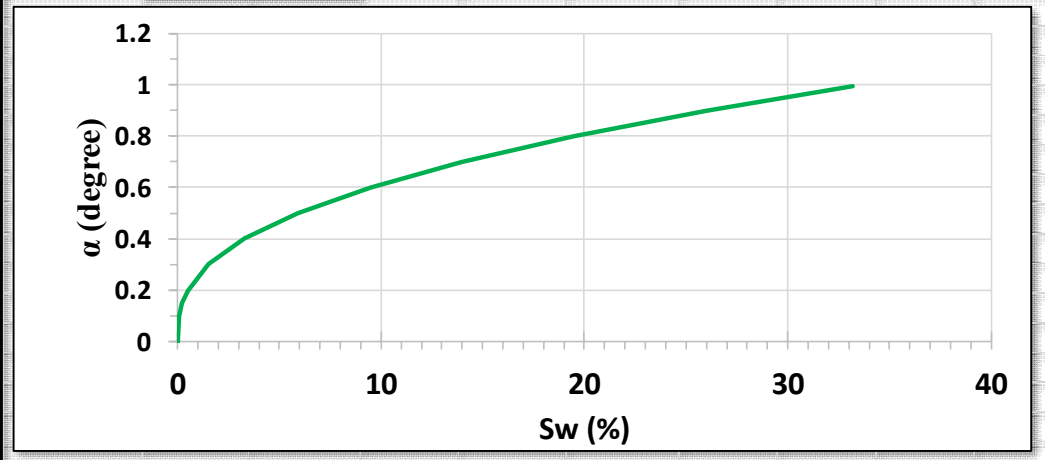

[after Han & Dusseault, 2002]

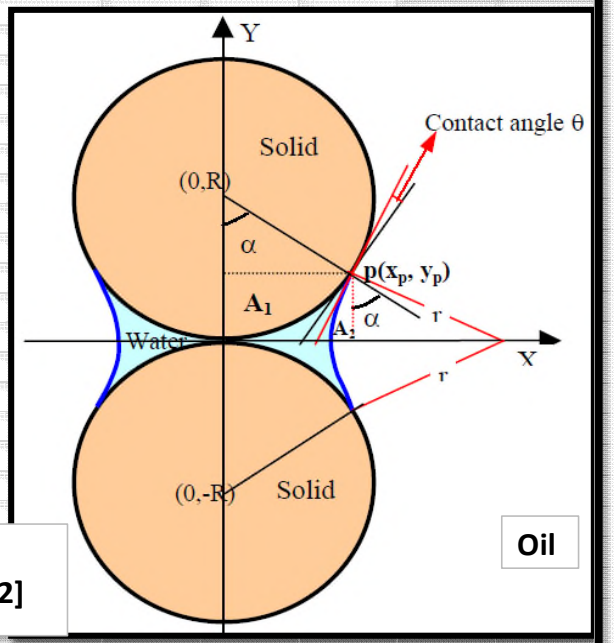

To see the effect of cohesion obtained from capillary force on the stability of sand during sand production, Equation 2.16 was used to do the calculation. The results of these calculations are shown in the following figure. It was determined that having around 2 kPa of cohesion would give enough strength to the sandpack to slow down the amount of failed sand in low drawdown pressures (NDD or MDD).

σa Kpa	Pw Kpa	U Kpa	(σa- P1) Kpa	ϕ degree	α degree	T radian	Sc0 Kpa	σT Kpa	rs/r1 -	rc/r1 -	
121	24	36	109	40	65.0	7.2	0.1	0.1	-3765.56	2.2	
121	24	36	109	40	65.0	7.2	0.2	0.2	-3765.56	2.0	
121	24	36	109	40	65.0	7.2	0.5	0.6	-3765.56	1.8	
121	24	36	109	40	65.0	7.2	1	1.2	-3765.56	1.6	
121	24	36	109	40	65.0	7.2	2	2.4	-3765.56	1.5	
121	24	36	109	40	65.0	7.2	3	3.6	-3765.56	1.4	
121	24	36	109	40	65.0	7.2	4	4.8	-3765.56	1.3	NDD
121	24	36	109	40	65.0	7.2	5	6.0	-3765.56	1.3	
121	24	36	109	40	65.0	7.2	6	7.2	-3765.56	1.2	
121	24	36	109	40	65.0	7.2	7	8.3	-3765.56	1.2	
121	24	36	109	40	65.0	7.2	8	9.5	-3765.56	1.2	
121	24	36	109	40	65.0	7.2	9	10.7	-3765.56	1.2	
121	24	36	109	40	65.0	7.2	10	11.9	-3765.56	1.2	
121	17.5	36	103	40	65.0	7.2	0.1	0.1	-3765.56	#NUM!	
121	17.5	36	103	40	65.0	7.2	0.2	0.2	-3765.56	#NUM!	
121	17.5	36	103	40	65.0	7.2	1.4	1.7	-3765.56	2.3	
121	17.5	36	103	40	65.0	7.2	1.5	1.8	-3765.56	2.1	
121	17.5	36	103	40	65.0	7.2	2	2.4	-3765.56	1.7	
121	17.5	36	103	40	65.0	7.2	3	3.6	-3765.56	1.5	
121	17.5	36	103	40	65.0	7.2	4	4.8	-3765.56	1.4	MDD
121	17.5	36	103	40	65.0	7.2	5	6.0	-3765.56	1.3	
121	17.5	36	103	40	65.0	7.2	6	7.2	-3765.56	1.3	
121	17.5	36	103	40	65.0	7.2	7	8.3	-3765.56	1.3	
121	17.5	36	103	40	65.0	7.2	8	9.5	-3765.56	1.2	
121	17.5	36	103	40	65.0	7.2	9	10.7	-3765.56	1.2	
121	17.5	36	103	40	65.0	7.2	10	11.9	-3765.56	1.2	
121	11	36	96	40	65.0	7.2	0.1	0.1	-3765.56	#NUM!	
121	11	36	96	40	65.0	7.2	0.2	0.2	-3765.56	#NUM!	
121	11	36	96	40	65.0	7.2	0.3	0.4	-3765.56	#NUM!	
121	11	36	96	40	65.0	7.2	2.68	3.2	-3765.56	2.8	
121	11	36	96	40	65.0	7.2	2.7	3.2	-3765.56	2.5	
121	11	36	96	40	65.0	7.2	3	3.6	-3765.56	1.9	
121	11	36	96	40	65.0	7.2	4	4.8	-3765.56	1.5	XDD
121	11	36	96	40	65.0	7.2	5	6.0	-3765.56	1.4	
121	11	36	96	40	65.0	7.2	6	7.2	-3765.56	1.4	
121	11	36	96	40	65.0	7.2	7	8.3	-3765.56	1.3	
121	11	36	96	40	65.0	7.2	8	9.5	-3765.56	1.3	
121	11	36	96	40	65.0	7.2	9	10.7	-3765.56	1.2	
121	11	36	96	40	65.0	7.2	10	11.9	-3765.56	1.2	

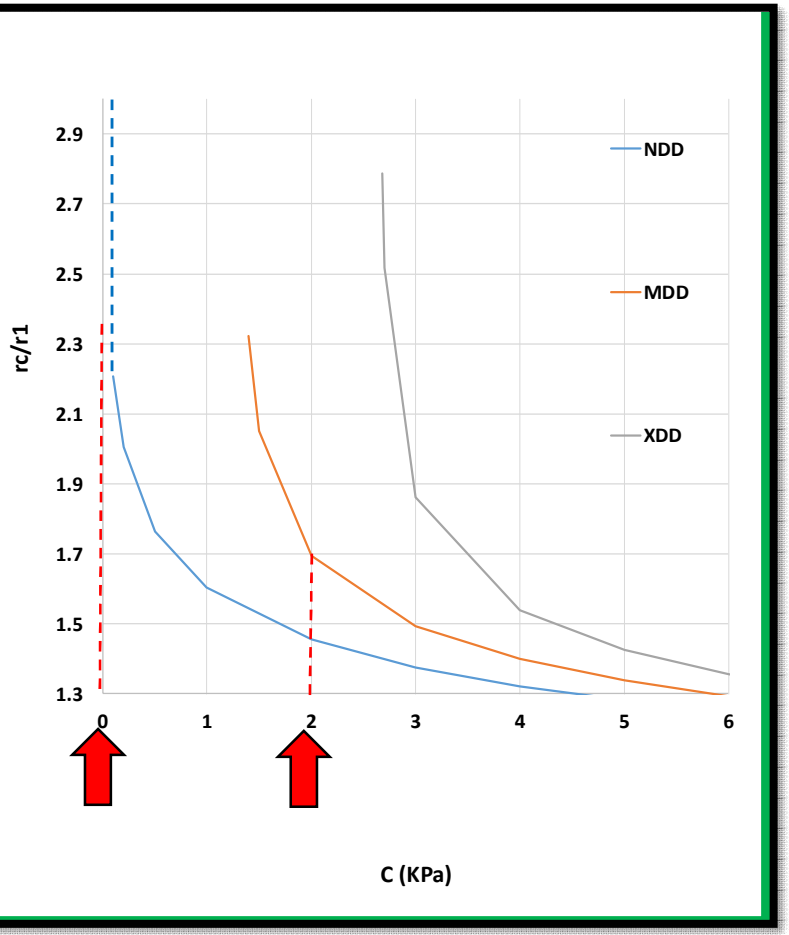

The figure above shows that when having zero cohesion, even without applying any draw down (NDD) the sandpack is highly exposed to yielding. This is while having 2 kPa of cohesion predicts that severity of the yielding zone should decrease to some extent. Furthermore, this figure shows that to make the sandpack stabilize in severe draw down or maximum drawdown (XDD), cohesion beyond 3 kPa is required.

W4-b Test:

Radius of Sandpack	Height of Sand Before Flight	Outer Diameter of Wellbore	Volume of Sand (including wellbore)	Volume of Well	Sand Volume	Sand Porosity	Volume of Water in Sandpack	Residual Water Saturation Target	-
m	m	m	m3	m3	m3	fr.	L	%	-
0.257	0.174	0.008	0.036	3.412E-05	0.036	0.38	2.4	18	-

α water angle	R Grain Size	γ Surface Tension	n Porosity	φ Friction Angle	θ Contact Angle	Xp	r	ΔP	F°c Capillary bond (capillary pressure)	Fs capillary bond (γ)	Fc	σ UCS	Cohesion
degree	m	N/m	-	Radians	-	m	m	Pa	N	N	N	KPa	KPa
0.77	8.15E-05	0.023	0.38	0.70	0	5.67E-05	3.2E-05	-316.901	-3.20E-06	5.78E-06	8.99E-06	7.94	1.85
	Oil/W 20C	0.023											

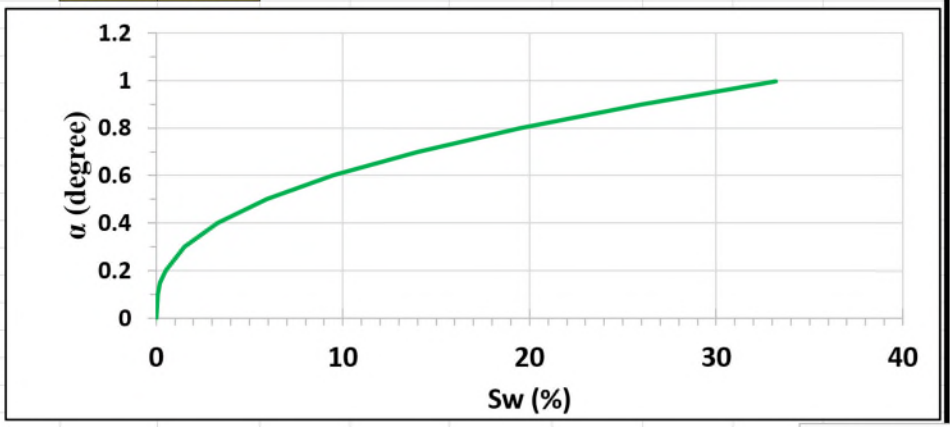

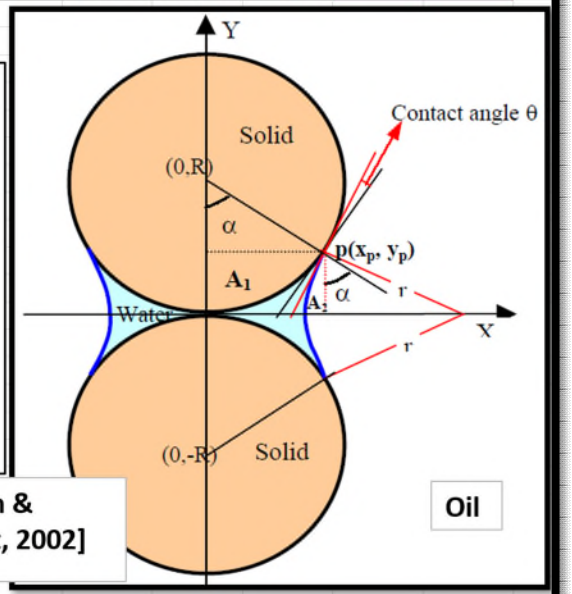

[after Han & Dusseault, 2002]

APPENDIX C. Saturation procedures

Revision 0:

UNIVERSITY OF ALBERTA GeoCERF	SOP for CHOPS Oil Saturation	Written by : Yazhao Wang
		Revision: 0 (2020-04-24)
		Date: 2020-04-24

Model Preparation

1) **Summary**
   a. This section provides safety precautions and guidelines to saturate the entire CHOPS system with canola oil.
2) **Safety Precautions**
   a. (**COVID-19 Special Precautions**) The model preparation procedures will be conducted with one person at any time. Shifts can be arranged during the sand dispensing stage as it will take more than 5 hours. N95 face mask, safety glasses and gloves will be worn at all times to protect the operator from silica dust, as well as potential spread of COVID-19. Hand washing is required before and after each shift change.
   b. Canola oil spills – Ensure spill kit is ready to deploy
3) **Procedure**
   a. Saturate Sand.
      a.1 Install C-CHOP lid to the container. Create a temporary seal at the top of the wellbore with liquid silicone and a rubber plug. Figure 10 shows an example of how the wellbore sealing with silicone will look once complete. **Note**: Curing time will vary depending on the type of silicone that is used. Allow sufficient time for the silicone to cure.

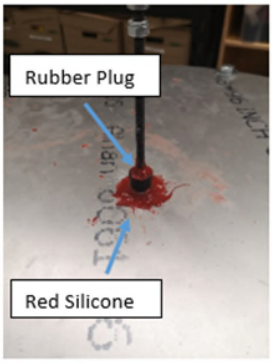

Figure 10: Securing the well plug with silicon rubber

      a.2 Remove 2 Plugs from the C-CHOPs tub. One plug from the top of the tub and one plug two fittings below. Install two needle valves with Teflon in the open ports and ensure needle valves are tightly closed. The valves can be installed on any side of the tub; however, they must be installed in the two rows as shown in Figure 11.

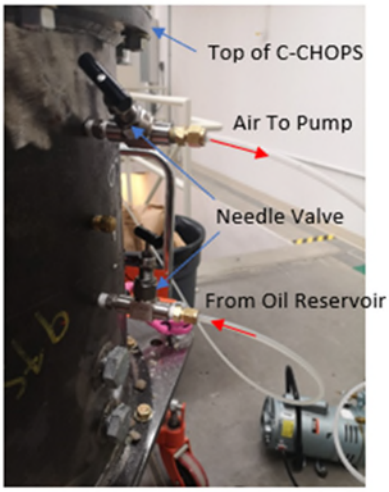

Figure 11: Installing needlw valves

a.3 Fit together the external reservoir system and vacuum pump for fluid saturation. The system should consist of (a) one reservoir, (b) 2 valves, (c) pipes and fittings (d) pressure gauge, and (e) vacuum pump. T-300 has been used previously for fluid saturation; Figure 12 shows both the reservoir and pump systems connected to pipes that are also connected to the C-CHOPS tub.

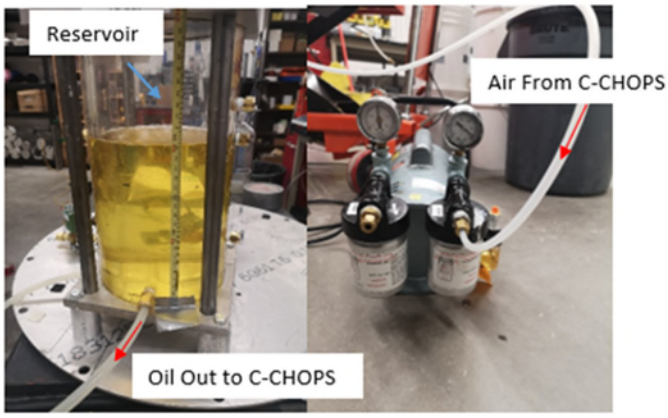

(a) (b)

Figure 12: (a) T-300 is filled with oil. A pipe is connected near the bottom of the reservoir that is then connected to the C-CHOPS tub, and (b) the vacuum pump is connected to a pipe the removes air from the C-CHOPS tub.

a.4 Fill the external reservoir with canola oil. Record the amount of oil inside the reservoir.

a.5 Open needle valve that is connected to the vacuum pump and turn the vacuum pump on for 10 seconds. Before turning off the vacuum pump, close the top needle valve so that the air can not enter C-CHOPS tub.

- a.5.1 With the vacuum pump off and the tub under a small amount of vacuum pressure ensures that the tub is not leaking by listening for air entering the tub and monitoring the pressure gauge on the C-CHOP tub.
- a.5.2 If the tub is leaking, repair the leak with silicone and repeat step 8.5.
- a.5.3 If the tub is not leaking, monitor the pressure gauge, and allow pressure to stabilize within the tub.
- a.5.4 Turn on the vacuum pump and open the needle valve for 5-10 seconds. Turn off the pump once needle valve has been closed. Monitor pressure within tub and allow pressure to stabilize. Also monitor sand trap fluid level with the clear pipe on the outside of the tub. If the fluid level begins to drop in the sand trap (indicated by a fluid level drop in pipe), this is an indication that to much vacuum has been applied at once to the tub, and pressure has not stabilized within the tub. If fluid level begins to drop within the sand trap open the top needle valve (with pump off) to allow air to enter the tub and increase the tub pressure. Allow pressure allow to stabilize before applying. Repeat step 7.5.4 until a vacuum pressure has been applied to the tub.
- a.5.5 Allow the tub to stabilize under vacuum pressure for two hours before introducing oil to the system.

  Note: A large amount of vacuum pressure at once will cause oil within the sand trap to flow through the perforations and into the sand pack. The vacuum must be applied slowly and incrementally to avoid this.

a.6 Open the external reservoir valve and allow fluid to flow from the external reservoir into the sand pack. Full saturation can take between 12-24 hours.

- a.6.1 A fluid flow rate of 10-20 ml/m should be used to avoid piping within the sand pack.
- a.6.2 Monitor the fluid flowrate by utilizing the drop in fluid level in the reservoir over a fixed period
- a.6.3 Allow the calculated porosity of fluid to fill the sand pack plus an additional volume of oil to fill the edging gravel.
- a.6.4 Continuously monitor pressure within the tub to ensure that no air is entering the system

a.7 Once the fluid has filled C-CHOPS tub, turn the vacuum pump off and close the external reservoir valve.

a.8 Remove the lid from the top of C-CHOPS.

a.9 Remove the synthetic capcock overburden and check to see is oil has reached the top of the sand pack. If too much oil is added, open the external reservoir valve and allow oil to backflow into external reservoir. If not enough oil is added to the sand pack then return the system to vacuum and

add additional oil to the system. Figure 13 shows how the top of the sand layer will look once the entire sand pack is fully saturated.

Figure 13: Once the caprock is removed from above the sand, oil should cover the top of the sand. If oil has not reached the top of the sand layer then further saturation is required.

a.10 Once saturation of the sand pack is complete, remove closed needle valves and disconnect and remove all equipment used for saturation. Needle valves may remain attached to the C-CHOPS tub as long as they are tightly closed. The pressure gauge used to monitor vacuum pressure should be removed from the tub.

Revision 1:

UNIVERSITY OF ALBERTA GeoCERF	Standard Operation Procedure for Sand Pack Saturation and Drainage in C-CHOPS Project	Written by : Yazhao Wang, Dmytro Pantov
		Revision: 1
		Date: 2020-08-05

Model Preparation

1) **Summary**
   a. This section provides safety precautions and operation procedures to saturate the sand pack inside C-CHOPS tub.
2) **Safety Precautions**
   a. Canola oil spills – Ensure spill kit is ready to deploy
3) **Materials needed:**
   a. 40L of water
   b. 40 L of food-grade canola oil
   c. Vacuum pump
   d. Needle valves
   e. Various lengths and diameters of swage lock piping
   f. Various swage lock fittings
   g. C-CHOPS tub with sand pack
4) **Significance and Use**
   a. Proper two-phase (water-oil) saturation of the sand pack will eliminate errors during the experiment. If the sample is not properly saturated then the experiment will not resemble in-situ conditions and the results will not accurately reflect the influence of capillary forces on sand production.
5) **Refereneces**
   a. SOP CHOPS Test in Centrifuge
6) **Procedure**
   a. The sand pack saturation procedure is the continuation of the sand pack preparation procedure of the C-CHOPS project as described in SOP CHOPS Test in Centrifuge.

Sealing the Tub

   b. Make sure the sandtrap is prefilled with oil, outlet tube is filled with oil and outlet is plugged with fittings.
   c. C-Chops tub needs to be sealed for both water and oil saturation. To create the seal, install lid to the container. Create a temporary seal at the top of the wellbore with liquid silicone and a rubber plug. Figure 1 shows how the wellbore sealing with silicone will look once completed.
   Note: Curing time will vary depending on the type of silicone that is used. Allow sufficient time for the silicone to cure.

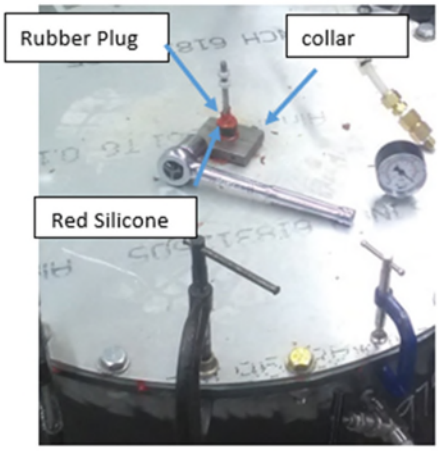

Figure 1: Sealing the C-CHOPS tub

d. Remove two plugs from the tub, including one plug from the top of the tub and one plug two fittings below. Install two needle valves with Teflon in the open ports and ensure needle valves are tightly closed. The valves can be installed on any side of the tub; however, they must be installed in the two rows as shown in Figure 2. Connect vacuum pump to the needle valve (A).

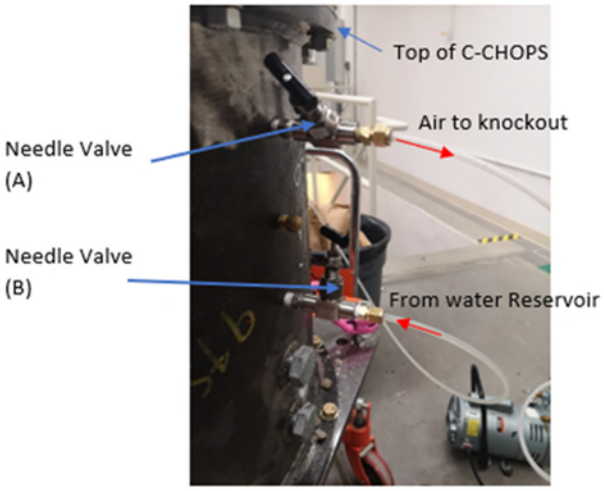

Figure 2: Tub connections for water saturation

Water Saturation

a. Figure 3 shows the setup for water saturation process.
b. Reservoir T-300 should be filled with water. The volume of the injected water should be tracked during the saturation.
c. Open Valve (B) that connects the reservoir and the tub, then open Valve (A). Turn on the vacuum pump and start injecting water into the sand pack.
d. Monitor pressure within tub and allow pressure to stabilize. Also monitor sand trap fluid level with the clear pipe on the outside of the tub. The saturated is completed when water is coming through Valve A into the knockout. Turn off the pump.

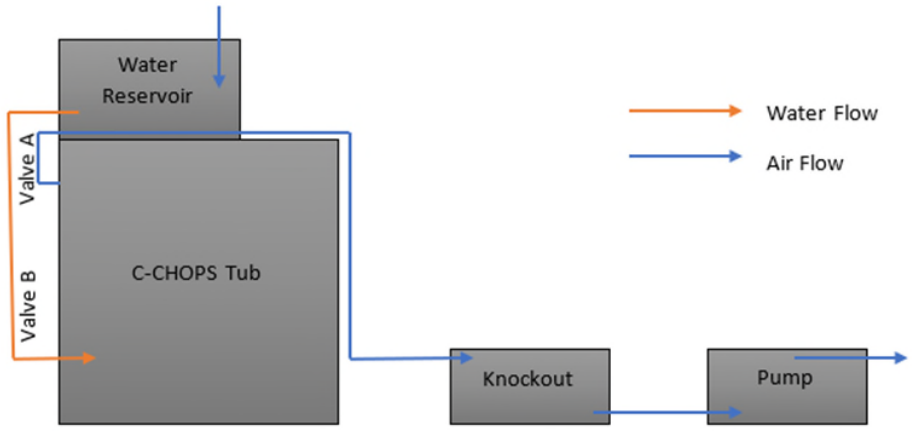

Figure 3. Schematics of water saturation setup

Water Drainage

e. Figure 4 shows the schematics of the water drainage setup. Water will be removed into the knockout (Figure 5) with the pump.
f. Disconnect water reservoir from valve (B). Disconnect vacuum pump from valve (A). Connect 4 fittings (as shown in Figure 6) and valve (B) through swagelock cross-unions to the knockout. Fitting's Lowest points for suction are placed in gravel section (between wall of the tub and mesh (Figure 7). This will prevent any damages to the sandpack during saturation and drainage procedures.

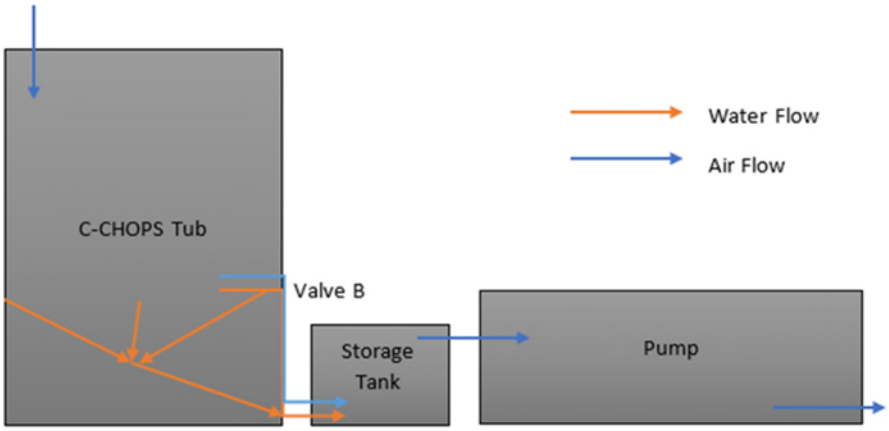

Figure 4. Schematics for water drainage setup

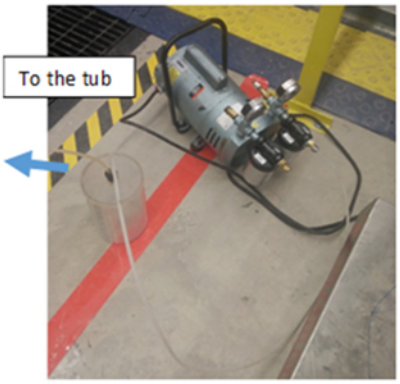

Figure 5. Pump with knockout for water drainage

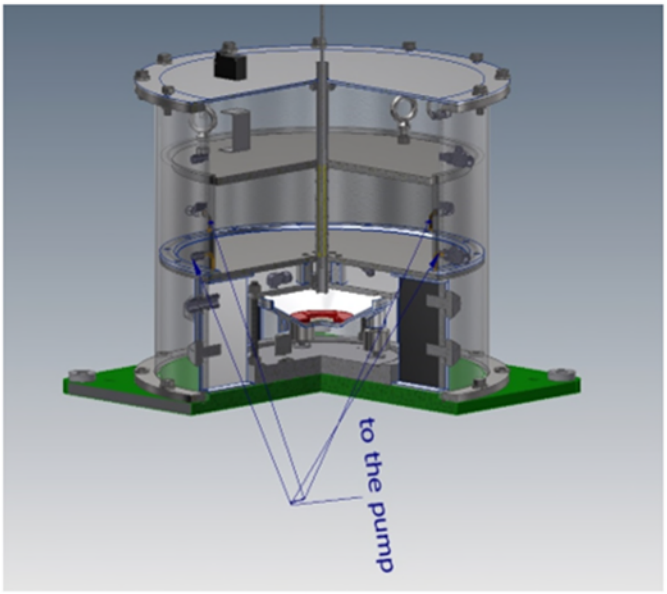

Figure 6. The tub with fittings for water drainage

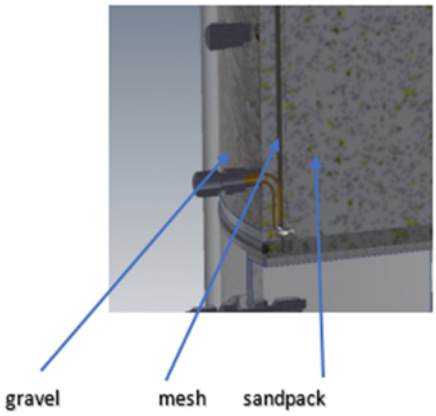

Figure 7. Fitting placement

g. Removing water from the tub should take 2-4 hours. After rate becomes negligible, stop process and wait 10 minutes. Then restart process until no water is coming out.
h. Record the extracted water and provide the net weight of the extracted water.Record the volume of water retained within the sandpack.

Oil Saturation

i. After mobile water has been extracted, the sand pack will be re-saturated with oil.
j. Connect needle valves and pipes as shown in Figure 4. Fit together the oil reservoir system and vacuum pump for fluid saturation. The system consists of (a) one reservoir, (b) 2 valves, (c) pipes and fittings (d) pressure gauge, and (e) vacuum pump. A reservoir filled with oil is placed on top of the tub. Figure 9 shows that both the reservoir and pump systems are connected to the C-CHOPS tub through pipes.

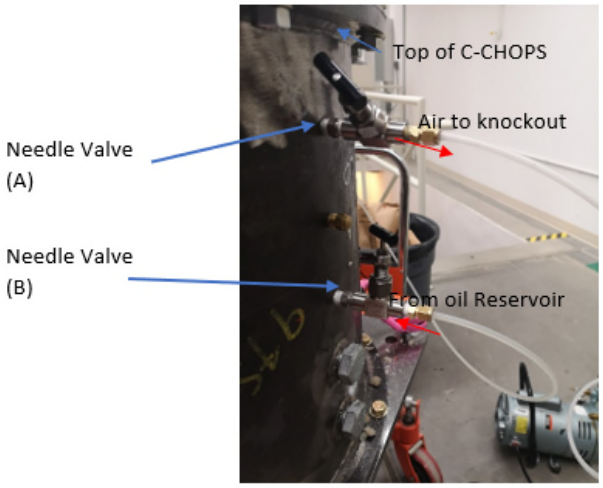

Figure 8. Tub connections for oil saturation

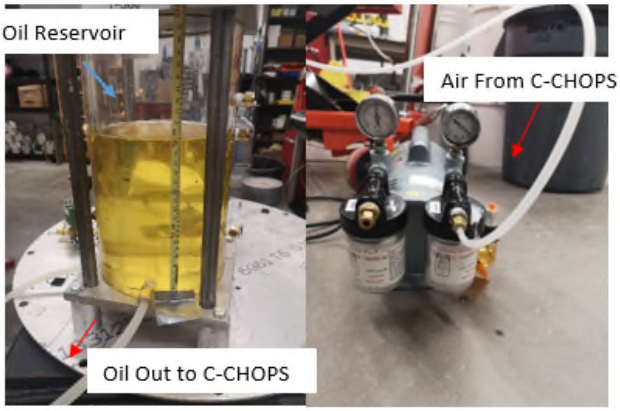

(a) (b)

Figure 9: Setup for oil saturation

k. The volume of oil inside the reservoir should be tracked during oil saturation.
l. Open needle valve (A) and (B). Turn the vacuum pump on for 10 seconds. Before turning off the vacuum pump, close the needle valve (B) so that the air can not enter C-CHOPS tub.
m. With the vacuum pump off and the tub under a small amount of vacuum pressure ensures that the tub is not leaking by listening for air entering the tub and monitoring the pressure gauge on the tub.
    i. If the tub is leaking, repair the leak with silicone.
    ii. If the tub is not leaking, monitor the pressure gauge, and allow pressure to stabilize within the tub.
n. Turn on the vacuum pump again and open the needle valve (B) for 5-10 seconds. Monitor pressure within tub and allow pressure to stabilize. Also monitor sand trap fluid level with the clear pipe on the outside of the tub. If the fluid level begins to drop in the sand trap (indicated by a fluid level drop in pipe), this is an indication that too much vacuum has been applied at once to the tub, and pressure has not stabilized within the tub. If fluid level begins to drop within the sand trap open the needle valve (B) (with pump off) to allow air to enter the tub and increase the tub pressure. Allow pressure to stabilize before applying vacuum again. Repeat until a constant vacuum pressure has been applied to the tub.
o. Allow the tub to stabilize under vacuum pressure for two hours before introducing oil to the system. Note: A large amount of vacuum pressure at once will cause oil within the sand trap to flow through the perforations and into the sand pack. The vacuum must be applied slowly and incrementally to avoid this.
p. Open the external reservoir valve and allow oil to flow from the external reservoir into the sand pack. Full saturation can take between 12-24 hours.
    iii. A fluid flow rate of 10-20 ml/m should be used to avoid piping within the sand pack.
    iv. Monitor the fluid flowrate by utilizing the drop in fluid level in the reservoir over a fixed period

v. Allow the calculated porosity of fluid to fill the sand pack plus an additional volume of oil to fill the edging gravel.

vi. Continuously monitor pressure within the tub to ensure that no air is entering the system

q. Once the fluid has filled the tub, turn the vacuum pump off, close the needle valve, and close the external reservoir valve.

r. Remove the lid from the top of C-CHOPS. If too much oil is added, open the external reservoir valve and allow oil to backflow into external reservoir. If not enough oil is added to the sand pack then return the system to vacuum and add additional oil to the system. Figure 10 shows how the top of the sand layer will look once the entire sand pack is fully saturated.

Figure 10. Final State of the oil saturation

s. Once saturation of the sand pack is complete, disconnect and remove all equipment used for saturation. Needle valves may remain attached to the C-CHOPS tub as long as they are tightly closed. The pressure gauge used to monitor vacuum pressure should be removed from the tub.

t. Continue the procedure for C-CHOPS test.

Oil drainage

u. After centrifuge test is completed, connect a pipr through valve (A) and (B) and let oil drain into a pail naturally. The drainage will take about 12 hours to complete.

Revision 2:

UNIVERSITY OF ALBERTA GeoCERF	Standard Operation Procedure for Sand Pack Saturation and Drainage in C-CHOPS Project	Written by : Yazhao Wang, Dmytro Pantov
		Revision: 2
		Date: 2021-03-23

Model Preparation

1) **Summary**
   a. This section provides safety precautions and operation procedures to saturate the sand pack inside C-CHOPS tub.
2) **Safety Precautions**
   a. Canola oil spills – Ensure spill kit is ready to deploy
3) **Materials needed:**
   a. 40L of tap water
   b. 40 L of food-grade canola oil
   c. Vacuum pump
   d. Needle valves
   e. Various lengths and diameters of swage lock piping
   f. Various swage lock fittings
   g. C-CHOPS tub with sand pack
4) **Significance and Use**
   a. Proper two-phase (water-oil) saturation of the sand pack will eliminate errors during the experiment. If the sample is not properly saturated then the experiment will not resemble in-situ conditions and the results will not accurately reflect the influence of capillary forces on sand production.
5) **Refereneces**
   a. SOP CHOPS Test in Centrifuge
6) **Procedure**
   a. The sand pack saturation procedure is the continuation of the sand pack preparation procedure of the C-CHOPS project as described in SOP CHOPS Test in Centrifuge.

Sealing the Tub

   b. Make sure the sandtrap is prefilled with oil, outlet tube is filled with oil and outlet is plugged with fittings.
   c. C-Chops tub needs to be sealed for both water and oil saturation. To create the seal, install lid to the container. Create a temporary seal at the top of the wellbore with liquid silicone and a rubber plug. Figure 1 shows how the wellbore sealing with silicone will look once completed.
   Note: Curing time will vary depending on the type of silicone that is used. Allow sufficient time for the silicone to cure.

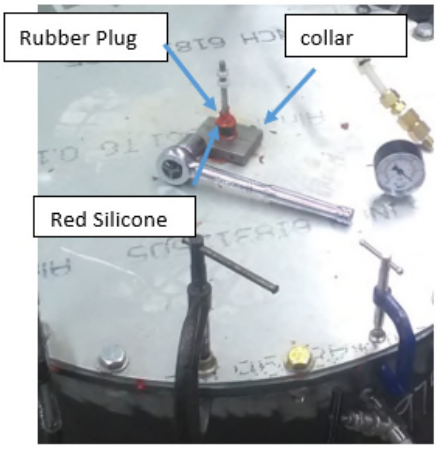

Figure 1: Sealing the C-CHOPS tub

d. Remove two plugs from the tub, including one plug from the top of the tub and one plug two fittings below. Install two needle valves with Teflon in the open ports and ensure needle valves are tightly closed. The valves can be installed on any side of the tub; however, they must be installed in the two rows on the same side as shown in Figure 2. Connect vacuum pump to the needle valve (A) and reservoir T-300 to needle valve (B).

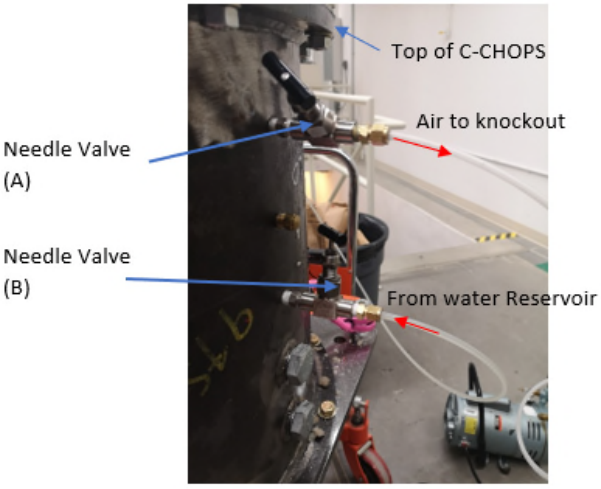

Figure 2: Tub connections for water saturation

Water Saturation

a. Figure 3 shows the setup for water saturation process.
b. Reservoir T-300 should be filled with water. The volume of the injected water should be tracked during the saturation.
c. Open Valve (B) that connects the reservoir and the tub, then open Valve (A). Turn on the vacuum pump and start injecting water into the sand pack.
d. Monitor pressure within tub and allow pressure to stabilize. Also monitor sand trap fluid level with the clear pipe on the outside of the tub. The saturation is complete when water is coming through Valve A into the knockout vessel. Turn off the pump.

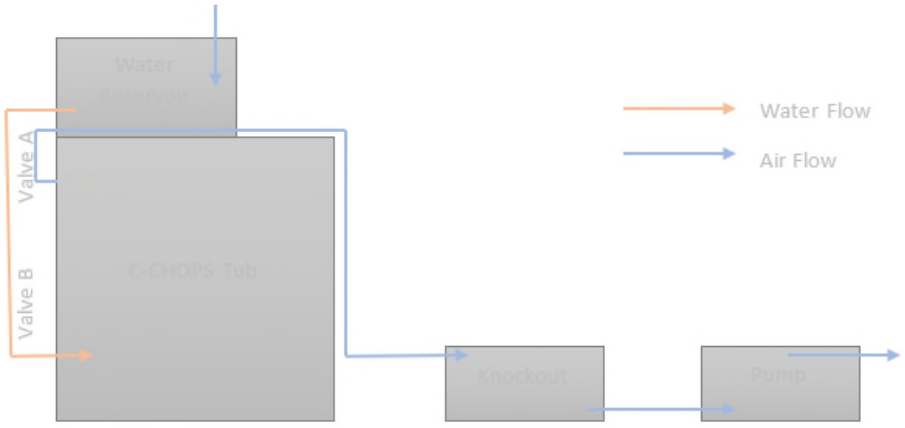

Figure 3. Schematics of water saturation setup

Oil Saturation

e. After the sand pack has been saturated with water, the sand pack will be re-saturated with oil. Figure 8 shows the schematic of the oil saturation setup.
f. Connect needle valves and pipes as shown in Figure 9. Fit together the oil reservoir system and vacuum pump for fluid saturation. The system consists of (a) one reservoir, (b) 2 valves, (c) pipes and fittings (d) pressure gauge, and (e) vacuum pump. The reservoir (T-300) is filled with oil and placed on top of the tub. The outlet from the oil reservoir will be connected to the sand trap drainage port. Pump and fluid knock will be connected to Valve A (Located at top of the sand pack) Figure 10 shows that both the reservoir and pump systems are connected to the C-CHOPS tub through pipes.

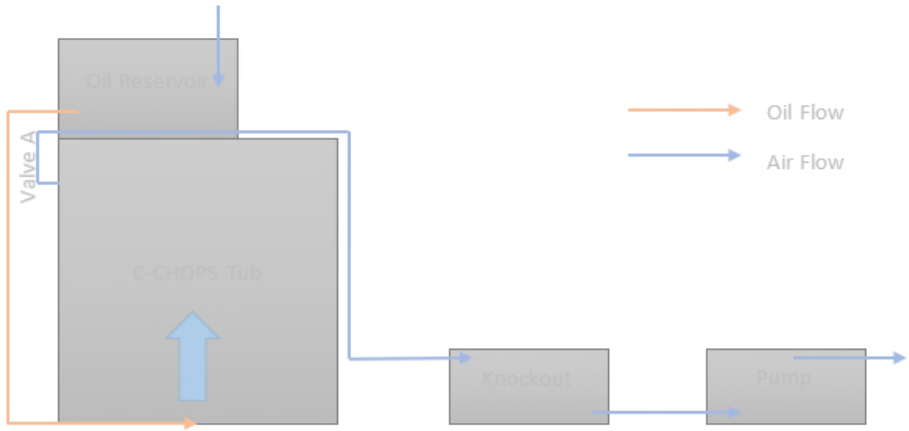

Figure 8. Schematics of oil saturation setup

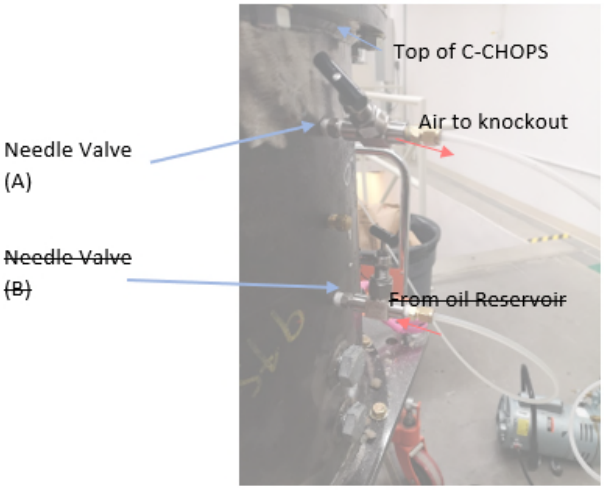

Figure 9. Tub connections for oil saturation

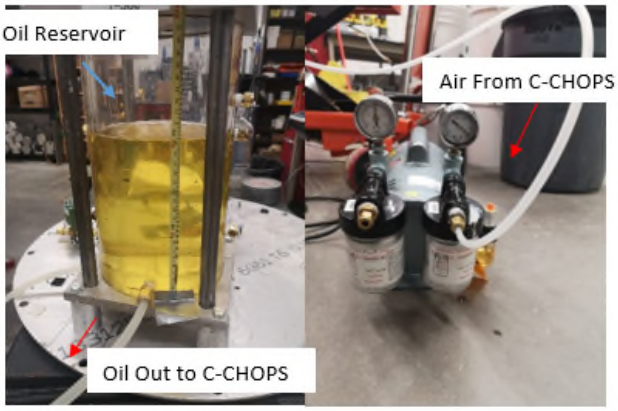

(a) (b)

Figure 10. Setup for oil saturation

g. The volume of oil inside the reservoir should be tracked during oil saturation.
h. Open needle valve (A) and sand trap drainage port. Turn the vacuum pump on for 10 seconds. Before turning off the vacuum pump, close sand trap drainage port so that the air can not enter C-CHOPS tub.
i. With the vacuum pump off and the tub under a small amount of vacuum pressure ensures that the tub is not leaking by listening for air entering the tub and monitoring the pressure gauge on the tub.
    i. If the tub is leaking, repair the leak with silicone.
    ii. If the tub is not leaking, monitor the pressure gauge, and allow pressure to stabilize within the tub.
j. Turn on the vacuum pump again and open the sand trap drainage port for 5-10 seconds. Monitor pressure within tub and allow pressure to stabilize. Also monitor sand trap fluid level with the clear pipe on the outside of the tub. If the fluid level begins to drop in the sand trap (indicated by a fluid level drop in pipe), this is an indication that too much vacuum has been applied at once to the tub, and pressure has not stabilized within the tub. If fluid level begins to drop within the sand trap open the sand trap drainage port (with pump off) to allow air to enter the tub and increase the tub pressure. Allow pressure to stabilize before applying vacuum again. Repeat until a constant vacuum pressure has been applied to the tub.
k. Allow the tub to stabilize under vacuum pressure for two hours before introducing oil to the system. Note: A large amount of vacuum pressure at once will cause oil within the sand trap to flow through the perforations and into the sand pack. The vacuum must be applied slowly and incrementally to avoid this.
l. Open the external reservoir valve and allow oil to flow from the external reservoir into the sand pack. Full saturation can take between 12-24 hours.
    iii. A fluid flow rate of 10-20 ml/min should be used to avoid piping within the sand pack.
    iv. Monitor the fluid flowrate by utilizing the drop in fluid level in the reservoir over a fixed period

v. Allow the calculated porosity of fluid to fill the sand pack plus an additional volume of oil to fill the edging gravel.
vi. Continuously monitor pressure within the tub to ensure that no air is entering the system

m. Once the fluid has filled the tub, turn the vacuum pump off, close the needle valve, and close the external reservoir valve.
n. Remove the lid from the top of C-CHOPS. If too much oil is added, open the external reservoir valve and allow oil to backflow into external reservoir. If not enough oil is added to the sand pack then return the system to vacuum and add additional oil to the system. Figure 11 shows how the top of the sand layer will look once the entire sand pack is fully saturated.

Figure 11. Final State of the oil saturation

o. Once saturation of the sand pack is complete, disconnect and remove all equipment used for saturation. Needle valves may remain attached to the C-CHOPS tub as long as they are tightly closed. The pressure gauge used to monitor vacuum pressure should be removed from the tub.
p. If the level of oil saturation is not desierable, the centrifuge can be used to assist while conducting steps i to step q.
q. Continue the procedure for C-CHOPS test.

Oil drainage

r. After centrifuge test is completed, connect a pipe through valve (A) and (B) and let oil drain into a pail naturally. The drainage will take about 12 hours to complete.

APPENDIX D. Event Logs

Event log for V1 test:

Time (min)	Notes
0	rpm = 111, N = 25
16	Centrifuge turned off to add more oil into T300 to be able to observe flow from overflow port
22	rpm = 111, N = 25
27	V2 opened to fill the tub up to the overflow port, there was an increase in tub upper and tub lower pressure transducers
30	T200 pressure increased meaning we are having overflow
31	Pump turns on to dump fluid from T200 to T300
37	V1 opened to create XDD
41	The leveling arm lowered all the way down
49	To dump fluid from T100 to T200, V3 opened, therefore T200 pressure increased and as a result T300 increased because of the pump
49	V3 closed soon to prevent data loss in T100
54	Leveling arm raised all the way up
56	PR
64	PR completed
66	The leveling arm lowered all the way down
67	To dump fluid from T100 to T200, V3 opened, therefore T200 pressure increased and as a result T300 increased because of the pump
70	Leveling arm raised all the way up
71	The leveling arm lowered all the way down
82	To dump fluid from T100 to T200, V3 opened, therefore T200 pressure increased and as a result T300 increased because of the pump
84	Leveling arm raised all the way up
85	The leveling arm lowered all the way down
93	Leveling arm raised all the way up
94	The leveling arm lowered 1.8 cm
98	The leveling arm lowered 1.8 cm
102	The leveling arm lowered 1.8 cm
104	The leveling arm lowered 1.8 cm
106	The leveling arm lowered 1.8 cm
109	The leveling arm lowered 1.8 cm
112	Leveling arm raised all the way up
112	The leveling arm lowered all the way down

Event log for G2 test:

Time (min)	Notes
0	rpm = 111, N = 25
3	The pump was ON during the whole experiment without changing its rate
6	V2 opened to fill the tub up to the overflow port, there was an increase in tub upper and tub lower pressure transducers
16	Everything got constant except the load cells, so we proceed to the next step; V1 opened, there was a reduction in sandtrap pressure
22	Lever dropped fully to create XDD, a period was given to have a better observation of the event
28	Plug was removed, sandtrap pressure increased which means we were producing sand
36	Plug removal was completed
42	V3 opened and closed quickly
74	V1 closed
84	V1 opened
117	V1 closed
123	V1 opened
135	V1 closed
144	V1 opened
159	V1 closed
190	V1 opened
216	End of the experiment (G2)

Event log for C3 test:

Time (min)	Notes
0	rpm = 111, N = 25
1	The pump turned ON and was on during the whole experiment without changing its rate
55	V2 opened to fill the tub up to the overflow port, there was an increase in tub upper and tub lower pressure transducers
74	Leveling arm lowered to create XDD
77	V1 opened, T100 pressure increased
96	V1 closed
96	V3 opened to dump fluid from T100 to T200
97	V3 closed
119	PR initiated and load cell reading increased because of sand production in the wellbore
126	PR completed
139	V1 opened
140	V3 opened
140	V3 closed
142	V3 opened
142	V3 closed
143	V3 opened
143	V3 closed
144	V3 opened
144	V3 closed
146	V3 opened
146	V1 closed
151	All valves closed, pump and centrifuge turned off
151	Test was abandoned

Event log for W4-a test:

Time (min)	Notes
46	rpm = 111, N = 25
47	The pump turned ON and was on during the whole experiment without changing its rate
56	V2 opened to fill the tub up to the overflow port, there was an increase in tub upper and tub lower pressure transducers
62	Leveling arm lowered to create XDD
63	V1 opened, T100 pressure increased
69	V3 opened
69	V3 closed
73	V3 opened
73	V3 closed
81	V3 opened
81	V3 closed
87	V3 opened
87	V3 closed
95	V3 opened
95	V3 closed
105	V3 opened
105	V3 closed
113	V3 opened
113	V3 closed
122	V3 opened
122	V3 closed
128	V3 opened
128	V3 closed
132	V1 closed
139	PR initiated
152	PR completed
152	V3 opened
153	V3 closed
158	Leveling arm raised all the way up to create NDD
162	V1 opened
162	V3 opened
162	V3 closed

Time (min)	Notes
163	Leveling arm lowered for 2.2 cm
167	Leveling arm lowered for 2.2 cm
169	Leveling arm lowered for 2.2 cm
171	Leveling arm lowered for 2.2 cm
173	Leveling arm lowered for 2.2 cm
175	Test was abandoned

Event log for W4-b test:

Time (min)	Notes	Time (min)	Notes
0	rpm = 111, N = 25	142	Pump's rate was set to maximum rpm
1	The pump turned ON, the load cells weren't responding correctly		
32	V2 opened to fill the tub up to the overflow port but no pressure drop was noticed	146	V3 closed and leveling arm lowered for 2.7 cm
44	Leveling arm lowered to create XDD	153	V3 opened
47	V1 opened, no fluid flow occurred	154	V3 closed and leveling arm lowered for 2.7 cm
51	Leveling arm raised all the way up	159	V3 opened
60	V1 closed	162	V3 closed and leveling arm lowered for 2.7 cm
80	Leveling arm lowered to create XDD	166	V3 opened
84	V1 opened, no fluid flow occurred	170	V3 closed and leveling arm lowered for 2.7 cm
90	Centrifuged was stopped, the range of leveling arm was lowered to allow bigger draw down to be applied	173	V3 opened
105	rpm = 111, N = 25	179	Leveling arm raised all the way up
		184	V3 closed, V1 close and leveling arm lowered all the way down
107	V1 closed	185	V1 opened
		186	V3 opened
117	V1 opened, no fluid flow occurred	188	V3 closed
117	Leveling arm raised all the way up	189	V3 opened and closed
120	The plug lifted for 3 mm to open the fluid path if it was blocked but that didn't allow for fluid flow	190	Leveling arm raised all the way up
		191	V3 opened
121	V3 opened and closed immediately	195	V3 closed, V1 closed, leveling arm dropped fully and V1 opened
122	PR initiated, increase T100 pressure was observed	197	V3 opened
131	V3 opened	202	The test was abandoned
132	V3 closed and opened		
136	V3 closed		
137	V3 opened		

Event log for W4-c test:

Time (min)	Notes	Time (min)	Notes
0	rpm = 111, N = 25	244	V1 opened, no fluid flow occurred
1	The pump turned ON	245	V1 closed
32	V2 opened to fill the tub	251	V1 opened, no fluid flow occurred
63	V2 closed	253	V1 closed
70	Centrifuged was stopped, more oil was added to T300 to raise the sandtrap's pressure	259	V1 opened, no fluid flow occurred
137	rpm = 111, N = 25	261	V1 closed
143	V2 opened to fill the tub	267	V1 opened, no fluid flow occurred
155	Arm dropped all the way down to create XDD	269	V1 closed
156	V1 opened, no fluid flow occurred, maybe because of the air in the sandtrap	275	V1 opened, no fluid flow occurred
167	V1 closed	277	V1 closed
170	Centrifuged was stopped, to change the leveling arm's range to create a bit of higher DD, V2 was closed	282	V1 opened, no fluid flow occurred
187	rpm = 111, N = 25	284	V1 closed
		290	V1 opened, no fluid flow occurred
195	Sandtrap pressure decreased a bit but raised again, maybe because of air in the sandtrap	291	V1 closed
		296	V1 opened, no fluid flow occurred
		300	V1 closed
200	V2 opened	306	V1 opened, no fluid flow occurred
203	V1 opened, no fluid flow occurred	314	V1 closed
208	V1 closed	317	PR initiated
		332	Leveler dropped by 2 cm
216	V1 opened, no fluid flow occurred	333	V1 opened
		334	V1 closed, V2 closed, V3 opened
		339	Leveler dropped by 2 cm, V1 opened,
219	V1 closed	341	V3 closed and opened shortly, V1 closed
		344	V1 opened
226	V1 opened, no fluid flow occurred	345	V3 closed and opened shortly, V1 closed
		348	Leveler dropped by 2 cm, V1 opened,
		350	V3 closed and opened shortly
229	V1 closed	351	V1 closed
236	V1 opened, no fluid flow occurred		
238	V1 closed		
		355	V3 closed and opened shortly, Leveler dropped by 2 cm, V1 opened
		356	V1 closed
		360	V3 closed and opened shortly Leveler dropped by 2.6 cm, V1 opened
		361	V1 closed
		368	The test was abandoned

APPENDIX E. Permeability Calculations before Sand Production

Permeability for V1 Test:

To calculate permeability before sand production, an average flowrate (obtained from the slope of T100 pressure versus time) was used. Then, permeability was calculated using the following equation after Craft et al. (1991):

$$k = \frac{q \times \mu \times ln\frac{r_e}{r_w}}{2\pi \times h \times (P_e - P_w)} \quad \text{(G1)}$$

Where:

k is the permeability for a radial flow;

q is the measured flowrate from T100 prior to sand production;

μ is the fluid viscosity;

r_e is the sandpack radius;

r_w is the wellbore radius;

h is the height of sandpack before sand production;

P_e is the reservoir pressure corrected to wellbore pressure as the common datum;

P_w is the wellbore pressure;

Permeability could be estimated as follow:

Permeability for V1 Test:

h	Reservoir head	Wellbore head	Pe	Pwf	re	rw	μ at 20C	q	K	K
m	m	m	Pa	Pa	m	m	Pa.s	m3/s	m2	D
0.154	0.25	0.15	56591	33955	0.26	0.011	0.0782	1E-07	1E-12	1.1

Permeability for G2 Test:

h	Reservoir head	Wellbore head	Pe	Pwf	re	rw	μ at 20C	q	K	K
m	m	m	Pa	Pa	m	m	Pa.s	m3/s	m2	D
0.161	0.24	0.15	56936	35585	0.26	0.011	0.0782	1.6667E-07	2E-12	1.9

Permeability for C3 Test:

h	Reservoir head	Wellbore head	Pe	Pwf	re	rw	μ at 20C	q	K	K
m	m	m	Pa	Pa	m	m	Pa.s	m3/s	m2	D
0.181	0.26	0.14	61680	33212	0.26	0.011	0.0782	2E-07	2E-12	1.5

Permeability for W4-a Test:

h	Reservoir head	Wellbore head	Pe	Pwf	re	rw	μ at 20C	q	K	K
m	m	m	Pa	Pa	m	m	Pa.s	m3/s	m2	D
0.152	0.5	0.4	122625	98100	0.26	0.011	0.001	1.5E-06	2E-13	0.21

In this test because the dominant fluid was water, viscosity of water (1 cp) was considered for the permeability calculations.

[Note]: No fluid flow was observed prior to plug removal and sand production in tests W4-b and W4-c. Therefore, the permeability for these two tests could not be determined.

APPENDIX F. Load Cell Data

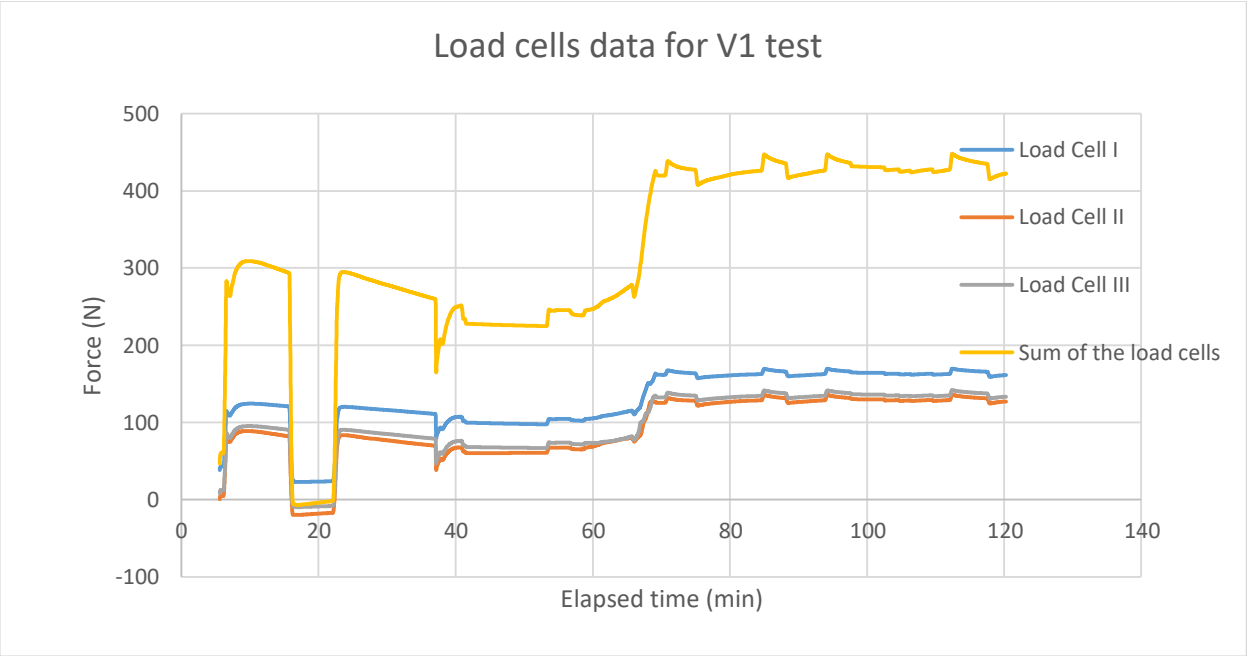

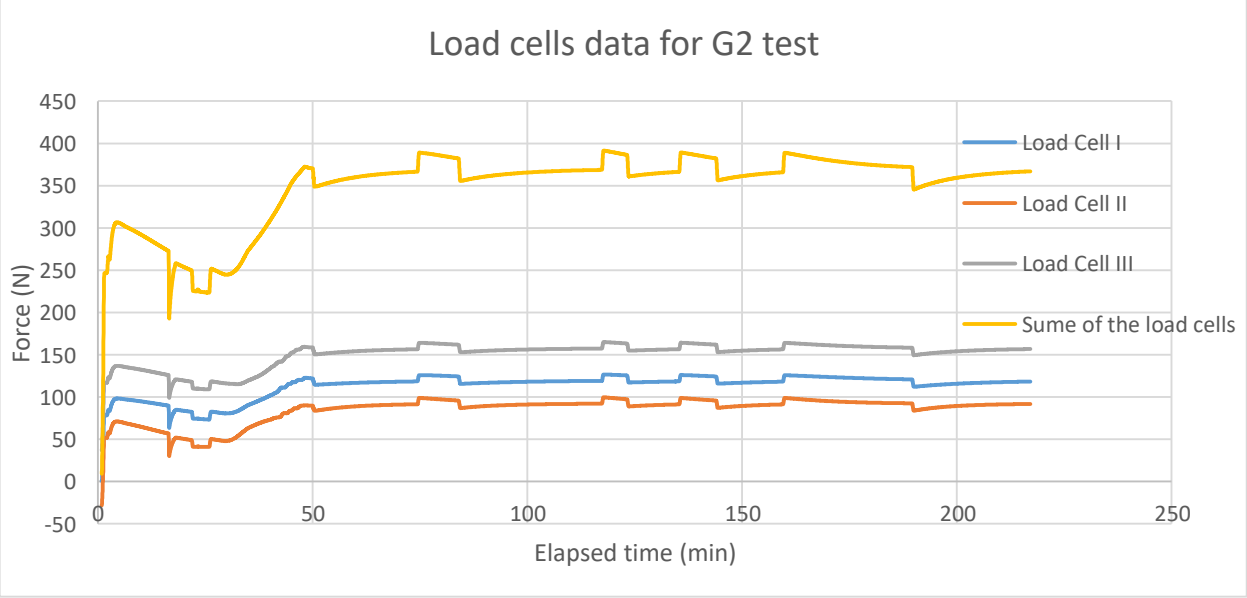

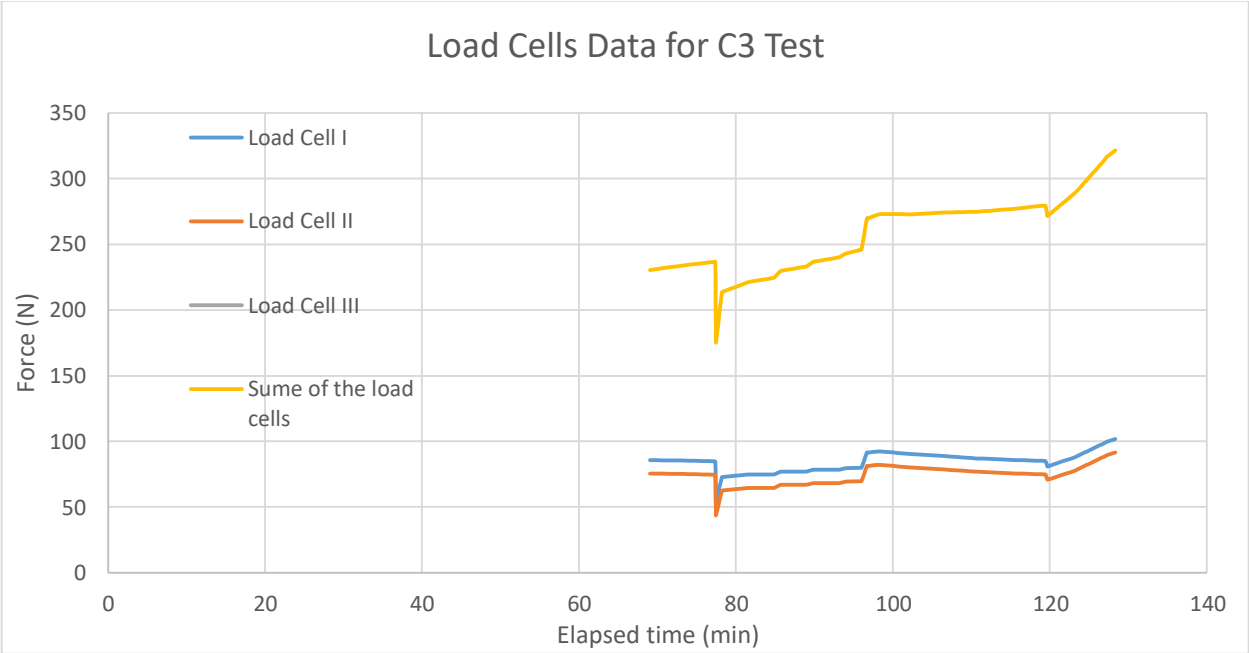
Load Cells Data for C3 Test
Load Cell I
Load Cell II
Load Cell III
Sume of the load cells
Force (N)
Elapsed time (min)
350
300
250
200
150
100
50
0
0
20
40
60
80
100
120
140

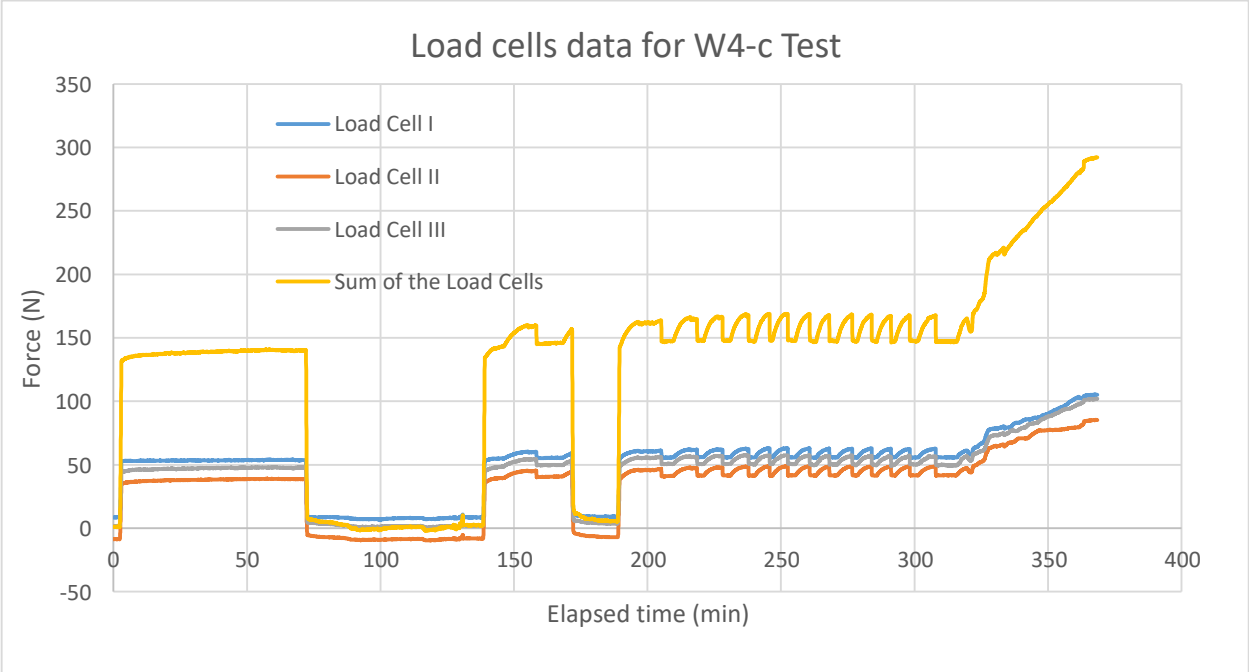
Load cells data for W4-c Test
Load Cell I
Load Cell II
Load Cell III
Sum of the Load Cells
Force (N)
Elapsed time (min)
350
300
250
200
150
100
50
0
-50
0
50
100
150
200
250
300
350
400

APPENDIX G. Stress Analysis Model

The height of the model (Figure G.1) was similar to the height of the sandpack in W4-c after the test which was 152 mm. To build the model as simple as possible to avoid complexity, it was tried to limit the number of boundaries and materials in this work. Therefore, instead of modelling the caprock/overburden material or the high permeable material around the reservoir, a distributed load on top of the sandpack accounted for the mass of caprock and overburden material, and a total head at the edge of the sandpack to model the layer of gravel around the reservoir was applied.

On the left segment of the model, wellbore was considered as 5 rows of perforations like the actual perforation on the wellbore in the physical model with free displacement. Displacement of other parts of this segment were only restrained in the X direction. The right segment of the models represents the edges of the sand reservoirs where again restrained in the X direction. The bottom segment of the model represent the bottom of sand reservoirs and they were restrained in the XY direction. The top segment of the reservoirs was restrained in the XY direction too. The bottom two corners of the models were restrained in the XY direction. To create NDD condition total heads of 0.24 was calculated based on the experimental model and was then applied to each perforations accounting for a datum at the base of the reservoir. Also as mentioned above, instead of accounting for modelling high permeable material around the sandpack like the gravel, a total head of 0.24 m was calculated based on the actual physical model and was then applied to the right segment for the model.

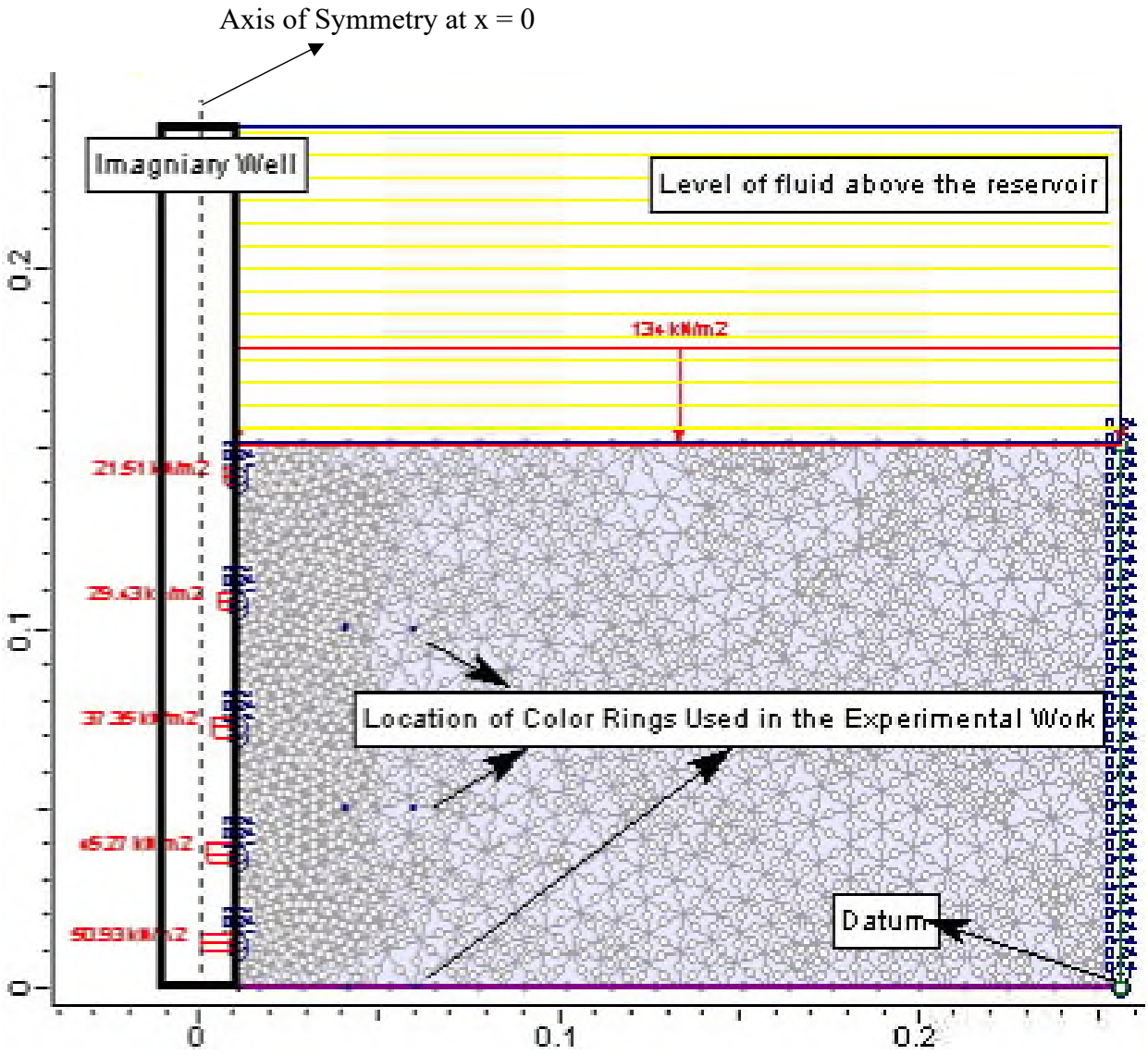

Figure G.1. The external boundary and boundary condition of the model (see Table G.1)

About 3243 of 6 Noded Triangles was used in the model to create approximately 1576 mesh elements. A finer mesh element (higher concentration) was used in the left segment where it is considered to be the wellbore. In the model a discharge section (green vertical line) was applied at the right segment of the model to calculate the total flowrate that is passing from that interval. This helped to interpolate the hydraulic conductivity prior to the sand production in the model by matching its flowrate with the observed experimental flowrate. However, it should be noted that the in W4-c test, there was no flowrate occurring prior to sand production. Also, this data could not be inherited from W4-b test because of facing the same issue. W4-a test, was not a good test to inherit the flowrate prior to the sanding because of high water saturation in that test. The best test that could serve this purpose was C3 test because of known flowrate prior to sand production, having synthetic caprock used in this test, and using a high permeable layer of gravel around the sandpack. Calculation regarding how the hydraulic conductivity was obtained from C3 test is shown in Appendix E. An important fact about the measured flow rate in RS2 in an axisymmetric model is that the RS2 calculates the flow rate in radian. That said, to calculate the flow rate of the whole model, the flow rate calculated by the model needs to be multiplied by 2π. However, because there was no flowrate prior to the sand production, a numerical model for C3 test was built and its hydraulic conductivity was estimated prior to the sanding. Then, it was assumed that in W4-c test, the hydraulic conductivity prior to sanding was similar to what was estimated in C3 test. Only one material (sand) was used for this modelling. A complete description of the model is provided in Table G.1.

Table G.1. Full description of the model

Type	Data
Radius of the wellbore	11 mm
Radius of the reservoir	256 mm
Height of the sandpack	152 mm
Fluid Flow Condition	Steady State
Pore Fluid Unit Weight (Canola Oil)	226.37 kN/m^3
Unit Weight (of sand)	462 kN/m^3
Material Behaviour	Drained
Porosity	35% (from C3 test)
Hydraulic Conductivity	1.07e^{-5} m/s (matched with experimental data of C3 test)
Initial Pore Water Pressure	53 kPa
Poisson's Ratio	0.25
Young's Modulus	18,000 kPa
Material type	Plastic (to be able to predict yielded zone)
Peak Tensile Strength	2 kPa
Peak Cohesion for the First Model	0 kPa
Peak Cohesion for the Second Model	2 kPa
Dilation Angle of Sand	12^o (Vermeer & Pieter, 1984)
Hydraulic Conductivity before Sanding	1.07e^{-5}
K2/K1	1
Soil Type	Sand
Material Behaviour	Drained
Reservoir head (head at the edge of the sandpack)	0.24 m
Wellbore Head in NDD mode	0.24 m
Wellbore Head in XDD mode	0.11 m
Overburden Stress	134 kN/m^2
$\sigma_H = (1 - \sin\varphi) \times \sigma_V$	48
Effective Stress Ratio (horiz/vert)	0.36
Field Stress Type	Gravity
Ground Surface Elevation	0.151 m
Locked-in Horizontal Stress	-17 kPa, Comp. +
Unit Weight of Overburden	2782 kN/m^3

For soil when applying a vertical stress, it will expand to lateral direction according to the lateral earth pressure coefficient. And, for passing loading, which is a scenario in C-CHOPS tests, there is an equation to calculate that coefficient based on the friction angle of the sand which is as follows:

$$\sigma'_H = (1 - \sin\varphi) \times \sigma'_V \quad \text{(G.1)}$$

Where:

σ'_H is the horizontal stress;

φ is the friction angle of the sand;

σ'_V is the vertical stress;

Therefore, effective stress ratio (horiz/vert) can be estimated for the modelling. Also, according to the Mohr circle, for such a soil, the circle should touch the failure criteria. Having the vertical stress and the friction angle, the horizontal stress which touch the failure criteria could be determined. Therefore, by adjusting the locked-in horizontal stress in the model by -17 kPa, the stresses in the model could be calibrated on top of the reservoir. The locked-in horizontal stress is simply shift the value of the horizontal stress up or down in the model. As mentioned above, the horizontal stress using the Mohr circle was estimated. Then, it was tried to manually change the values of locked-in horizontal stress in the model to match the estimated horizontal stress on top of the reservoir at the interface where effective stress is applied.

APPENDIX H. Seepage Analysis Model

W4-c test was considered for this modelling because of the most available sets of data compared to other tests. Therefore, a similar model was built with the same description as provided in Table G.1, except this time, a cavity was considered in the model (Figure H.1.a) and the fluid flow condition was set to be XDD by applying a total head of 0.11 m at the calculated. To model a cavity in RS2 simulator, the excavation feature was used. Likewise, in the previous model, the hydrostatic pressure at each perforation was calculated and applied at each of them in addition to the base of the cavity and part of its side slope (Figure H.1.b). However, because of the existence of the cavity and level of fluid in the wellbore and cavity, air was occupied the empty volume of the cavity and was getting into the sand that plugged off some of the pores and made it more difficult for oil to flow in that area. So, all the pressure above the oil needed to be set at zero. So, to apply the atmospheric pressure, part of the boundary condition of the side slope of the cavity that was not in touch with fluid was defined as zero pressure.

The dimension and location of the cavity was similar to what was observed in W4-c test. To be able to determine the remolded zone near the wellbore/cavity, the model with only cavity was run first. Then, two remolded zones were determined. One was a simple vertical line near the wellbore and the other one a line with the same slope angle as the cavity according to the maximum shear plastic strain graph (Figure H.2). The reason for assuming the remolded zone was based on Figure **4.15** where shear displacement had occurred near the perforations. Then, based on these zones, the model was modified meaning that these zones were added to the model (Figure H.3).

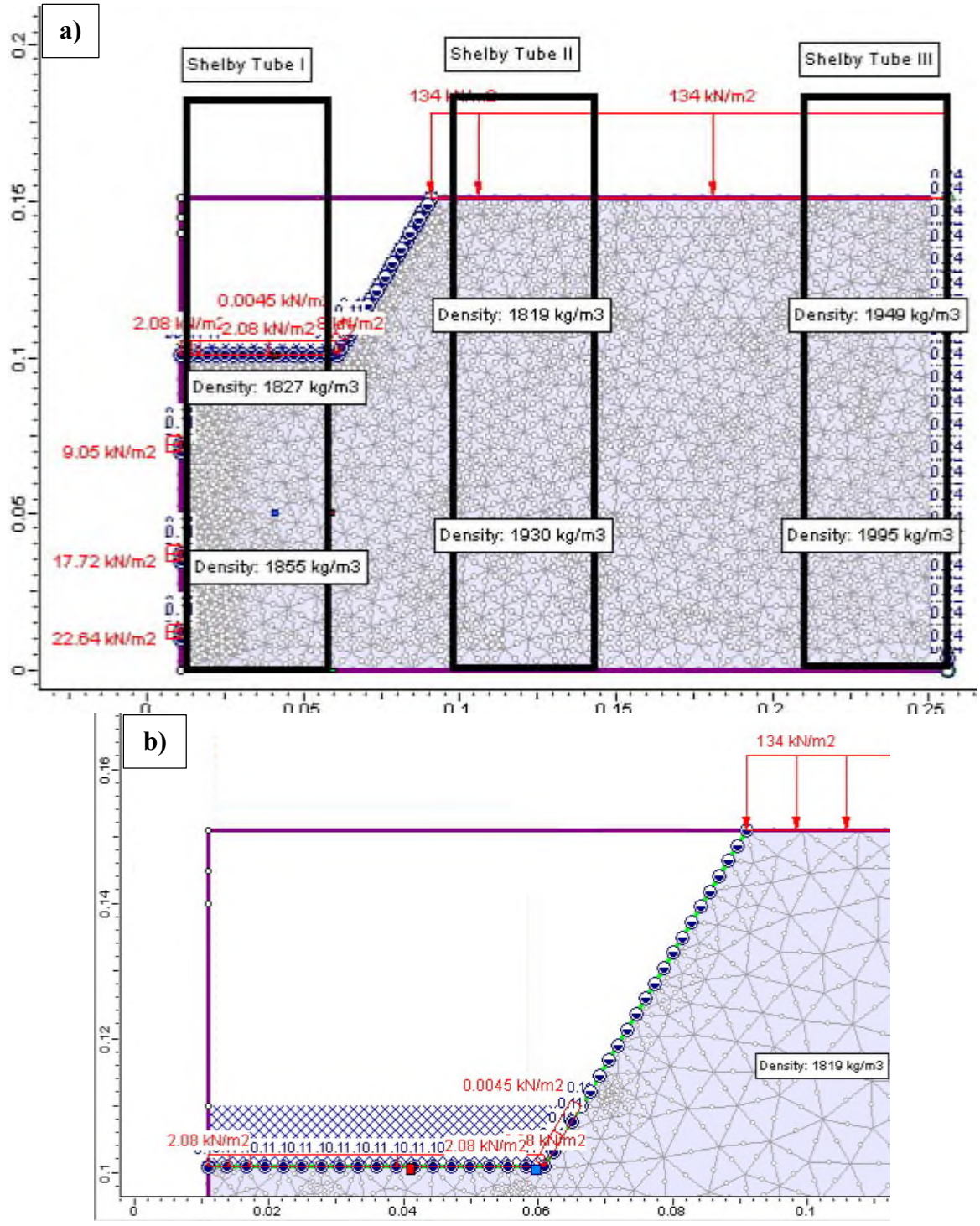

Figure H.1. a) The model with a cavity similar to the experimental work in W4-c test. Shelby tubes that were inserted in the experimental work are shown in the models including the density measurements from each tube; b) A closer look at the cavity and its boundary conditions.

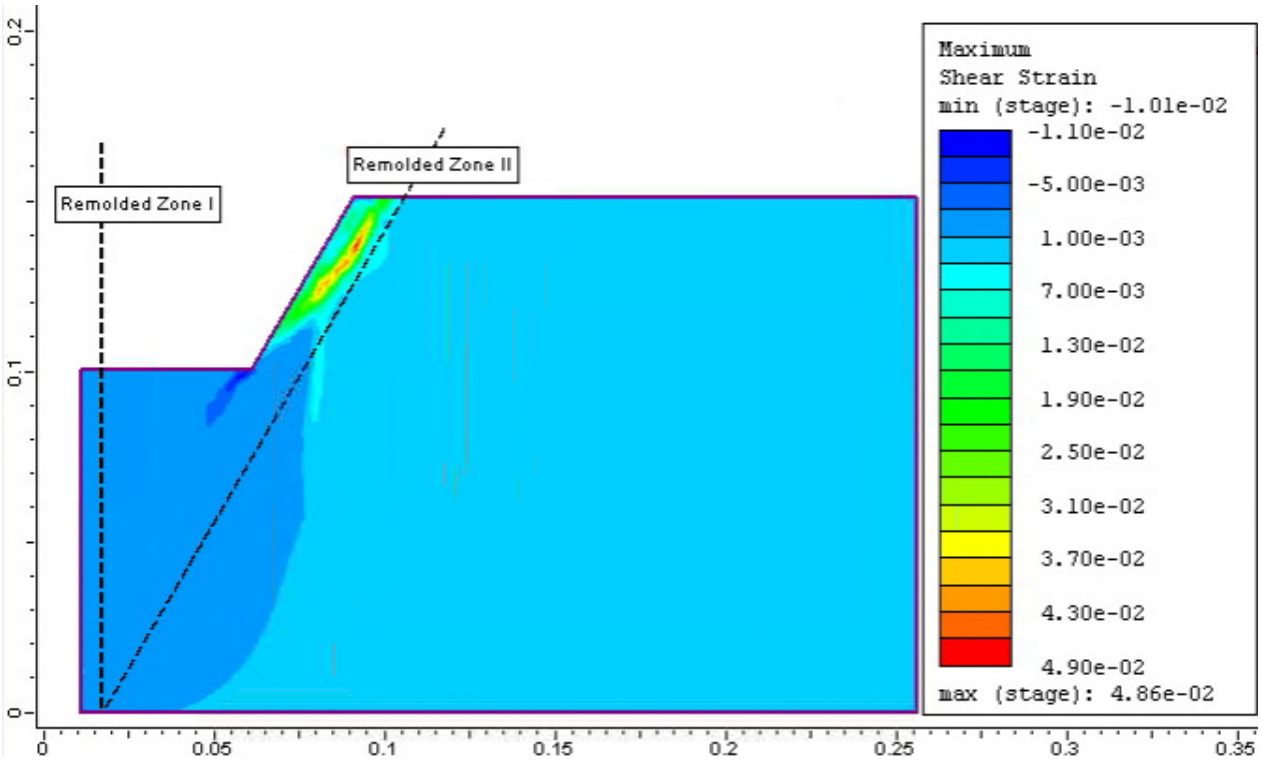

Figure H.2. The interpreted remolded zones in the model with cavity. Two zones were assumed for the remolded zones. Zone I is an approximate representation of the near-perforation zones of intense yielding and dilation, as demonstrated in the pre-sanding stress analyses presented in Chapter 4. Zone II is an approximate representation that captures an area of relatively low stress below the cavity, and yielded and dilated rock adjacent to the cavity surface.

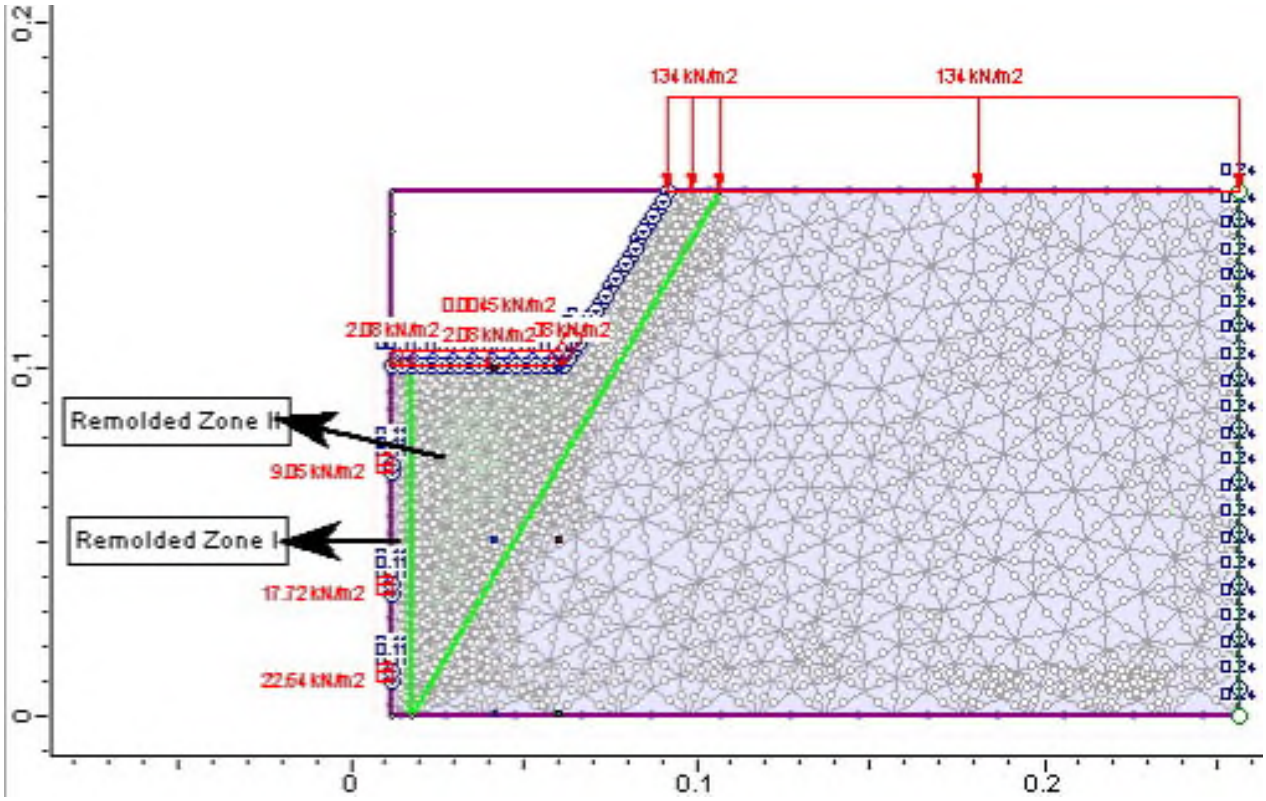

Figure H.3. The modified model with remolded zones

Having remolded zones determined in the model, two models were originated from the model as follow:

1. The hydraulic conductivity of remolded zone I to be increased to match the experimental flowrate after the sand production while using the hydraulic conductivity before sand production for the rest of the reservoir (Figure H.4).

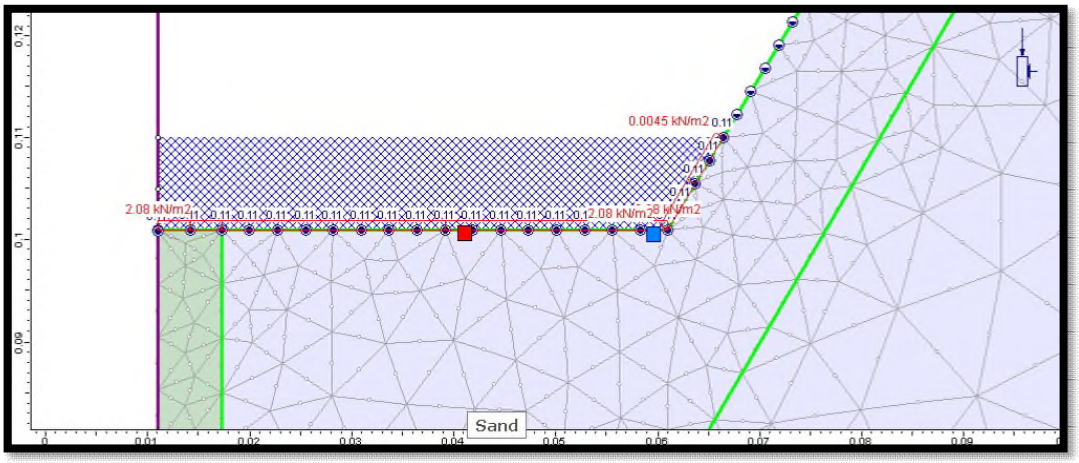

Figure H.4. The model which the hydraulic conductivity of remolded zone I (close to the wellbore has been altered. The red and blue squares in the model or just tools to demonstrate where the color rings located in the experimental test.

2. The hydraulic conductivity of remolded zone I and II to be increased to match the experimental flowrate after the sand production while using the hydraulic conductivity before sand production for the rest of the reservoir (Figure H.5).

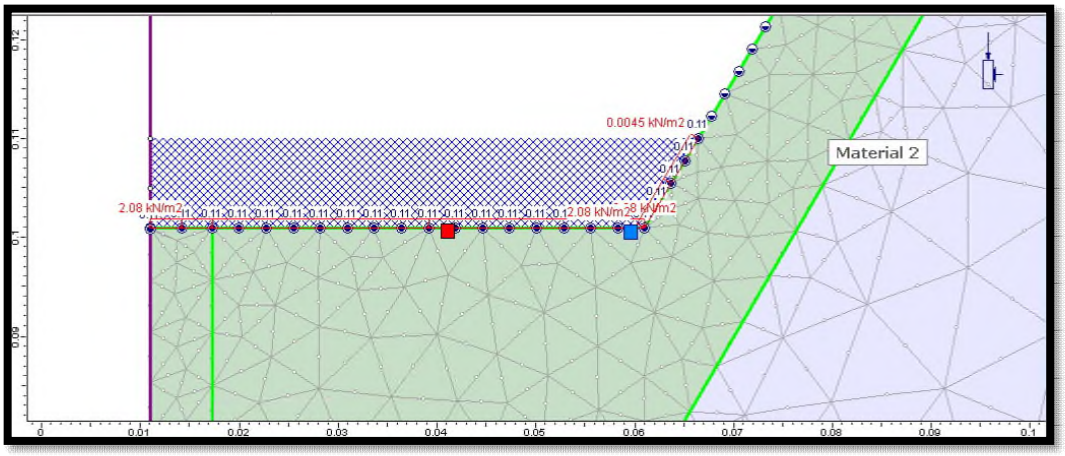

Figure H.5. The model which the hydraulic conductivity of remolded zone I and II (close to the wellbore and the cavity has been altered.

Attempts to match the flowrate by changing the hydraulic conductivity of the remolded zone(s) to the observed flowrate in the experimental work for both models are shown in Figure **4.18**.

Figure H.6 shows how flow paths preferentially bend towards the cavity as result of flow's preference toward shorter paths compared to the lower parts of the wellbore that are surrounded by sand.

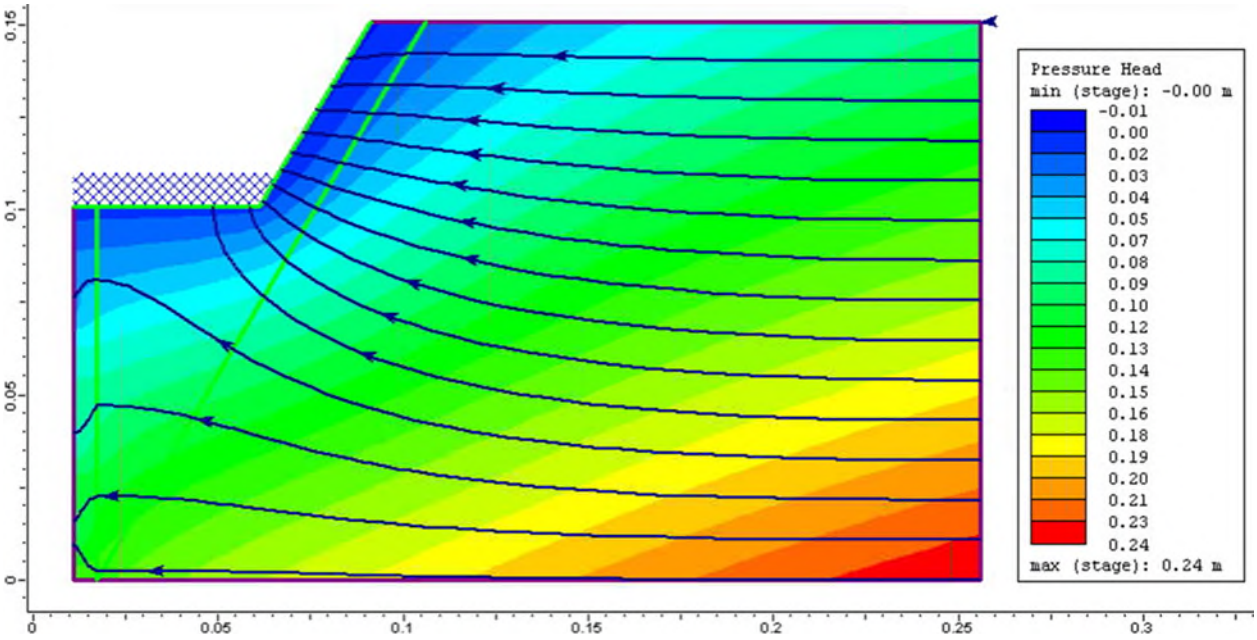

Figure H.6. Modeled flowlines for the W4-c test

APPENDIX I. Submerged angle of slope estimation for a planar slope of infinite length

For a friction angle of 33.7° (calculated after (Lambe & Whitman, 1969):

Parameter / Equation	Comment	Value(s)
N	Scaling factor	25
γ'	Buoyant specific weight of sand	10.54 kN/m^3
γ_{sat}	Specific weight of saturated sand	19.56 kN/m^3
ϕ	Angle of friction measured under dry conditions	33.7°
$\tan(\phi') = \frac{N \cdot \gamma'}{N \cdot \gamma_{sat}} \tan(\phi) = \frac{\gamma'}{\gamma_{sat}} \tan(\phi)$	Equation for calculating effective friction angle (ϕ') of wet (i.e., oil-saturated) sand. Note that the value is independent of the gravitational scaling factor	-
$\phi' = \tan^{-1}\left(\frac{10.54}{19.56}\tan(33.7°)\right)$	Effective friction angle of wet sand	19.7°
$F = \frac{tan(\phi')}{tan(\alpha)}$	Equation for calculating factor of safety for a submerged slope of infinite length	-
$\alpha = \tan^{-1}\left(\frac{\tan(19.7°)}{1}\right)$	Slope angle at frictional equilibrium ($F = 1$)	19.7°

For friction angle of 40°:

Parameter / Equation	Comment	Value(s)
N	Scaling factor	25
γ'	Buoyant specific weight of sand	10.54 kN/m^3
γ_{sat}	Specific weight of saturated sand	19.56 kN/m^3
ϕ	Angle of friction measured under dry conditions	40°
$\tan(\phi') = \frac{N \cdot \gamma'}{N \cdot \gamma_{sat}} \tan(\phi) = \frac{\gamma'}{\gamma_{sat}} \tan(\phi)$	Equation for calculating effective friction angle (ϕ') of wet (i.e., oil-saturated) sand. Note that the value is independent of the gravitational scaling factor	-
$\phi' = \tan^{-1}\left(\frac{10.54}{19.56}\tan(40°)\right)$	Effective friction angle of wet sand	24.5°
$F = \frac{tan(\phi')}{tan(\alpha)}$	Equation for calculating factor of safety for a submerged slope of infinite length	-
$\alpha = \tan^{-1}\left(\frac{\tan(24.5°)}{1}\right)$	Slope angle at frictional equilibrium ($F = 1$)	24.5°